University of Alberta

A Low-Power Wearable Microcomputer System for Posture Monitoring

by

Michael Dean Bazzarelli

A thesis submitted to the Faculty of Graduate Studies and Research in partial fulfillment of the requirements for the degree of Master of Science

Department of Electrical and Computer Engineering

Edmonton, Alberta
Fall 2004

Library and Archives Canada

Published Heritage Branch

395 Wellington Street
Ottawa ON K1A 0N4
Canada

Bibliothèque et Archives Canada

Direction du Patrimoine de l'édition

395, rue Wellington
Ottawa ON K1A 0N4
Canada

Your file Votre référence
ISBN: 0-612-95705-5
Our file Notre référence
ISBN: 0-612-95705-5

The author has granted a non-exclusive license allowing the Library and Archives Canada to reproduce, loan, distribute or sell copies of this thesis in microform, paper or electronic formats.

L'auteur a accordé une licence non exclusive permettant à la Bibliothèque et Archives Canada de reproduire, prêter, distribuer ou vendre des copies de cette thèse sous la forme de microfiche/film, de reproduction sur papier ou sur format électronique.

The author retains ownership of the copyright in this thesis. Neither the thesis nor substantial extracts from it may be printed or otherwise reproduced without the author's permission.

L'auteur conserve la propriété du droit d'auteur qui protège cette thèse. Ni la thèse ni des extraits substantiels de celle-ci ne doivent être imprimés ou aturement reproduits sans son autorisation.

In compliance with the Canadian Privacy Act some supporting forms may have been removed from this thesis.

Conformément à la loi canadienne sur la protection de la vie privée, quelques formulaires secondaires ont été enlevés de cette thèse.

While these forms may be included in the document page count, their removal does not represent any loss of content from the thesis.

Bien que ces formulaires aient inclus dans la pagination, il n'y aura aucun contenu manquant.

Canada

ACKNOWLEDGEMENT

This thesis was made possible by the support and help of many people to whom I am gratefully thankful.

I would like to thank my supervisor Dr. Nelson Durdle for his guidance and help with this thesis work, his encouragement, and friendship.

I owe a great deal of thanks to Dr. Edmond Lou for his help with this thesis work, his expertise, and his willingness and availability for discussion.

I would also like to thank the Glenrose Rehabilitation Hospital for providing a research lab and support. In particular I thank Mr. Jim Raso for providing advice and reviewing some of the first draft chapters. Also, I thank Mr. Doug Hill for sharing his scoliosis knowledge and help with the daily activities at the Glenrose Research Center.

The National Research Council's Industrial Research Assistance Program, whom provided support for this thesis, is greatly acknowledged. Also, the financial support from the University of Alberta is appreciated.

I would like to thank Dr. Igor Filanovsky for his help and discussion. Also, I would like to thank Dr. Eugene Paperno, at Ben-Gurion University of the Negev, for his EM expertise and willingness to discuss my work.

Words can not describe what is owed to my parents. I thank them for their love and selfless support allowing me get to where I am.

I am grateful to Ms. Amy Fingas for her support, motivation, and help with this thesis.

In close, all thanks is owed to God who made all this possible.

TABLE OF CONTENTS

1 Introduction 1
1.1 Application and Significance of Portable Posture Monitoring to Scoliosis 2
1.2 Objectives 5
1.3 Scope of Work 6
1.4 Thesis Overview 8
2 Background 10
2.1 Anatomy 10
2.2 Scoliosis Background 14
2.2.1 Types of Scoliosis 15
2.2.2 Evaluation of Idiopathic Scoliosis 17
2.3 Treatment of Idiopathic Scoliosis 19
2.3.1 Conservative 19
2.3.2 Neuromuscular Electrical Stimulation 19
2.3.3 Bracing 20
2.3.4 Surgery 22
2.3.5 Physiotherapeutic Treatments of Scoliosis Using Posture Correction . 23
2.4 Existing Tracking Systems 26
2.4.1 Posture Monitoring Systems 27
2.4.2 Portable Scoliotic Posture Systems 28
2.4.3 Motion Tracking Systems 30
2.4.4 Existing Hybrid Systems 33
3 Measurements of a Scoliotic Patient 35
3.1 Types of Postural Measurements 35
3.1.1 Anatomical Torso Movements 35
3.1.2 Seven Topographical Features 37
3.2 System Overview and Measurement of Posture 40
3.2.1 System Use in Identifying Posture 41
3.3 Determining Measurements and Postures Using the System 43
3.3.1 Background 43
3.3.2 Calculating Postural Positions 44
3.3.2.1 Shoulder Height 44
3.3.2.2 Shoulder Angle Difference 47
3.3.2.3 Decompensation 47
3.3.2.4 Scapula asymmetry 48
3.3.2.5 Waist Crease 49
3.3.2.6 Waist Asymmetry 49
3.3.2.7 Pelvis asymmetry 50
3.3.3 Determining Movements and Postures in Real Time Using Simplified Methods 51
3.3.3.1 Determining Flexion Movements 51

3.3.3.2 Determining Yaw Movements 52
3.3.3.3 Determining Elevation Movements 53
3.3.3.4 Shoulder Height, Shoulder Angle Difference and Pelvis asymmetry 53
3.3.3.5 Decompensation 54
3.3.3.6 Scapula Asymmetry 54
3.3.3.7 Waist Asymmetry 55
3.4 Evaluating Posture 55
3.4.1 Complete Posture Monitoring 56
4 System Theory 57
4.1 Accelerometer Theory 57
4.1.1 Technology of Accelerometers 57
4.1.2 Calculating Tilt Angles 61
4.2 Electromagnetic Theory 66
4.2.1 Overview 66
4.2.2 Electromagnetic Dipole Field 67
4.2.3 Deriving Position and Orientation Derivation For One Sensor Coil 68
4.2.4 Reciprocity Principle to Derive Position and Orientation 72
4.3 Network 73
4.3.1 Communication System 73
4.3.2 I^2C-Bus Hardware and Protocol 74
5 System Design 76
5.1 System Overview 76
5.2 Hardware Design 78
5.2.1 Receivers 78
5.2.1.1 Sensing Coil and Resonating Circuit 79
5.2.1.2 Electronically Controlled Gain 82
5.2.1.3 Band Pass Filter 86
5.2.1.4 RMS to DC Conversion 88
5.2.1.5 Microcontroller 90
5.2.1.6 Accelerometer 93
5.2.1.7 Power Supply 95
5.2.2 Transmitter 96
5.2.2.1 Microcontroller 97
5.2.2.2 Analog Signal Generation 97
5.2.2.3 Transmitting Coils and Circuit 98
5.2.3 Master Computer 100
5.3 Software Design 104
5.3.1 Receivers 104
5.3.1.1 Receiver Initialization Routine 105
5.3.1.2 Receiver Mode Selection Routine 108
5.3.1.3 Receiver Calibration Routine 110
5.3.1.4 Receiver Sleep Routine 112
5.3.1.5 Receiver Awake Routine 112

5.3.1.6 Receiver Get Data Routine 112
5.3.1.7 Receiver Send Data Routine 114
5.3.1.8 Receiver Interrupt Service Routine 115
5.3.2 Transmitter 119
5.3.3 Master Computer 121
5.3.3.1 Initialization 123
5.3.3.2 Configuration 124
5.3.3.3 System Operation 125
6 Results and Discussion 126
6.1 Test Methods 126
6.1.1 Angle Detection Test Methods 126
6.1.2 Distance Test Methods 129
6.2 Test Results 131
6.2.1 System Accelerometer Angle Measurement Stability Test Results 131
6.2.2 System Accelerometer Repeatability Test Results 133
6.2.3 System Accelerometer Accuracy Test Results 133
6.2.4 System Accelerometer Resolution Test Results 136
6.2.5 System Electromagnetic Stability Test Results 138
6.2.6 System Electromagnetic Angle Accuracy Test Results 140
6.2.7 System Electromagnetic Angle Resolution Test Results 141
6.2.8 System Electromagnetic Distance Test Results 142
7 Conclusions and Recommendations 145
7.1 Conclusions and Results 145
7.2 Future Recommendations 147
References 150

LIST OF TABLES

Table 5-1. Coil evaluation. 81
Table 5-2. EM signal measurements. 83
Table 5-3. RMS to DC conversion comparisons. 89
Table 6-1. Actual and theoretical error comparison. 132
Table 6-2. Repeatability test. 133
Table 6-3. Acceleration data analysis. 135
Table 6-4. Accelerometer angle error. 136
Table 6-5. Change of accelerometer resolution. 137
Table 6-6. Five hour EM standard deviations. 139
Table 6-7. EM accuracy test results. 141
Table 6-8. Repeatability of EM distance tests. 143
Table 6-9. Distance measurement test summary. 144

LIST OF FIGURES

Figure 2-1. Planes of the body. 11
Figure 2-2. Vertebral column. 12
Figure 2-3. Vertebra. 13
Figure 2-4. Cobb angle. 18
Figure 3-1. Postures due to shoulder girdle movement. 36
Figure 3-2. Postures due to spine movement. 36
Figure 3-4. Shoulder height measurement due to flexion. 45
Figure 3-5. Shoulder movement model. 46
Figure 3-6. Discrepancies with mounting. 47
Figure 3-7. Decompensation mounting and measurement. 48
Figure 3-8. Pelvis asymmetry calculation. 50
Figure 4-1. Structure of MEMS accelerometer. 60
Figure 4-2. Accelerometer PWM output. 62
Figure 4-3. Magnetic dipole. 67
Figure 4-4. Diagram for field derivation. 70
Figure 4-5. Orientation of sensor. 71
Figure 5-1. System block diagram. 78
Figure 5-2. Receiver block diagram. 78
Figure 5-3. Prototype receiver. 79
Figure 5-4. Controllable gain circuit. 84
Figure 5-5. Variable gain circuit simulation. 85
Figure 5-6. Band pass filter first cascadable 2nd-order section. 87
Figure 5-7. RMS to DC rise and settling time. 90
Figure 5-8. ADC and RMS to DC results. 93
Figure 5-9. Transmitter block diagram. 96
Figure 5-10. Transmitter prototype. 97
Figure 5-11. Transmitter drive circuit. 97
Figure 5-12. Transmitter Orthogonal Coil. 99
Figure 5-13. Transmitter output. 100
Figure 5-14. Master computer. 102
Figure 5-15. System network busses. 103
Figure 5-16. Receiver program flow chart. 105
Figure 5-17. Receiver initialization flow chart. 108
Figure 5-18. Receiver mode selection flow chart. 110
Figure 5-19. Receiver calibration selection flow chart. 111
Figure 5-20. Receiver get data flow chart. 114
Figure 5-21. Receiver send data flow chart. 115
Figure 5-22. Receiver interrupt service routine high level flow chart. 117
Figure 5-23. Transmitter flow chart. 120
Figure 5-23. Transmitter flow chart (continued). 121
Figure 5-24. Main computer high level flow chart. 122
Figure 5-24. Main computer high level flow chart (continued). 123

Figure 6-1. EM rotational test fixture. 128
Figure 6-2. EM distance test fixture. 130
Figure 6-3. Standard deviation. 131
Figure 6-4. Theoretical angle error. 132
Figure 6-5. Accelerometer acceleration data. 134
Figure 6-6. Accelerometer resolution measurements. 138
Figure 6-7. Sample rate effect on droop and settle time. 139
Figure 6-8. Overview of EM system 140
Figure 6-9. EM angle resolution test results. 142
Figure 6-10. EM coil calibration. 143

Chapter 1

1 INTRODUCTION

Scoliosis is a lateral curvature of the spine producing the characteristic 'S' shaped curve in the frontal plane. It is usually accompanied by rotation of the vertebrae on their axes. Over 80% of the cases are of unknown etiology and are termed idiopathic. Not only can idiopathic scoliosis lead to physical deformity but also pain and medical complications that require some form of treatment [49]. The most common form of non-operative treatment used in arresting the progression of the adolescent idiopathic scoliotic curve is bracing [8, 49, 50].

Although bracing is the gold standard against which new nonoperative treatments are evaluated, its mechanism is not fully understood. The brace exerts a force on the patient's body moving it into an alternate posture. This is termed the passive form of treatment. At the same time the brace causes the patient to pull away from its pressure points. This is the active form of treatment. It is this active component of the brace treatment that has been suggested as the most important mechanism for halting curve progression [6, 7, 9, 51].

Based on this active component of treatment, research into physiotherapeutic treatment methods are being explored with apparent successful results [7, 12, 18, 32, 44]. These programs focus on using active treatment methods such as posture correction and physical exercises to halt curve progression. These new treatment methods help to overcome some of the drawbacks of bracing [4, 5, 6, 18].

There are both physical and psychological problems when wearing a brace. Physically, braces have several drawbacks: they are hot, restrictive, heavy, bulky, and worn up to 23 hours a day. The majority of the patient population are adolescents and may

struggle with decreased self image as a result of bracing at one of the most sensitive times of their lives. These drawbacks can greatly affect the patient's quality of life and negatively impact the treatment; non-compliance rates are high [7]. Alternative physiotherapeutic treatment methods are being investigated to overcome these drawbacks.

Aside from monitoring the success of treatment to halt curve progression, a quantitative means of assessing all scoliosis treatment methods is required to determine their effects on trunk asymmetries. Primary evaluation methods rely on radiographs. These provide a poor image of overall trunk distortion, often the major concern of the patient and their family. Work has been done to create a set of clinical measures that can be used to evaluate a scoliotic patient [28]. Any means of obtaining quantitative data will help in the evaluation of treatment outcomes and the investigation of treatment methods.

This thesis proposes a portable posture monitoring device to be used for the treatment of idiopathic scoliosis in conjunction with physiotherapeutic treatment methods. In addition to being used as a device that can monitor a patient's posture or body positions, the data from the device can be used to calculate clinical measurements to quantitatively analyse a patient's progress for a particular treatment method [28]. Also, the collected data will aid in reducing unknowns in treatment studies and provide more insight into the development of the disorder and the mechanism of the treatment methods.

1.1 Application and Significance of Portable Posture Monitoring to Scoliosis

This thesis focuses on the application of portable posture monitoring to idiopathic scoliosis treatment and research. A posture monitoring system is applied as an alternative treatment method to the brace, in conjunction with a behavioural treatment method. A portable posture monitor is a discrete and small device that is worn by the patient. Small sensors are placed at key locations to detect the desired posture or

movement. The discreetness of the posture monitor helps overcome drawbacks associated with brace treatment and provides a better quality of life for the patients during their treatment. Physical problems such as skin rashes and irritations, discomfort due to heat or restriction, and fatigue due to heavy bulky braces can be avoided. Also, the emotional factors can be lessened with a much less obtrusive device and treatment method.

The posture monitor is able to provide real-time feedback. The novelties of a system that can do this with low computing power, while still acquiring high resolution data, will be elaborated on. The real-time biofeedback that the patient receives allows them to make adjustments to their posture, or to be prompted to perform a required movement or exercise. This means that the system can be used with existing physiotherapeutic treatments to form new methods of treatment. The system bridges the gap not met by other treatment methods by providing the ability to aid in proprioception. Proprioception is the patient's awareness of body position and movement. The patient receives verification that he has performed a movement, exercise, or obtained a desired posture correctly, helping them with any proprioceptive deficiency. Problems with proprioception in scoliotic patients have been observed and have been suggested as a causative factor of spinal asymmetry [26]. In addition, aside from just performing exercises, research has shown that scoliotic patients need to perform specific repetitive exercises that place the spine at certain angles to gain the most beneficial results [3]. The posture monitor will facilitate these types of exercises and provide the feedback that has been provided by a physiotherapist or a mirror [32].

Another benefit of using posture monitoring over bracing is that researchers and clinicians benefit from having information that was previously unavailable with brace treatment. From quantitative data that the system obtains, the clinician can verify if the patient is performing the treatment method as prescribed as well as monitor compliance. The patient is provided with a system that reminds and motivates him to comply with the treatment program.

Obtaining quantitative measurements is significant for scoliosis research. The posture monitoring system provides the data to obtain the clinical measures for cosmetic deformity. These can be monitored throughout a patient's treatment. This allows investigation of the relationships between the clinical measures and both scoliosis severity and treatment methods. True compliance rates, and other information specific to a treatment, for example the actual number of exercises performed or treatment times and lengths, would reduce the number of unknowns in studies. Research of both brace and behavioural treatments suffers from these variables being unknown.

The evaluation of physiotherapeutic methods of treatment and outcomes can occur more easily with the posture monitor. With the help of the quantitative data, research can be performed to evaluate and determine which particular exercises may be successful. Also, patient evaluations can be made safer. Currently, radiography is the method of choice to evaluate progress of scoliosis treatment. A posture monitoring system will provide a simple and safe way to evaluate treatment progress and avoid the health risks associated with radiographs. In addition, a posture monitor provides 3D information as opposed to a 2D radiograph. Radiographs do not always reflect the 3D deformity. In fact, it is not known how to assess the 3D aspect of the deformity in a repeatable fashion and surface topography is an attempt.

Posture monitoring has other applications in addition to scoliosis treatment. There are other medical conditions that could benefit from the use of a posture monitor. These include post operative monitoring for posture or movement restrictions such as in hip replacement surgery or anterior cruciate ligament (ACL) repair. Any type of posture treatment for back pain caused by postural dysfunction, kyphosis, lordosis, or osteoporosis would benefit from the device [5, 57]. People with certain disabilities or neuromuscular difficulties can also use posture monitoring. An example of this is to detect general head position or maintain appropriate body position of severely disabled people [31]. The benefits of proper trunk alignment to patients with neuromuscular difficulties include prevention of deformity, improvement of fine motor activities such

as speech, improvement of balance to free up arms and hands for movement and manipulation, and promotion of motor activities required for learning and independence [31]. There are other non-medical applications such as job safety. Workers could be monitored and reminded about their posture during heavy lifting. It could also be applied in the fine arts such as in dance education.

It should be clarified that the posture monitor in this thesis is designed for posture monitoring and for use as a research tool. It is proposed as a possible treatment tool for use with brace treatment or for use with active posture treatment methods. However, active posture treatment for scoliosis treatment remains to be proven effective.

1.2 Objectives

The objectives of this thesis are:

- to evaluate position sensors that might be used to measure trunk alignment;
- to study and develop a list of postural movements, and postures specific to idiopathic scoliosis treatment;
- to develop a method to perform posture monitoring to help improve and develop alternative treatments to scoliosis;
- to analyse alternate treatments to scoliosis;
- to design, build, debug, and test a novel, hybrid, networked posture monitoring system;
- to compare a new posture monitoring system against alternatives;
- to determine accuracy and resolution of the system;
- to verify the ability to detect an incorrect posture consisting of a rotation (yaw) movement, flexion of the spine, or shoulder elevations for quick posture evaluation;
- to verify the ability to record data that can be used to compute a clinical measurement, for example shoulder angle asymmetry.

1.3 Scope of Work

There are several requirements when creating a portable posture monitoring system for use with physiotherapeutic treatment of idiopathic scoliosis. The application needs to be studied and evaluated to achieve new methods to overcome existing problems with monitoring posture and motion when using a portable device versus a non-portable system. Existing methods need to be evaluated and improved upon. The system needs to detect a patient's posture and provide real time feedback, and to record data to calculate clinical measurements. Also the device will form a base system tool for new research.

The end application is described to highlight the most appropriate application-specific system requirements. Physiotherapeutic treatment methods are presented. A connection between human posture and movement, and scoliosis treatment methods is determined. This involves studying human postures and movements and how they relate to scoliosis monitoring and treatment methods. In particular, study is required to determine the key motions that are monitored in idiopathic scoliosis treatment, and whether quantitative clinical measurements can be obtained at the same time. Methods to obtain existing clinical measurements using such a system are created and will be presented. Some of the key measurements required are flexion movements and rotation or yaw movements of the spine, also shoulder girdle movements. A novel method is described for detecting a yaw measurement that does not rely on continuous monitoring by the system, such as gyroscope technology requires.

The system requirements include a small, low power, portable system that could alert a patient to a poor posture and provide biofeedback, as well as log high-resolution data. It has to be fast and able to obtain multiple sensor measurements at the same time. It has to be accurate and have high resolution. A novel intuitive approach is presented for posture and motion monitoring as opposed to calculation-intensive methods that prevented system expansion and could not give fast timely feedback to the patient. Posture tests can be created in an easy intuitive manner.

Novel methods are implemented to obtain measurements in a low-power portable environment. Several features are implemented that overcome problems with previous devices to create a system that is intuitive, fast, and accurate with a higher resolution. A hybrid system concept is developed that uses electromagnetic (EM) and Micro-Electro-Mechanical Systems (MEMS) sensor technology. Distributed computing increases speed and takes advantage of parallel data acquisition. A communications network is set up between the microcontrollers to allow multiple computers to be easily added to the system when using different system configurations. This minimizes impact to the system performance, and provides for future transition to a wireless system. Manufactured coils are investigated to reduce the system cost of building custom EM coils.

These features allow for both a high-resolution data collection system and a data processing system to be implemented with low power, low sophistication microcontrollers. Previously, only one or the other, of either data collection or biofeedback, had been done. A less computationally intensive solution avoids the limitations of the previous devices that could only record data from two sensors due to the required computing power. The hybrid design allows for the recording of sensor data and determining sensor location with fewer computations, yet maintaining a high resolution of measurement. It also has the option to perform lower resolution calculations, particularly useful depending on the feedback resolution being provided to the user. For example, if the user is receiving a single feedback signal alerting them about a raised shoulder, only one angle calculation from a sensor measuring the shoulder angle needs to be made. In contrast, with an EM six degrees of freedom (6DOF) system, there are no shortcuts in the computation that can be made. The polar coordinates need to be calculated, and then they need to be related back to the patient's body location.

In summary, the system can perform several things that were not previously done: several sensors can be used to obtain intuitive information and the calculations that are

made can be tailored to provide posture feedback, while high resolution data are collected to compute clinical measurements; the sensors can be placed in different configurations to obtain a desired measurement; angles can be measured with respect to gravity; yaw can be determined without the need for continual sensor monitoring; distances can be measured in 1-D; and, important for future work, distances can be determined by placing two of the sensors coils orthogonally and using both data sets, collected in parallel, for calculations.

The posture monitor is investigated to determine its accuracy and resolution. It is able to detect an incorrect posture consisting of either a yaw movement or flexion of the spine, centering the trunk over pelvis, and shoulder elevations for fast posture evaluation. It can record data to compute clinical measurements, for example shoulder angle asymmetry.

1.4 Thesis Overview

This thesis consists of seven chapters. These elaborate on the development of a portable posture monitoring device for physiotherapeutic treatment of idiopathic scoliosis and its use as a tool for scoliosis research.

Chapter 1 provides the introduction to this work. An overview of the application of posture tracking to scoliosis is presented. The scope of the work is given along with the objectives and a summary.

Human anatomy background pertaining to scoliosis is presented in chapter 2, along with information on idiopathic scoliosis. Treatment methods of scoliosis are discussed leading to the introduction of the behavioural or physiotherapeutic treatment methods that would benefit from a posture monitoring device. Finally an overview of motion tracking systems is presented.

Chapter 3 describes methods to obtain the measurements that can be made on a scoliotic patient. The types of human postures and movements and their relation to a scoliotic patient are studied. The methods are presented on how to obtain each clinical scoliosis measurement. This is followed by methods that show how a patient's posture can be evaluated in real-time using methods that do not require clinical measures to be computed. In particular, we discuss is methods that are in relation to the resolution of the feedback signal being given to the patient.

The system theory is presented in chapter 4. This covers the MEMS accelerometer sensor technology and how the angle can be calculated for both high and low-resolution methods. The electromagnetic technology used is explained with an example of how measurements can be made for distance and angle. The system networking communications protocol is presented.

Chapter 5 describes both the hardware and the software to create a posture monitoring system. The hardware requirements are presented along with the final hardware selections and designs. An outline of the software that was created for the embedded systems is given.

The results and discussion are presented in Chapter 6. The tests are presented and the results for angle measurements, yaw measurement, and 1-D distance measurements of the system are presented. Next a clinical measurement result is calculated as an example of how measurement is obtained from the system. This chapter will end with a discussion of the results.

Chapter 7 is a summary of the thesis work. Concluding remarks are made along with a summary of the results. Future recommendations for this work are made including a discussion of the next steps for this research and any changes or suggestions that should be implemented.

2 BACKGROUND

This chapter introduces the background information relevant to this work. An overview of the basic human anatomy is presented to facilitate clearer discussion and descriptions. To aid in understanding the motivation for this thesis, scoliosis background information is presented along with information regarding state of the art equipment for posture monitoring.

2.1 Anatomy

When describing the body in three dimensional space, the planes are defined as shown in figure 2-1. The median plane divides the body into left and right halves. Any plane parallel to this is called a sagittal plane. The vertical plane normal to the sagittal plane is the frontal or coronal plane. It divides the body into anterior, or front, and posterior, or back, portions. At right angles to both these planes is the horizontal or transverse plane that divides the body into upper and lower portions.

There are three axes of rotation. The longitudinal or vertical axis runs through the body from head to toe. The horizontal or transverse axis is perpendicular to the longitudinal axis and runs from left to right in a frontal plane. Perpendicular to both these axes is the sagittal axis; it runs anterior to posterior.

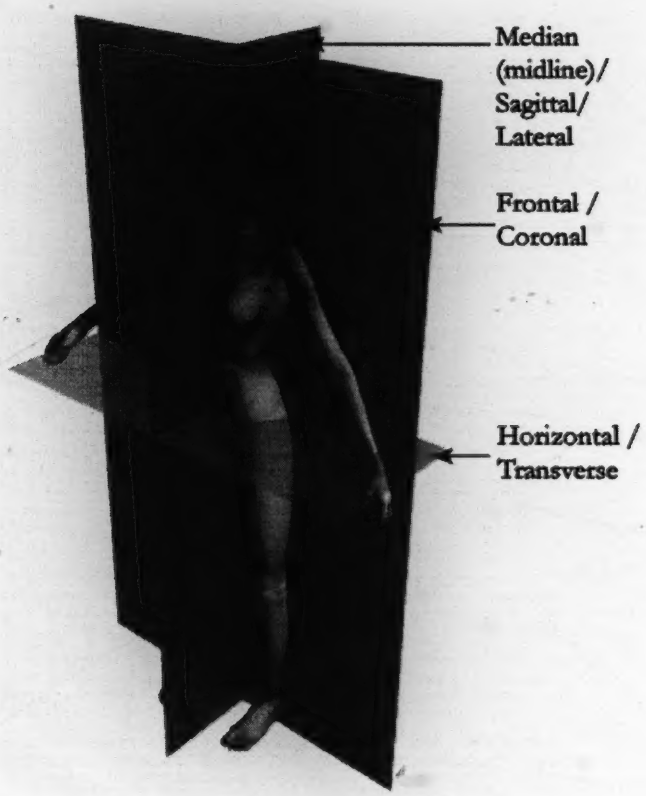

Figure 2-1. Planes of the body.

The spinal column starts at the base of the skull and ends at the pelvis. The spinal column consists of bones called vertebrae separated by intervertebral disks. The spinal column is composed of five sections, namely the cervical, thoracic, lumbar, sacrum, and coccyx pictured in figure 2-2. The cervical region consists of seven vertebrae. Following this is the thoracic region that consists of twelve vertebrae each attached to two ribs. The rib movement along with the vertebra is what can cause the characteristic rib hump that is seen in scoliosis when the vertebra has rotated. Next is the lumbar section of the spine which consists of five of the largest vertebrae. The sacrum is a fusion of five sacral vertebrae that joins with the pelvic bones. The coccyx is an extension of the sacrum and the fusion of four coccygeal vertebrae. Each of the

vertebrae in these sections are often referred to using a letter for the region the vertebra is found in and the numbered position of the vertebra. For example, in the cervical region the vertebra are referred to as C1, C2, C3 to C7 moving from the head down. Likewise, the thoracic region is referred to as T1 to T12, lumbar vertebrae as L1 to L5 and the sacrum as S1 to S5.

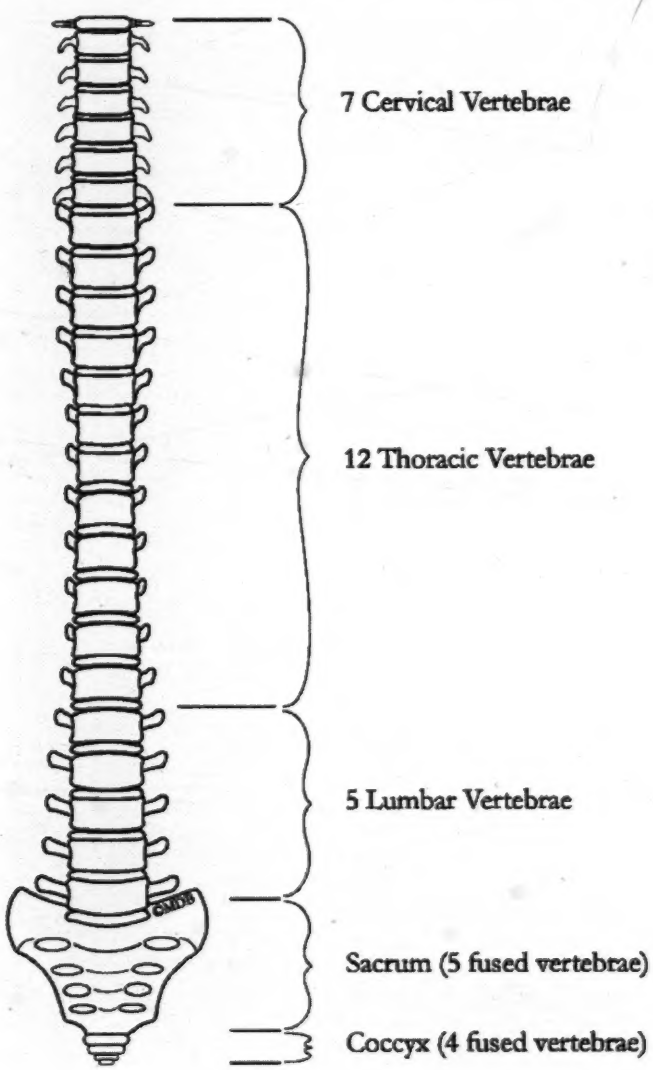

Figure 2-2. Vertebral column.

The general parts of the vertebra are labeled in figure 2-3. The bodies of the vertebrae are stacked upon each other with the intervertebral disk in between. The vertebral foramen is a hole that lines up to form the spinal canal which houses the spinal cord. The spinous process is the bony part that protrudes posteriorly and is a muscle attachment site. The transverse process protrudes laterally and is a site for rib or muscle attachments. The superior articulating facet on the articulating process of one vertebra forms a joint with the inferior articulating facet of the vertebra above. Vertebrae differ from each other and are classified into groups. Named from the head toward the pelvis they are called: atlas, axis, cervical vertebrae, thoracic vertebrae, lumbar vertebrae, sacrum, and coccyx.

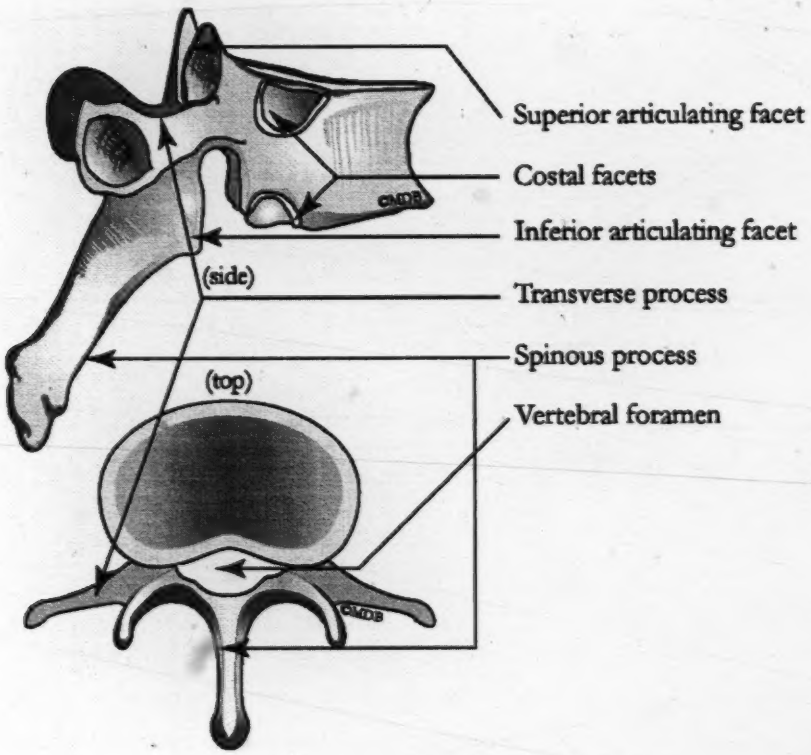

Figure 2-3. Vertebra.

The shoulder girdle consists of several joints and bones that attach the upper limbs to the torso. The scapula is often called the shoulder blade. The lower part of the scapula that is seen as a high point on the back is called the inferior angle. Towards the top of the shoulder the scapula is called the acromion, here it joins to the clavicle, or collar bone, via the acromioclavicular joint. The clavicle connects to the sternum, or breast bone, via the sternoclavicular joint.

2.2 Scoliosis Background

Scoliosis is a lateral curvature of the spine with axial rotation. This causes distortion of the ribs and leads to characteristic rib humps more prominently seen during forward flexion. The spine may have one or more curves. The curve with the most significant structural deformity is called the major or primary curve. The minor, secondary, or compensatory curve is the curve which brings the head back to midline. Defining some of the vertebrae aids in discussing the scoliotic curves. The transitional vertebra is the vertebra between two curves that is not rotated. The apex vertebra is found at the apex or most lateral point of the curve.

Curves are classified according to the area in which their apex is found. A cervical curve has an apex between C1 and C6. A cervicothoracic curve has an apex at C7 or T1. A thoracic curve has an apex between T2 and T11. This curve often exhibits the worst cosmetic deformity because the ribs are attached in this region. Thoracic curves also tend to progress more than other curves [10, 14]. A thoracolumbar curve has an apex at T12 or L1. A lumbar curve's apex is between L2 and L4 and a lumbosacral curve has an apex at L5 or S1.

Scoliosis is often accompanied with other abnormal curvatures in the sagittal plane. Kyphosis is a backward curve of the spine. To distinguish kyphosis from poor posture, a forward bending test will exhibit a sharp bend in the back as opposed to a smooth curve. Lordosis is a forward curve in the spine.

2.2.1 Types of Scoliosis

There are different types of scoliosis. Non-structural scoliosis has no bony deformity and no rotation in the vertebrae. The spine is not structurally changed, the curve usually does not progress, and normal flexibility is maintained. It can be either postural or compensatory. Postural non-structural scoliosis is a postural misalignment problem and can be corrected with postural exercises. Compensatory scoliosis develops to correct the body's alignment due to a physical problem such as a leg length discrepancy. A compensatory curve is also seen above or below a structural curve to compensate for malalignment. In both of these cases the curve would disappear during forward flexion.

Structural scoliosis usually has bone deformity present. It may be progressive and has reduced normal flexibility. Cobb identified four different subgroups of structural scoliosis [50]. Osteopathic scoliosis is congenital and due to abnormal bone development. During embryonic development the structures fail to correctly develop. Neuropathic scoliosis is due to central nervous system disorders. Examples include cerebral palsy or poliomyelitis. Myopathic scoliosis is caused by muscular disorders such as muscular dystrophy which is gradual irreversible wasting of skeletal muscle. The last classification, idiopathic scoliosis, is the most common and accounts for about 90% of all scoliosis cases [50]. The cause is unknown. Its essential features include lateral curvature and rotation of the vertebrae. Vertebral bodies rotate into the convexity of the curve meaning the spinous process moves towards the concave side.

Idiopathic scoliosis can be divided into infantile, juvenile and adolescent scoliosis. Infantile occurs in the age range of 0 to 3 years old and usually only requires monitoring. Juvenile idiopathic scoliosis occurs in the age range of 4 to 9 and is highly progressive. Adolescent idiopathic scoliosis (AIS) is found in 2 to 8 percent of the population [17]. The age range is from 10 to skeletal maturity. Approximately 80 percent of the adolescents affected are female. Of the adolescent group approximately

8 percent, which is 0.2 percent of the general public, will have progression in their curves and will require treatment [6, 19].

There are several medical complications that can occur due to scoliosis such as pain, malfunctioning body systems, and even death [10, 14, 33]. As previously described the skeletal system is affected and becomes deformed. In particular, the vertebrae are deformed and the spine is distorted and twisted. The twisting of the vertebrae causes the ribs to distort, and can produce a rib hump. The pelvis can be distorted. The muscular system is affected having reduced flexibility [16]. The nervous system is also affected. Nerves can be pinched between the deformed vertebrae. For severe thoracic curves, the respiratory system function is decreased [16, 33, 10]. It is manifested as shortness of breath. This lung dysfunction has been reported to cause heart failure in severe scoliosis [33]. These medical repercussions depend on the severity and location of the curve.

One of the repercussions that is common to most types of scoliosis is the cosmetic aspect of the deformity. This has psychosocial effects on the patient. In one study, patients have reported various ways scoliosis has limited their life aside from the medical problems. A number of the responses dealt with issues involving difficulties in purchasing clothing, a decreased physical capacity, and self consciousness [34]. Body image is a psychological factor that affects the adolescent and can lead to non-compliance in treatment [17]. In the SF-36 test, a quality of life test, AIS patients had decreased scores in all categories which included: limitations in physical and social activities due to health problems, limitations in usual role activity, bodily pain, general mental health, limitations in usual role activity because of emotional problems, vitality, and general health perceptions [35]. In a different study using the Pediatric Outcomes Data Collection Instrument questionnaire, scores for AIS patients were significantly lower than children without orthopaedic disabilities in the test areas of transfers, sports, comfort and happiness [36].

2.2.2 Evaluation of Idiopathic Scoliosis

During the initial assessment of a scoliotic patient the clinician tries to determine if there are any underlying pathologies that are treatable and then to determine the type of scoliosis. The assessment also provides a baseline to which future curve progression can be compared. The physical examination for idiopathic scoliosis begins with a front and back inspection of the patient for asymmetries such as in the shoulders, skin folds, scapulae, hips, or spinal alignment. Then the forward bending test is performed. The patient keeps their knees straight, hips are flexed close to 90 degrees and arms hang down toward the floor with the palms together. The patient's back is observed for asymmetry such as rib prominence. Due to the vertebral rotation the prominence of the rib or paralumbar muscle will be prominent on the convex side of the curve [37]. This test helps to rule out non-structural scoliosis.

For early detection and screening, however, use of the forward bending test alone is somewhat qualitative and has led to reports of too many false negatives. This means that significant curves have gone undetected [38, 39]. This has lead to more quantitative screening methods and the requirement of more than the forward bending test alone. These back shaping techniques attempt to predict scoliotic deformities from back shape and trunk deformity.

A scoliometer can be used to measure the rib prominence and to quantify the angle of trunk rotation when the patient is in the forward bending test position. This is like a spirit level that is placed on the patient's back over the spinous processes at the level of maximal prominence. A measurement of 7 degrees correlates to approximately 20 degrees of Cobb angle [37].

The Cobb angle is the standard measurement of the scoliotic curve. Scoliosis is present, by definition, if this angle is equal to or greater than 10 degrees. The angle is measured using a posteroanterior radiograph of the spine as shown in figure 2-4. The upper and lower vertebrae are the vertebrae that have maximal tilt above and below

the apex of the curve. A parallel line along the superior aspect of the upper vertebra is drawn, and likewise for the lower vertebra along its inferior aspect. The angle is read from the intersection of these lines as the Cobb angle.

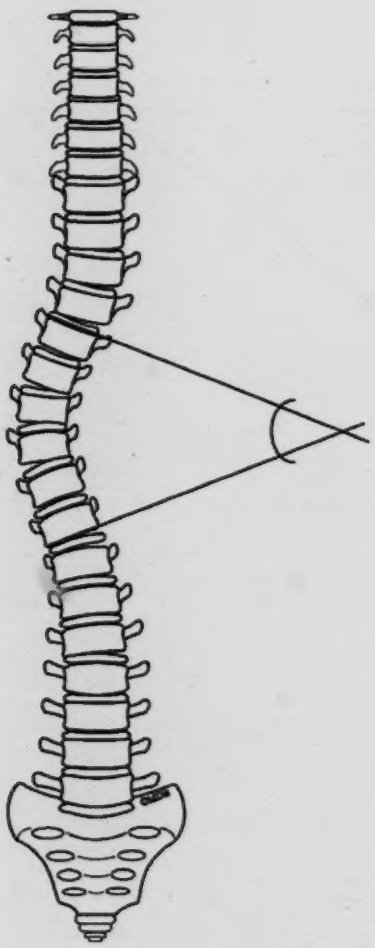

Figure 2-4. Cobb angle.

Moiré topography is a more accurate method of mapping the back surface in three dimensions. This method projects a grid of lines onto a patient's back and the illuminated surface is viewed through a similar grid. One picture is produced from two pictures: the first picture is of the grid projected onto a flat white surface, the second

picture is from the grid projected onto the patient. When combined, contours are produced that correspond to discrete distances [52]. Other methods have since been introduced that produce three dimensional mappings of the patient's back. These back shaping methods have been shown to correlate to the Cobb angle, however, they both provide different aspects of measurement and have not replaced the Cobb angle measurement. The benefit of surface topography is to reduce the health risk to the patient by reducing the number of radiographs required to monitor the patient's progress [40].

2.3 Treatment of Idiopathic Scoliosis

The primary goal of all treatment methods are to halt progression of the curve, or if possible to reduce the curve. Treatments are considered successful if they halt curve progression. All treatments are controversial in deciding when to treat the patient and in deciding how effective the treatment is [37].

2.3.1 Conservative

Conservative treatment is the first course of treatment if the patient's curve is less than 20 degrees before skeletal maturity [8, 37]. This means that the patient will be monitored for curve progression by being reevaluated at regular intervals. If the curve begins to progress reaching an unacceptable limit, then another form of treatment will be chosen.

2.3.2 Neuromuscular Electrical Stimulation

Electrical stimulation was a newer type of treatment that began clinical trials in 1974. It is not used anymore. It induces muscular contraction on the patient. The treatment is carried out at night while the patient is sleeping and has found good patient acceptance. In contrast, Bylund et al. found that compliance in their study was actually a problem, and that some patients found it too uncomfortable [45]. What makes electrical stimulation different than other therapies is that only a few muscle groups are brought into play, and it is considered a passive therapy [44].

This treatment is considered when the curve progresses from 20 to 30 degrees, or if the patient initially presents with a curve of 30 degrees. Curves of 40 degrees or more are not considered good candidates for this treatment [2].

The efficacy of the treatment is controversial. Some studies report a high success rate [2, 19, 20]. However, others report it as low or no treatment at all [2, 8, 45]. Enthusiasm for this treatment appears to be decreasing.

2.3.3 Bracing

Bracing is the oldest and most common form of treatment for idiopathic scoliosis. All other non-surgical treatments are compared against it. Although it began centuries ago in various forms it was not until the Milwaukee brace that enthusiasm began for its use in treatment of idiopathic scoliosis (IS).

The Milwauke brace consists of a pelvic girdle with upright bars that attach to a plastic collar encircling the patient's neck. It is used to treat patients with curves in the upper part of the spine. For curves in the middle or lower spine, low profile braces have been developed such as the Boston brace, which are called thoracolumbarsacral orthosis (TLSO). These braces are made of plastic material fitted to the body and padded inside. Pressure pads inside the brace help to correct the lateral curvature and rotation. They do not extend to the neck and are less visible on the patient.

Bracing treatment is considered for the patient whose curve progresses past 20 degrees, and is done for curves over 30 degrees [8, 37]. However, this number is coming down to 25 degrees. They are prescribed to be worn for up to 23 hours per day.

In a meta-analysis, Rowe et al. [8] showed that the most successful results occurred in patients who wore their braces for 23 hours per day. However, compliance is a problem with bracing. In contrast to the traditional 23 hour treatment, others have claimed that part-time brace wear might be as effective as full-time brace treatment [9,

2]. In fact it has been hard to determine true compliance rates. For example, in a study from Oxford using a hidden compliance meter a compliance rate of 10 percent was discovered, contrary to what the patients and parents claimed [14]. Years later however, a different author claims there might have been an error in this study [42]. Another study found patients wore their braces 65 percent of the recommended time. Thus, the lack of true compliance rates, and the controversy between studies showing there is no difference between full and part-time use, leaves questions about the true effect of the brace [50]. Until there is objective data for true compliance rates, it will be hard to define the acceptable wear time for bracing.

Why are the noncompliance rates high? Most believe it has to do with the discomfort and psychological distress it causes to the patient. Braces are hot, restrictive, and uncomfortable. Furthermore, aside from just being worn, braces must be worn correctly to be effective. This involves fastening the brace to the correct tension. Along with the physical there are psychological issues. The patient might feel pressure to fit in with her peers during adolescence and might not want to wear the brace. Likewise, they might withdraw from social settings affecting their quality of life. One study summarized this idea when 75% of the females said, they viewed the brace as a prison and wore it less than prescribed [17].

There are also some medical drawbacks to wearing a brace. Rashes or skin irritations can develop. Muscle atrophy can occur. Pulmonary capacity can be decreased by 18 percent, and mild transient alteration of renal function can occur [37].

The major controversy surrounding brace treatment is whether it can influence the natural history of IS. Several studies have been published that claim braces do work [8, 9, 11, 30, 42]. Rowe's meta-analysis found the Milwaukee brace the most effective when used 23 hours per day. This brace and the Boston brace's effectiveness decreased significantly when bracing for 8 or 16 hours per day. Most studies agree that bracing does not work with curves over 45 degrees. Only recently has success with larger

curves in the area of 35 to 45 degrees been claimed [30]. It also seems to be agreed that bracing is more effective if the treatment is started early.

However, recently more articles have been published questioning these claims and even stating that braces do nothing [14, 15, 41, 52]. Questions have been raised regarding the length of time required in the brace, as already mentioned, by the Scoliosis Research Society. In a literature review by Dickson, he points out that the literature on brace treatment for AIS is inadequate in proving the efficacy of brace treatment [14]. He states many of the studies have no control group and are retrospective studies. He points out that more work is required to determine which deformities will progress. The negative effects of bracing are questioned. Also, many questions about the exact mechanism of how the brace works needs to be answered. Brace treatment still requires more investigation.

The brace exerts forces on the patient while at the same time the patient pulls away from pressure points induced by the brace [6, 54]. This is referred to as the brace's passive and active components, respectively. The active component of the brace has led to a therapeutic treatment of scoliosis, where the patient moves into a position to minimize the scoliotic deformity and will be discussed later. The active component has been suggested to be more important in improving the spinal curvature and the cosmetic appearance [6, 9, 51, 54].

2.3.4 Surgery

To avoid medical complications that can occur when a curve progresses, such as breathing problems and heart disease, surgery can be performed. Other reasons include preventing further curve progression, to prevent or improve the cosmetic appearance, reduce the risk of arthritic problems and pain due to the curve, and to reduce the risk of paralysis. Once the curve reaches 40 to 45 degrees, surgery is often considered [8, 37]. Typically some indicators for surgery are significant pain, the progression and magnitude of the curve, and other cardiopulmonary symptoms.

The most common type of scoliotic surgery is spine fusion. The vertebrae that form the abnormal curve are fused together fixing the curve and preventing the curve from progressing. Metal rods are often used in surgery and are attached along the spine with small hooks, screws or wires. Primarily these help the spine remain fixed during the time that the fusion takes to heal. Usually they are not removed.

2.3.5 Physiotherapeutic Treatments of Scoliosis Using Posture Correction

Of most interest to this thesis is the physiotherapeutic, or behavioural, type of treatment. These treatments focus on correcting the posture and performing exercises that focus on decreasing the deformity. The goal is to treat AIS without using a brace or to recognize physiotherapeutic treatment's place in a treatment program with a brace. This treatment overcomes the problems associated with the brace, and actually introduces some benefits that the brace cannot provide. In particular, these treatments focus on using active treatment, which is believed to be an important component of brace treatment. This is where the patients are involved in making the correction themselves.

Something else that this type of training does is to retrain the patient's proprioception. This is the unconscious perception of movement and the body's spatial orientation arising from stimuli within the body itself. It is the mechanism that the body uses to control posture and movement using stimuli from the nerves in muscles, joints, and tendons. It has been suggested that defects in proprioceptive posture control are linked to the etiology of idiopathic scoliosis. Studies have shown significant differences in the scoliotic group versus the control group [26]. Byl et al. tested IS patients and found patients with curves over 25 degrees had decreased proprioception and had decreased balance [3]. They recommended that balance and proprioceptive exercises be included in patient treatment programs. For example, they recommended exercises that would challenge the orientation of the spine, such as having the patient try to obtain a particular angle or posture with his spine. This would require some type of biofeedback system. These thoughts were echoed in another study that felt

proprioception could be a cause, and recommended focusing on specific proprioceptive exercises so the spine itself can be located in space correctly [16]. These studies all pointed to the possibility of retraining the patient.

The lateral shift procedure is a specific exercise type of treatment with promising results and it is currently being used at the St. Maartenskliniek Hospital in the Netherlands [29]. The physical movements that will be described for this treatment are not themselves new, but have been around since 1929 and were used as exercises in the Milwaukee brace treatment program. However, around 1983 Mehta discovered, by accident, that these exercises alone in repetition can stabilize and even correct early idiopathic scoliosis [18]. The treatment involves having the patient actively correct their back curve by moving opposite to the convexity of the primary curve. In Mehta's preliminary study they noted that compliance varied and did affect the patient outcome. She noted the need for some type of electronic device that could remind the patient, thereby addressing the compliance issues. Another benefit of side-shift treatment is that it can be started sooner than bracing because it doesn't interfere with a child's activities, and it is not as traumatic a decision to make as choosing to start brace treatment [18].

Recently, den Boer et al. published another study on side-shift or lateral shift therapy [44]. It is very similar to Mehta's treatment program and included more details on how the treatment program is carried out at their clinic. In particular, they focus on a few more of the physiotherapeutic deficiencies that have been reported with IS patients. First, exercises are taught to the patient to strengthen and stretch their muscles. Then standing and sitting stretching exercises are taught to counteract lordoscoliosis that is often present in IS patients. These are followed by balance exercises. When the patient shifts their spine into the correct position, they hold it for 10 seconds and then learn to relax into that position. They are encouraged to do this as often as they can and to incorporate it into their daily activities such as when watching television. Mirrors and parents are used for feedback when teaching the patient the correct shift position.

Their results were as successful as their brace treatment. In particular they would like to be able to research how much time the patient should spend performing the shifting. This could be obtained with a monitoring device.

Posture correction is another related type of treatment that does not specifically associate itself with side-shift therapy, although they are very similar. It focuses on the posture of the patient by using active correction, via specific exercises, to focus on the specific postural defect of the patient. Ferraro et al. encourages incorporating the exercises into everyday life. A mirror and proprioceptive stimuli are used when teaching the exercises [4]. They found that increased participation, 30 minutes per day, slowed curve progression, or halted it, as compared to those who participated less than 10 minutes per day. In another study, Weiss used active exercises such as elongating the spine, derotating it, and using lateral deflection to correct the deformity [32]. Feedback was given with a mirror so that the patient could associate the feeling he was experiencing with the correct posture. Even in a resting state, a pillow was used to maintain the position to continue the proprioceptive training. The patient's goal being the association of how a correct posture feels. Over time this allows it to become second nature. Their results were successful and they recommended it to be tried before bracing. Fifty-three percent did not change, 44 percent improved, and 3 percent progressed. Interestingly, one of the 3 percent that progressed actually appeared to look better cosmetically.

The evidence of muscle asymmetry is thought to be another contributing factor to idiopathic scoliosis. This has lead to focusing on the correction of the muscle imbalance through strength training exercises [12]. Strength training to correct the torso rotation strength asymmetries, was carried out. In the small study only one of the patients progressed out of the twelve. However, their curve was 60 degrees to begin with. This is generally accepted as beyond non-operative treatment methods. Four of the patients had reductions in their curves.

One study was found that did not see any significant difference between the scoliotic patients and the control group when using a general exercise program [13]. However, this seems reasonable as there was no particular rationale for the exercises that were given. The exercises appeared to be general exercises that were not trying to target the curvature or a specific IS defect. It was also noted that in the study strength measurements were not made to document any changes, or verify the exercises were doing something such as correcting a muscle imbalance [12]. Furthermore, the study admitted that most patients did not comply with the program.

From looking at several of the physiotherapeutic methods of treatment, one common thread is the requirement for compliance. Unfortunately, as with brace treatment, poor compliance occurred in some of the trials [13]. The use of a monitoring system would aid in promoting and verifying compliance. Another common thread is the need for feedback to aid in performing the exercises correctly and to help the patient improve their proprioception. A posture monitoring system could provide continual, accurate, quantitative feedback. More studies are required. In addition, much of the confusion that has occurred in brace studies could be avoided. By quantifying compliance and by reducing the treatment study unknowns with the use of a monitoring system, better treatment studies could be obtained.

2.4 Existing Tracking Systems

Some work has been done on portable posture monitoring systems, however as will be explained, they tend to be too simplistic, or essentially too complex. The majority of the technology has been developed for environments that do not have portability, size, or power restraints. Nor are these applications specifically for posture monitoring. They can be grouped in the general category of motion tracking systems.

When discussing motion tracking systems, a few of the terms should be explained. The term 'degrees of freedom' is used to describe the minimum number of position and orientation measurements of an object. In cartesian coordinates the position of an

object could can be specified with the X, Y, and Z locations. The orientation of the object could be stated in degrees and described as pitch, roll, and yaw. Using cartesian coordinates, pitch is rotation around the Y axis. Roll is rotation around the X axis, and yaw is rotation around the Z axis. For example, a 4 degrees of freedom (4DOF) system might mean it can measure the 3 locations, X, Y, Z, and one of the orientations of the object. So although a 3 degrees of freedom (3DOF) system usually refers to the three position measures, it could be any combination of position and orientation.

2.4.1 Posture Monitoring Systems

There are a few systems that exist for monitoring a patients posture that are not specifically for scoliosis treatment. The posture monitor proposed by George is capable of monitoring the vertical axis of the trunk [31]. It was used to help people with neuromuscular difficulties. By alerting patients to poor posture they could make corrections thereby enhancing motor activities, head control, learning, respiration, and circulation. Six 2" x 2" sensors containing miniature mercury switches are logged and monitored by a 6" x 4" x 2" portable computer. When the sensors tilt out of alignment by increments of 5 degrees in either the left or right direction from the vertical axis, an auditory prompt notifies the patient.

Using mechanical technology an exoskeleton has been built by Biodynamics Laboratory at Ohio State University to study ergonomics and industrial biomechanics [46]. It is called the Lumbar Motion Monitor and it is used during the performance of industrial tasks. Back motion in 3D space can be monitored using this device and the back injury risk of a task can be assessed. The system uses potentiometers to measure twisting motions of the exoskeleton spine. The signals are converted to digital signals and passed to a portable 386 computer. It provides angular: position, velocity, and acceleration as a function of time.

There are some systems that have been built to monitor posture that are not portable. The posture monitor systems developed by Nishida et al. is designed to monitor

patients only when they are in bed; it uses 221 pressure sensors built into a bed [47]. Another system developed by Tanka et al. [48] used electromagnetic inclinometers for long-term ambulatory monitoring of posture change. The resolution of the system was 12 degrees and it obtained two-dimensional information.

2.4.2 Portable Scoliotic Posture Systems

To date there appear to have been only two systems developed for portable scoliotic posture monitoring, that is, with the goal of the systems to be able to monitor and record information specific to scoliosis treatment or posture monitoring. One of these systems has had three studies performed with it.

Dworkin believes a posture training device is less physically restraining, more cosmetically acceptable to adolescents, and overcomes many of the drawbacks of a brace. His study of twelve girls using a posture monitoring device resulted in an average of 1 degree (SD=7.5 degrees) Cobb angle improvement [6].

The device measured torso length continuously in real time and provided audio feedback after 20 seconds of incorrect posture. The posture monitor consisted of a vertical fishing line loop harness that ran over the patients torso from C7, around the pubis, and back. As the patient stood up straight this loop would lengthen with the spinal extension. A horizontal loop harness ran around the chest to remove the effects that breathing has on lengthening the vertical loop. The resolution is reported to be 0.5 mm. The device kept a tally of the total amount of time of erroneous posture.

All the patients preferred the device to bracing. Initial complaints of fatigue ended quickly as the patients learned to use the device. There was however, occasional soreness due to pressure from the harness.

Treatment with the device is distinguished from an exercise program because it provides continual feedback. It is thought to work with the same principles as the brace but it also adds the benefit that the patient develops learned muscle control

through their own nervous system, rather than through external stimulation. Another benefit was that it prompted the patients to make choices in their environment, and ergonomics, that aided them to obtain the correct posture. Thus they were continually working on their posture and retraining their proprioception.

Another study with the device showed successful results using the same device as Dworkin [5]. They concluded that non-compliance resulted in a deterioration of the curve, full compliance being 23 hours per day treatment. The scoliotic patients who were compliant showed significant improvements in spinal curvatures. Follow up data after seven months did show that permanent correction can occur and that patients were unconsciously maintaining correct posture.

Most recently, in 2001, Wong et al. used the Dworkin device, now called "Micro Straight" [7]. The device measures 5 x 12 x 2.5 cm. His results were successful at approximately 69%. This is comparable to the success rate of brace studies, however the group size was a lot smaller. Similar to Dworkin, the patients experienced discomfort with the tension loops but preferred the device over the brace. One problem that he mentions is that the device can not detect whether the trunk is shifted over to one side. There is a need to monitor the upper trunk in relation to the pelvis.

Lou developed a system for 6DOF tracking of sensors located on a patient [54]. The POCO system is a portable data acquisition and electromagnetic measurement system used to measure the topographical features of a scoliotic trunk. It weighs 50 grams. One transmitter and up to two receivers, each consisting of three orthogonal coil sensors, are used to obtain the measurements of distance and angle relative to the transmitter. The maximum distance error in the range of 30 to 47 cm is 0.5 cm with a maximum angle error of 5 degrees [22]. Power consumption is 1.2 mA in stop mode and 120 mA during sampling mode.

The electromagentic (EM) portion of the system uses the strength of the received signal to compute the position of the receiver relative to the transmitter. The

transmitter emits a low frequency 12 kHz magnetic sinusoidal signal. Measurements are performed by transmitting on one of the three mutually orthogonal loops in the transmitter and then obtaining the receivers signal strength on all three of the receiver's orthogonal loops. This sequence is repeated for the remaining two loops on the transmitter. Interference due to metallic objects was detectable when the object was within 10 cm of the sensors.

It was experimentally determined that it takes approximately 18 ms to obtain the nine samples from one receiver. This is considering only the time it takes for the receiver to obtain full scale after the transmitted signal was turned on. The settling time of the RMS-to-DC converter requires approximately 50 ms of time for every single loop measurement. A total of one second per receiver is required, which is what has limited the system to two receivers.

The MC68HC16Z1 microcontroller was used for the data acquisition system. It provides a 10-bit A/D converter, a UART, and low power consumption. The system is capable of storing 14563 samples.

Prior to using the system it must be calibrated. The procedure is aided by computer software, however it is quite tedious. The transmitter and receiver measurements are made using the range of distances that the system will be applied to, starting from the lower limit and increasing to the upper distance limit. At each particular distance, increasing by 2 cm intervals, nine measurements are made for each 10 degree rotation in the x-y plane to a total of 360 degrees. Each receiver must have its gain physically adjusted for the range of distances from the transmitter.

2.4.3 Motion Tracking Systems

There are several systems that have been developed for motion tracking that are not specific to scoliosis. An overview of the technologies that are being utilized by all tracking devices is covered here. Some examples of existing equipment that utilizes one of these technologies will be given.

There are several other uses for motion tracking systems. The animation industry is utilizing these devices for animating characters in movies and games. This allows animators to quickly produce realistic animations by using human or animal actors, and mapping their motion to computer models. Similarly, virtual reality applications use motion tracking devices to provide realistic interactive environments. Some of these applications include training vehicle operators such as pilots. Also, athletes can benefit from the use of motion tracking to produce a better golf swing, for example.

The medical field has multiple uses for motion tracking equipment. Medical simulation is an important application. Operations can be simulated while monitoring the medical student's use of surgical tools. Expanding on this concept, tracking is being used in real surgeries to track steerable instruments for minimally invasive surgeries. This avoids the cost and dangers of radiographs, and decreases healing times. Biomechanics research is also benefiting from the use of motion tracking systems. Tools can be tracked to investigate forces involved in orthopeadic reconstructive surgery. Also, injury prevention can be studied by investigating workplace environments and human biomechanics. An example is to provide lifting training.

The majority of commercial motion tracking systems are not portable as defined for this work; that being a device that could be worn by a person during their daily activities. The methods used by these devices follow.

Electromagnetic systems use low frequency AC or pulsed DC fields. Typically three coil receivers and transmitters are used to derive 6DOF measurements from nine signal measurements. However, other coil configurations exist to obtain different DOF. For example, Northern Digital Inc. uses a transmitter with more than three coils configured in a pyramid configuration to obtain 5DOF measurements with one receiver coil.

The main disadvantage of these systems are ferromagnetic interference and electromagnetic noise. Polhemus and Ascension are two companies that sell AC and

DC trackers, respectively. Each technology claims an advantage over the other technology. Polhemus originated the DC concept but opted to pursue AC tracking. The fundamental argument between these two technologies is that by using a DC pulse, noise due to ferromagnetic material is reduced because induced eddy currents die out. However, this comes at a cost of speed of acquisition. In addition AC, trackers report higher accuracy measurements. The Polhemus Liberty provides up to 240 Hz sample rate with an accuracy of 0.3 inches RMS, and 0.15 degrees RMS for angles. The Ascension MotionStar uses pulsed DC EM fields and provides up to 120 Hz sample rate with an accuracy of 0.3 inches RMS and 0.5 degrees RMS for angles. The fields for AC trackers can be lower than for DC trackers. This allows for smaller signal source electronics and lower power consumption. This is because DC trackers need to produce an EM field that overcomes the earth's field while AC trackers can operate well under the earth's 60 μT magnetic field. This also contributes to AC trackers operating at larger distance ranges.

Optical tracking systems utilize infrared (IR) cameras and are capable of obtaining 6DOF measurements. Active or passive markers emit or reflect back, respectively, IR to the cameras. The position is calculated by image comparison if using two cameras, or by the intersection of three planes if using three linear cameras. The advantages of these systems are that they are accurate and fast. The disadvantages are they are sensitive to ambient or optical noise, and that they are line of sight systems. The Optotrack Certus by Northern Digital Inc. has an accuracy of 0.1 mm and a maximum 4.6 kHz sample rate.

Acoustic tracking systems use approximately 40 kHz ultrasonic waves. The distance is calculated using time of flight or phase coherence. Time of flight calculates the distance to the nearest reflector by using the speed of sound in the air and emitted pulse and echo arrival times. Or it can measure the time for the sound emitted from the transmitter to arrive at the transmitter. Phase coherence measures the phase difference between the sounds waves emitted by a transmitter at the target and those

emitted by a transmitter at a reference point to determine distance. A 3D position calculation requires either one transmitter and three receivers, or three transmitters and one receiver. 6DOF requires three transmitters and three receivers. Advantages to this system are the working distance range and small system size. The disadvantages are that it is slow sensitive to temperature, pressure, and humidity.

Mechanical tracking systems come in numerous forms. Mechanical sensors are used to measure angles or distances. Typical sensors either measure the amount that they are bent or measure the variance of resistance. The Gypsy from MetaMotion is a motion capture system that utilizes an exoskeleton with sensors to measure angles between the joints. It is strapped to an actor to record their motion. This provides a low cost, accurate, fast system. It lends itself well to application that have some type of feedback such as medical simulators. The disadvantages are that it is very specific to its application and potentially bulky.

Inertial tracking utilizes gyroscope and accelerometer technology. Gyroscopes measure changes in orientation. Accelerometers measure acceleration. Distance is obtained through integration. The latest accelerometers can also measure angles by measuring static displacement. The disadvantages of these systems are the calculations that are required to obtain data and drift errors. Specifically errors accumulate when performing the double integration to obtain distance. Likewise errors with the gyroscope accumulate over time and periodic recalibration is necessary.

2.4.4 Existing Hybrid Systems

Due to limitations in each of the individual tracking methods, it would be advantageous to create a tracking system that utilizes more than one technology. These hybrid systems would gain from using the strength of two technologies.

An EM and accelerometer system was developed to investigate its use as a complement to EMG study to compensate for gravity's effect on measurements of movement and to know the actual position of the body [52]. Its future goal would be

to provide long-term ambulatory monitoring to diagnose movement disorders. Measurements were taken to obtain 3D orientation of objects in azimuth and inclination coordinates. The sensors used three accelerometers and three electronic miniature compass sensors that were digitized and sent to a personal computer. Large metal objects were required to be kept at least one meter away to correctly sense the earth's magnetic field. It was able to obtain 0.75° average and 3.3° maximum for inclination measurements and 4.2° average and 14.3° maximum for azimuth lab tests.

Existing motion tracking systems are combined to make or complete a hybrid tracking system. MetaMotion's Gypsy which utilizes a potentiometer exoskeleton added a gyroscope to track rotation. Northern Digital Inc. used the same optical tracking technology in its Polaris Optical system however it added both active and passive IR markers to account for the limitations of using only one type. Other researchers combine single technology tracking systems. For example, an EM trackers was combined with an optical tracker to overcome the weaknesses of both systems in an attempt to produce a hybrid tracking system with the robustness of an EM tracking system and accuracy of an optical tracking system [55].

3 MEASUREMENTS OF A SCOLIOTIC PATIENT

To monitor a scoliotic patient's posture we must determine the types of postures and torso movements to be detected, and how the monitoring system will detect these positions. This chapter discusses some of the types of measurements that are used to assess a scoliotic patient. In particular, the seven topographical features that have been identified to characterize trunk deformity will be investigated to determine which of these measurements can be made with a hybrid posture monitoring system [28]. The theory to calculate the position of the torso will be determined for the wearable posture monitoring system. This will illustrate what measurements the system can perform and allow us to summarize some of the best uses for the system. This may lead to a particular deformity that best lends itself to measurement and treatment.

3.1 Types of Postural Measurements

3.1.1 Anatomical Torso Movements

The spine and shoulders are the sources of motion for the torso. To detect all the torso positions or postures, we must be able to measure these motions. These key motions have been categorized and depicted in figure 3-1 and 3-2 illustrating the possible movements of the shoulders, hips, and spine that produce different postures.

---

[1] Material in this chapter has been published in: M. Bazzarelli, N. Durdle, E. Lou, J. Raso, "A wearable networked embedded system for the treatment of scoliosis," in *Research into Spinal Deformities 4*, Vol. 91, *Series Studies in Health Technology and Informatics*, T.B. Grivas, Ed., Oxford: IOS Press, 2002, pp. 383-386.

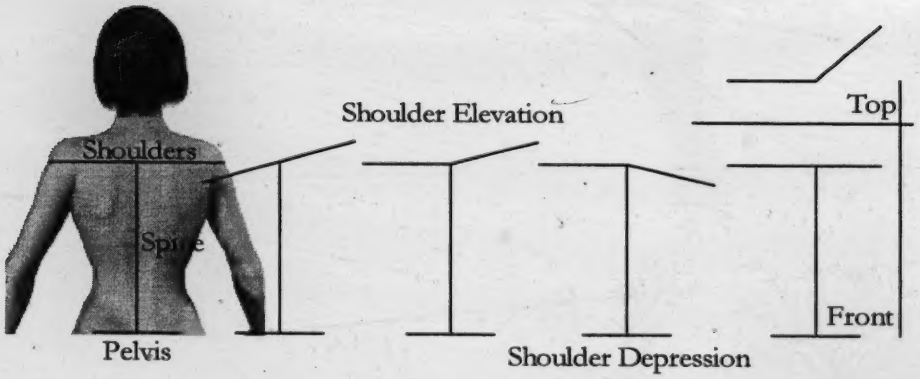

Figure 3-1. Postures due to shoulder girdle movement.

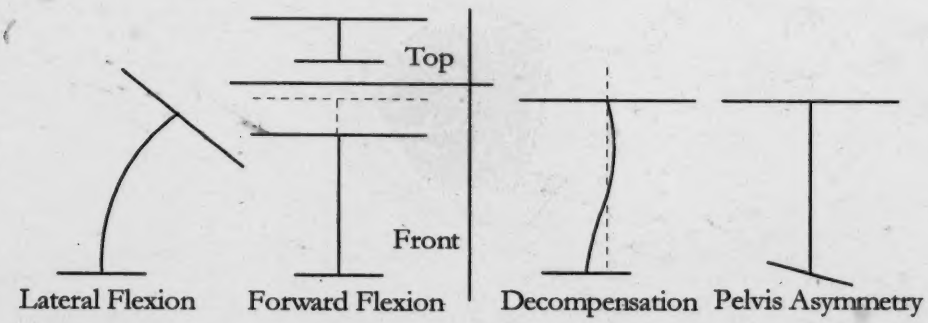

Figure 3-2. Postures due to spine movement.

Figure 3-1 depicts shoulder girdle movements, that is movements involving the scapula and clavicle. Shoulder shrugging motions are called shoulder girdle elevation and depression. Elevation is a movement where the scapula moves in a superior or upward direction. Shoulder girdle depression, opposite to elevation, is when the scapula moves in an inferior direction. The normal range of motion is 40 degrees for elevation and 10 degrees for depression [58]. Scapular abduction or protraction is a lateral movement of the scapular away from the spine. Scapular adduction or retraction is pushing the shoulders back and pulling the scapula together. The normal range of motion is 20 degrees for scapular abduction and 15 degrees for scapular adduction

[58]. Scapular rotation is the rotation of the scapula initially around an axis passing through the sternoclavicular joint. Scapular upward rotation is a rotary movement of the scapula moving the inferior angle of scapula laterally and upward. Downward rotation moves the inferior angle of the scapula medially and downward.

Figure 3-2 depicts movements of the spine. Flexion is forward bending of the spine, extension is backward bending, lateral flexion is left or right side bending. The spine can rotate left or right around the longitudinal axis. Postural decompensation can occur in all three planes and is when the distribution of body mass is away from the ideal. An example is when the spine moves into an 'S' shaped position. Finally, pelvis movement is shown, however this would be combined with lateral flexion and thus the mechanism is really a spine movement.

3.1.2 Seven Topographical Features

Along with these anatomical movements, there are other measurements that have been defined as objective measures of scoliotic deformity. The system can be used to obtain some of these clinical measurements to aid in the evaluation and development of treatment outcomes.

Scoliosis assessment has changed through out the ages. Originally it had been evaluated based on postural distortion [50]. After the introduction of radiography it concentrated on the assessment of the misalignment of the spine resulting in the Cobb angle measurement. Today the Cobb angle is the standard in the assessment of scoliosis [50]. However, modern treatments rely on techniques not limited to frontal-plane correction. Objective measures are required to evaluate these treatment outcomes, however there are few objective measures aside from the Cobb angle. To avoid subjective judgments as to the effectiveness of treatment, outcome measures have been established to assess the effect of treatment on trunk distortion in children with idiopathic scoliosis. In addition to evaluation and development of treatment methods, these measures can be used to obtain more insight into what relative

contribution these features make to the overall deformity and to the study of idiopathic scoliosis.

In total, seven topographic features that contribute to the impression of trunk deformity in adolescent idiopathic scoliosis have been presented as objective measures [28]. These measurements are: shoulder height, shoulder angle difference, decompensation, scapula asymmetry, waist crease, waist asymmetry, and pelvis asymmetry. Figure 3-3 shows an example of these measurements.

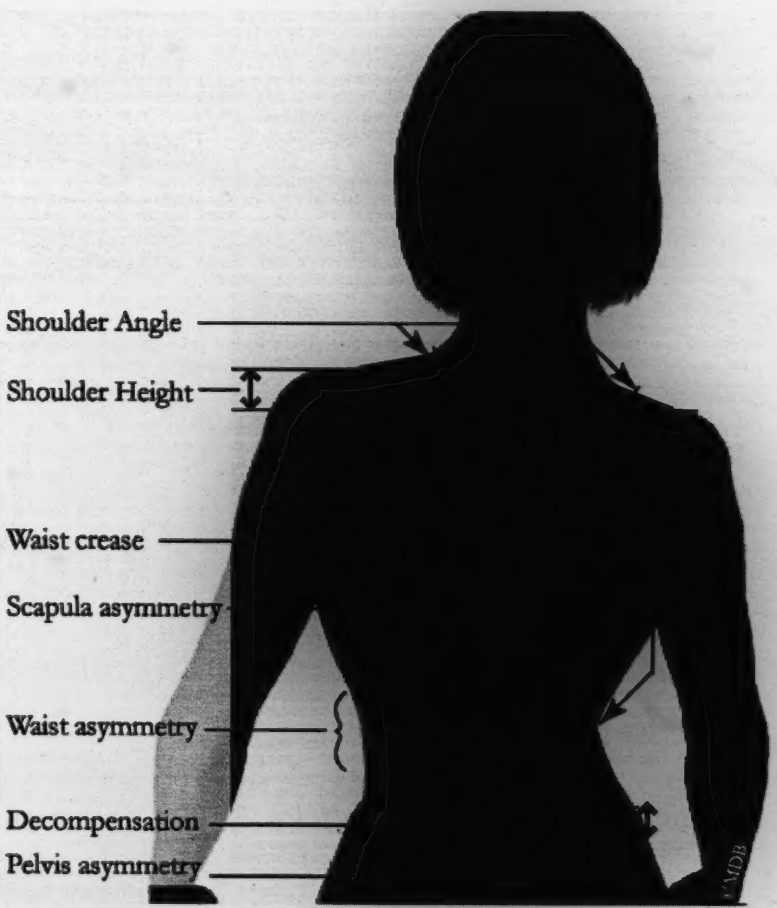

Figure 3-3. Cosmetic feature measurements.

Shoulder height is the difference in height of the shoulders. Horizontal lines are drawn on each shoulder and the distance between the two is recorded.

Shoulder angle difference is the difference in the angles of the left and right shoulders. Each shoulder angle is taken from a horizontal line up to a line along the slope of the shoulder.

Decompensation is a measure of the distribution of the body mass away from the ideal. It can occur in all planes but is classified by the major planes affected. In the sagittal plane, postural decompensation are kyphotic or lordotic changes. In the horizontal plane, postural decompensation are rotational changes. Scoliotic changes are in the frontal plane, this is, the plane that is used to measure decompensation. The horizontal distance from a vertical line through the center of the pelvis to a vertical line through the center of the head is the decompensation measurement.

Scapula asymmetry is the angle formed between a line through the high points of the scapula, usually the inferior angle points, and the horizontal.

Waist crease is a visible fold of the skin on either side of the body and is either present or not.

Waist asymmetry is an index to measure how much the waist has shifted. The waist can appear shifted visibly to one side or the other in severe cases and is primarily due to a scoliotic curve in the lower part of the spine. The waist asymmetry scores range from 0 to 2, with 1 being perfect symmetry. A score less than 1 represents the waist being shifted to the right, and a score greater than 1 represents the waist being shifted to the left.

The formula for waist asymmetry is given as [28]:

$$Waist\ asymmetry = \frac{R_l U_l U_r}{R_r L_l L_r} \qquad 3.1$$

Figure 3-3 shows the variables' locations on the torso. They are obtained by drawing four lines. A vertical line is drawn through the center of the pelvis. A horizontal line is drawn through the waist, that is the minimum distance across the torso's waist region. The distance from the vertical line to the edge of the body provide R_l (reference left) and R_r (reference right). Horizontal lines are drawn above and below this line at a vertical distance equal to 10 percent of the trunk length, which is the vertical distance from the pelvis to the shoulder. The upper line provides the measurements U_l (upper left) and U_r (upper right). The lower line provides the measurements L_l (lower left) and L_r (lower right).

Pelvis asymmetry is the difference in height of the pelvis. Horizontal lines are drawn at the left and right points of the pelvis and the vertical distance between these lines is measured as the pelvis asymmetry.

3.2 System Overview and Measurement of Posture

The system is composed of three pieces of hardware: the CPU or master control unit, the transmitter, and the receiver. All are embedded systems having software and a microcontroller networked to communicate with each other. The CPU is the master device that oversees the collection of data, processing of data, and the user interface. The transmitter is capable of generating an electromagnetic field in three orthogonal axes. The receiver is capable of measuring these electromagnetic field strengths. This information, along with known geometries, can be used to determine a single coil receiver's distance or angle in one degree of freedom. Of particular interest, a yaw movement can be detected with out requiring continuous monitoring of a sensor. The receiver also measures pitch and roll providing two 2D angle measurements with respect to gravity. Thus using telemetry, angle measurements and information for

deriving distance or orientation changes are obtained from all the receivers by the master control unit.

The system will be worn by the patient in a configuration that best facilitates the optimal monitoring of their defective posture. The master control unit can be clipped to the patient's belt. A typical monitoring situation will locate the transmitter at the base of the patient's spine and a variable number of receivers can be placed at different points on the patient's back. The receivers and transmitters can either be taped to the patient's torso or they can be mounted inside pockets on a tight fitting spandex t-shirt. Using a shirt with piping sewn in for the wiring and pockets for the receivers would provide the most user friendly method to mount the system, however, it would introduce another motion artifact due to the movement between the skin and the spandex.

3.2.1 System Use in Identifying Posture

There are two different ways that the system is used. In the first method, called real time portable posture monitoring, data are collected and instant sensory feedback is provided. This method may not necessarily process all the information contained in the collected data when identifying an incorrect posture. The second method, in the clinical setting, will use the data, which are downloaded to a PC, to calculate clinical measurements and treatment progress. Furthermore, data can be analysed in a clinical setting with information that could not be known in a portable posture monitoring setting to yield clinical measurements that might not be obtained without supervision.

When using the system in a portable setting it uses minimal calculations to quickly determine if the trunk is misaligned and to provide the appropriate sensory feedback while the patient is wearing the system. The novelty of this is that the large amount of calculations used by EM 6DOF systems can be avoided due to the use of the two sensor technologies. This coupled with the parallel processing and known sensor placement geometries eliminates the need to first calculate the topography and then

interpret the coordinates. This reduction in calculation reduces the processing time and processing power requirements, and thereby the overall physical size and power requirements. The primary focus of this method of operation is to simply determine that the posture is not in the favoured position. This can be likened to one telling you to stand up straight. Even though one does not know the quantitative measurement, that is exactly how much lower the right shoulder was than the left shoulder, one can tell it is not correctly positioned. Note that the data are saved and can be further analysed at the clinic to obtain such an objective measurement and to record the progress of the patient. Because the user feedback is of low resolution, the patient only needs to know something was incorrectly positioned, and they can deduce what it is from there. The system may be set to monitor one particular posture feature in particular, or the patient will be on a physiotherapeutic program so they will be aware of what to look for. However, depending on the complexity of the system, such as the complexity of a fuzzy logic system, the feedback resolution can be of a higher resolution providing more details to the user. In summary, the posture is determined using a qualitative method, similar to fuzzy system theory.

The second method is performed in a clinical setting. The data that are collected can be downloaded and analysed thoroughly on a PC. Clinical measurements can be made that can not be obtained from the portable data. This is because it is possible to bypass motion artifact present in measurements such as scapula asymmetry that would prevent reliable readings. For example, to avoid motion artifacts the clinician can verify that the receivers are directly over the scapular inferior angle points when making a scapula asymmetry measurement. While both uses of the system record objective data that can be used in evaluating patient posture and treatment outcomes, the clinical method is primarily focused on determining clinical measurements.

3.3 Determining Measurements and Postures Using the System

This section describes the posture measurements that can be made and how they are calculated or determined using the posture monitoring system.

3.3.1 Background

There is a certain amount of motion artifact due to the movement of the soft tissue [59]. Thus we cannot directly measure the motions of the bones nor precisely track their movement through the skin. Using a test subject a marker was placed on the skin over the inferior angle of their scapula. They were instructed to move their scapula laterally. The test subject moved their scapula 1.6 cm laterally before the skin started to move. When the scapula was moved vertically toward the head the skin moved more proportionately.

The main problem this posses is a discontinuity when comparing the clinical measurement versus what the system might measure with skin and clothing motion artifact. The actual clinical measurements tend to be made using radiographs or physically by a clinician who can verify where the bone is in relation to the measurement being made externally. However, obtained measurements can still be compared against themselves when looking for quantitative comparisons of progress. When the system is used in a clinical mode the clinician can verify the location of the sensors to obtain a motion article sensitive measurement.

When considering using the system in a qualitative posture analysis mode, only simple measurements are required to detect a misaligned posture. It will be most important to consider the type of patient and the primary postural defect. This will lead to the optimal method to mount the system. There is a difference in tracking and measuring certain torso movements versus simply determining if the movement is what we consider good or bad. The tilt and EM signals obtained from each of the sensor technologies could be used alone, on their own, to determine an incorrect posture. For example, in the first measurement we will consider the shoulder height measurement.

However, an accelerometer tilt signal alone or a distance measurement alone compared against a threshold level is enough to inform you that the user requires a posture correction before one even calculates the shoulder height. Tilt measurements from the accelerometers will provide: shoulder height, decompensation, asymmetries, and flexions. EM measurements from the receiver can be used to determine if a yaw motion has occurred or to monitor if a distance has changed in one dimension. Due to the ambiguities in an electromagnetic field, any constraints that are required will be given. Combinations of both measurements can be utilized in a fuzzy system to derive varying degrees of feedback resolution regarding the patient's posture beyond a binary good or bad posture feedback.

3.3.2 Calculating Postural Positions

To determine which clinical measurements can be made with the system, each motion attributed to the clinical measurement will be examined. For each motion the system's method of measurement will be presented. This will show an optimum method for mounting the system depending on the measurement that is being made and if there is any external data or assumptions required.

3.3.2.1 Shoulder Height

The postural movement required to correct or produce a shoulder height difference, and thus shoulder height measurement, are side flexion of the spine, shoulder elevation or depression, or a combination of these movements. In the case of scoliosis, the lateral flexion component of the motion is the most important.

When considering the side flexion of the spine, only one measurement is required; that is, a tilt angle measurement as depicted in figure 3-4. This can be obtained by mounting the receiver on top of the patient's shoulder. The distance from the sternoclavicular joint to the acromioclavicular joint can be measured in the clinic to obtain the distance d_R. The tilt angle measurement, θ_R is obtained from the receiver and the calculation of the shoulder height difference can be computed as:

$$h_R = d_R \sin\theta_R$$
$$h_L = d_L \sin\theta_L \qquad 3.2$$
$$shoulder\ height = |h_R - h_L|$$

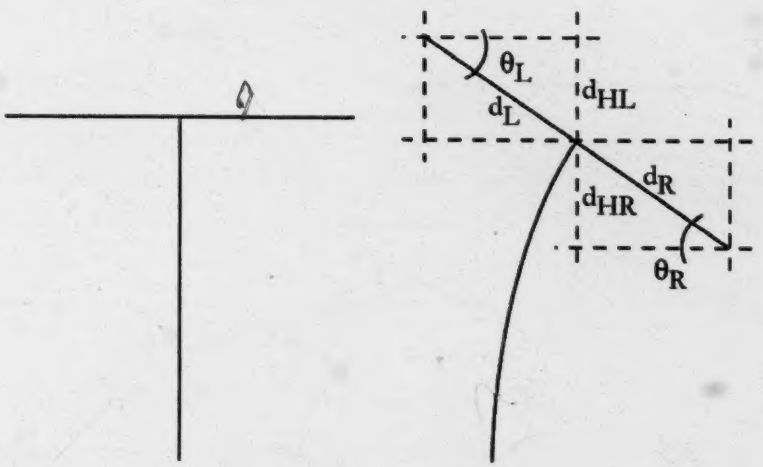

Figure 3-4. Shoulder height measurement due to flexion.

When considering shoulder elevation or its combination with lateral flexion, the height can be determined in a similar way. In this case a new model was created to depict shoulder movement more accurately, as seen in figure 3-5. This model takes into account the axis of rotation of the shoulder and allows for shoulder height to be measured using the same technique as presented for a flexion movement. This is accomplished by determining the actual distance from the pivot point to the shoulder. Although the system could measure the distance from a central point between the two sensors, using a transmitter at the base of the neck, this can be avoided by using the known, or measured, geometry of the patient. Being application-specific in this manner simplifies things, for example to obtain repeatable measurements, which is required for evaluating treatment progress. This is done by requiring less precision in remounting the sensors. Using the single angle measurement method only requires that the receiver

measuring the angle be mounted on the shoulder in such a way that there is good coupling with the clavicle. However, if the system has to measure the distance, the transmitter must be positioned in the same location, and the receiver must be in the same location, to avoid creating a different geometry as seen in figure 3-6. There are more possible sources of error in this configuration. Figure 3-6 shows that the distance and angle are not related unless mounted in the exact position. Also, the shoulder height measurement will change if either the receiver or transmitter move in any direction, providing a greater possibility of different measurements with each mounting of the system.

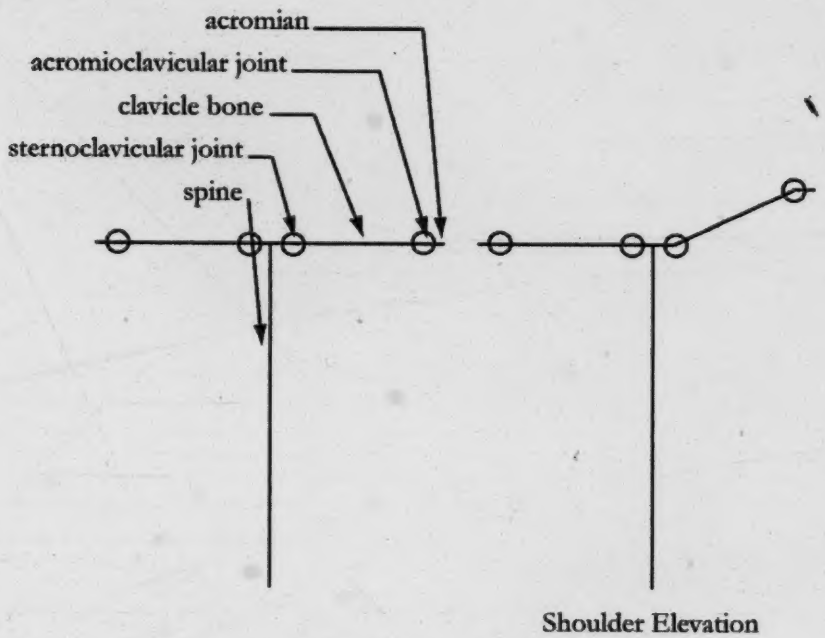

Figure 3-5. Shoulder movement model.

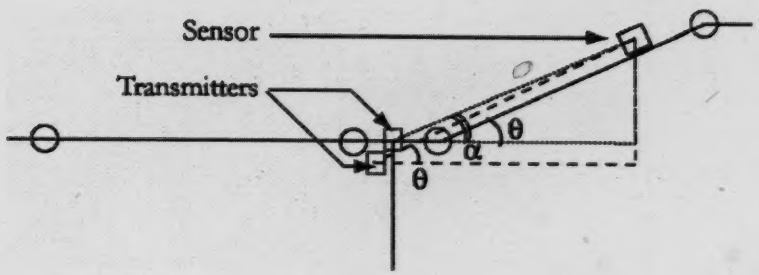

Figure 3-6. Discrepancies with mounting.

In figure 3-5 the pivot point of the shoulder is at the sternoclavicular joint. The acromioclavicular joint is at the opposite end of the clavicle bone where the acromian connects to the clavicle bone. The distance d_R from equation 3.2 now becomes the distance between these two joints. The receiver is mounted between these two joints to obtain the angle measurement. The distance along the shoulder remains constant and the height can be solved for using only one angle measurement.

In summary, to monitor patient progress these errors will need to be taken into account. The method given will help to minimize these errors. However, to use the system to monitor incorrect posture and provide discrete feedback, these errors are of little consequence.

3.3.2.2 Shoulder Angle Difference

The shoulder angle difference can be computed from the shoulder angles as described in the shoulder height section above. Note that this measurement is one of the three features that was determined to be the most significant predicators of cosmetic impression and is simple to obtain.

3.3.2.3 Decompensation

Decompensation can be measured in all planes. In the sagital plane kyphosis results in a rounded or hunched back. The plane of interest to scoliosis is the frontal plane. Here the characteristic 'S' shaped curve can been seen. The system can obtain measurements

in both of these planes at the same time because it can measure tilt angles in two dimensions.

To calculate decompensation in the frontal plane several receivers would be mounted along the patient's spine at measured intervals, d_s, as shown in figure 3-7. A line of best fit will be created that matches the angle at each receiver with a line of length d_s between each receiver. This final curve is a representation of the patients spine that can be processed to find the decompensation measurement. Or, as shown, the horizontal contribution d_h can be added from each sensor to provide the decompensation measurement. The variables for equation 3.3 the calculation are shown in figure 3-7, where θ_s is the tilt angle and d_s is known.

$$d_h = d_s \sin\theta_s \qquad 3.3$$

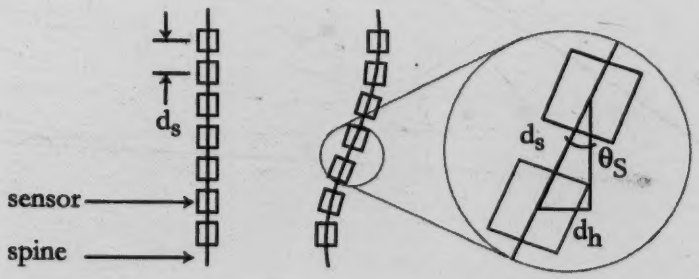

Figure 3-7. Decompensation mounting and measurement.

3.3.2.4 Scapula asymmetry

This measurement does not lend itself well to a skin-mounted posture monitoring system outside of the clinic because of the motion artifact between the skin and the inferior angle of the scapula. A scapular upward rotation movement will cause a marker placed on the skin over the inferior angle of the scapula to move to a new location relative to the inferior angle of the scapula. A test revealed up to a 2.3 cm distance. Furthermore, this measurement is also affected by other positions. Acquiring this measure can be likened to measuring your height. To do this one must stand tall

and take the measurement. Recording your height for the rest of the day while you walk around doesn't really reflect your actual height measurement. Thus, to obtain a measurement that would agree with a measurement taken in the clinic, one would verify that the data are obtained when the transducers are over the correct locations on the scapula. To acquire this measurement a sensor would be placed on one of the scapula's inferior angle point with its a tilt axis pointing towards the other scapula's inferior angle. The angle measured is the scapula asymmetry.

Measurement during daily-unsupervised wear would not be practical, as the scapula will move depending on what activity the patient is involved in. It would be difficult to correlate their activity to a relaxed posture without utilizing transducers on the patient's torso and arms to determine their stance at the time of the measurement.

3.3.2.5 Waist Crease

This observation is either present or not. Using the system there is no direct measurement that needs to be made. The crease is a reflection of extreme concavity caused by the curve.

3.3.2.6 Waist Asymmetry

This measurement was deemed one of the three most significant of cosmetic impression. It involves measuring horizontally from a vertical line from the center of the pelvis, to the edge of the body on the right and left sides. A total of six distance measurements are required. The transducers mounted on the waist should not change orientation when the patient is not twisting their lumbar spine nor flexing forward or backward extensively. The tilt sensors of the transducers will determine if the patient is in flexion. Valid measurements occur once the correct posture is achieved. The asymmetry will be calculated using the distance from a transmitter centered on the pelvis to the single coils. Using this distance, the transducer's measured angle, and the pre-measured distance on either side of the transducer, the new horizontal distances to the pelvic mid line can be calculated and thus the waist asymmetry obtained. There will

be an error introduced in this measurement because by definition the vertical distance is constant between the U,R and L lines in figure 3-3. Thus the actual measurement that would match a clinical value, can only be taken when the sensor is at that distance. Thus measurements taken while the patient is moving could introduce a variable locating U, R, and L; this variable would confirm if the measure was the true clinical waist asymmetry measurement. Similar to scapular asymmetry, this measurement by definition is taken when the patient is in a particular posture.

3.3.2.7 Pelvis asymmetry

This measurement is computed using the angle measurements from a receiver mounted on the pelvis. The height difference of the pelvis is calculated from the tilt of the hips, angle θ_p, and the known width measurement of the hips, d_h. Figure 3-8 shows the placement of the receiver for the calculation:

$$d_{\text{Pelvis asymmetry}} = d_h \cdot \sin\theta_p \qquad 3.4$$

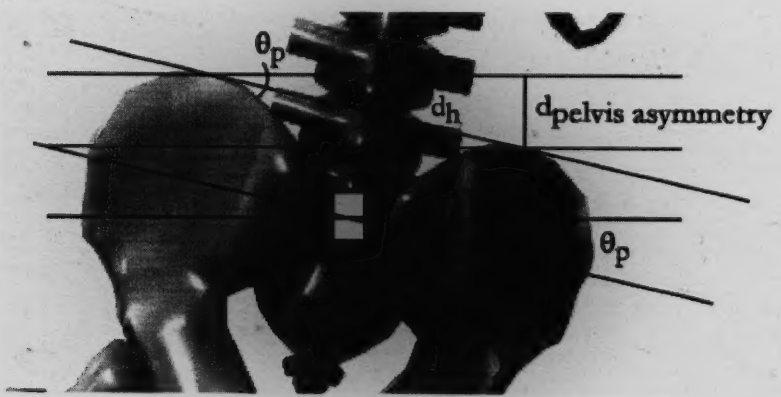

Figure 3-8. Pelvis asymmetry calculation.

3.3.3 Determining Movements and Postures in Real Time Using Simplified Methods

When using the system as a qualitative measure of posture with a low means of feedback resolution, that being a single signal indicating if the posture needs correction or not, many things can be simplified for a less computationally intensive solution than posture topography. If only parts of a posture are being monitored, even more simplification can take place. For example, simplification is possible if shoulder height, Kyphosis, or any one particular flexion or elevation is the only feature being monitored for correctness. The actual angle measurements can be monitored and the real data can be used and compared with a rule base. If all these movements are to be monitored and a reference drawn from them, regarding the patient's posture, then a fuzzy system would serve this purpose. Depending on the complexity of the implemented fuzzy system there is the possibility for a higher resolution of feedback.

Posture movements will be presented explaining how the system could detect them. Also, how the system detects the movement involved with clinical measurements will be presented. This allows for a choice when using the system if one is monitoring or focusing on one particular movement, one particular clinical measurement, or a combination of these.

3.3.3.1 Determining Flexion Movements

All flexion movements can be determined using the tilt angle from the accelerometers in two dimensions. This allows forward, backward and side flexion angle measurements. Using just these angles the amount any part of the body is leaning forward, backward or to a side can be measured and quickly compared against an acceptable value. Only one receiver would be required placed along the spine to monitor any two-dimensional flexion of the spine.

The coil on the receiver can sense flexions provided certain constraints are met and the coil is mounted in a known position. If the coil's distance from the transmitter changes

with the flexion, the resolution of the signal's interpretation as flexion will degrade. To obtain the measurement, set the transmitter directly below the receiver coil, with the normal of the receiver's coil to the y axis mounted on the patients back along the spine. The flux linkage from the z axis of the transmitter to the sensor coil will be nil. However, as the patient leans forward or backward the flux linkage on the coil will increase allowing detection of a forward or backward flexion. In a like manner, mounting the sensing coil with its normal to the x axis, or frontal plane, will cause it to sense side flexions.

3.3.3.2 Determining Yaw Movements

Yaw movements can be determined using the transmitter as a reference point and a single coil sensor. Note that this method of yaw detection on a posture monitoring device is novel due to the fact that it does not involve a gyroscope or any of the common methods that require continual integration and monitoring. Using this method the system can be in a low power mode or turned off, not monitoring anything, then upon waking up sample the sensors and determine that a yaw movement has occurred.

For the case of the torso's yaw, the sensor coil is placed with its normal to the y-axis at the top of the thoracic spine. The transmitter's orthogonal coils are placed at the top of the sacrum. Both coils are lined up in the sagittal plane. As the patient rotates their torso left or right in a yaw movement, the sensor coil will turn into the flux fields caused by the x and y coils on the transmitter. In this example the normal of the coil is receiving half the maximum magnitude of the flux density generated by the y transmitter coil. As the patient twists, the coil turns out of this plane and less of the y transmitter signal will be received, while the flux contribution from the x coil will begin to increase.

Scapular abduction and protraction yaw about the sagittal axis can be detected by monitoring a single receiver coil on the shoulder itself and the tilt angles of the

shoulder. This measurement is more complex because the radius between the transmitter and receiver can change due to the possible elevation movement of the shoulder thus introducing ambiguities to the EM signal interpretation. The angle measurement would be used to determining if elevation was the cause for the change in the receiver coil signal. This allows one to determine if a single shoulder is being abducted or protracted on its own. In this particular case it might be best to have the transmitter mounted between the shoulder blades to reduce the amount the radius could be changed.

Scapular abduction and protraction due to shoulder yaw movements have little involvement with scoliosis as forward displacement of the shoulder in the transverse plane is caused by spinal deformity. Thus sensing a shoulder abduction or protraction would be of little use in a scoliotic case because the abduction or protraction would require a posture correction of the spine, not of the shoulder girdle. Sensing the position of the spine would be more practical and important as it is the source of a protracted or abducted shoulder in scoliosis.

3.3.3.3 Determining Elevation Movements

Shoulder elevations can be determined from the shoulder angle measurements which are obtained as described in the clinical measurements section.

3.3.3.4 Shoulder Height, Shoulder Angle Difference and Pelvis asymmetry

To monitor a patient for shoulder height differences, the angles from the receivers mounted on the shoulders are used. Instead of calculating the actual height measurements of the shoulders, the angles of the left and right shoulders can be compared to determine if shoulder height are appropriate. In a similar manner, the angle from a receiver mounted on the pelvis is used to determine if pelvis asymmetry is present with no need to calculate the height difference. Shoulder angle difference is calculated directly from the angle measurement.

3.3.3.5 Decompensation

To determine if decompensation is present in any plane, several receivers can be placed along the spine as described when doing the clinical measurement. However, instead of calculating the decompensation clinical measurement, the system would only monitor the angles on the receivers. If one of the receivers exceeds a specified angular threshold then the system can alert the patient to a decompensation movement in one of the planes.

The type of decompensation measurement needs to be specified with respect to a movement. For example, if it is a scoliotic 'S' curve that we wish to detect, the angles of the sensors in the x-z plane would be monitored. A rare case to make note of is it is possible for the patient to lean to the left or right side and keep his back straight. In this case the angles would need to be monitored so they all were within a specified range of a common value to detect this rare instance.

3.3.3.6 Scapula Asymmetry

This measurement does not lend itself well to continual monitoring, nor is it really practical to measure outside of the clinic. As previously explained, it is not really a measurement that you would monitor during the day because so many movements, such as reaching, change your scapula's locations. The distances between the sensors on the scapula change. The orientation of the sensors would change with the expected skin artifact.

Thus to monitor scapula asymmetry in a portable setting, the goal would be to distinguish between the accepted and unacceptable scapula asymmetry. This would mean that when in a relaxed position and the sensors are mounted correctly this posture would be considered a correct scapular asymmetry. The transducer's deviation from this would be recognized as an unacceptable asymmetry. However, to overcome false positives due to daily movements the incorrect measurement would be required to remain constant for a set period of time. This would help in reducing false positives

due to a repetitive motion that would appear incorrect but would have different incorrect positions. Thus the system is waiting for the patient to remain in a stationary position to evaluate their scapula asymmetry.

3.3.3.7 Waist Asymmetry

Waist asymmetry is primarily caused by a left convex curve in the lumbar. The sensors monitor the lumbar curve to detect a change in waist asymmetry. The similar method to monitor decompensation can be used.

Three sensors are mounted along a vertical line from the center of the pelvis at the intersection of the horizontal lines that form the six distance measurements used in the clinical measurement. The sensors are mounted vertically when the patient has the desired corrected posture, or acceptable waist asymmetry measurement. Now if the patient relaxes and allows the curve to worsen the vertical line through the sensors will also curve to the left. Thus, the top sensor will tilt in the x-z plane clockwise while the bottom sensor will tilt in the opposite direction attempting to stay parallel with the original vertical line which is now bent. This change in tilt angles can be detected and the patient notified to make a correction.

3.4 Evaluating Posture

Using the given methods the data obtained can be used to evaluate a patient's posture. In the case of clinical measurements the data will be downloaded from the system and processed off line to obtain the clinical measurements. In the case of real time posture monitoring, the acquired data must be processed in a way to recognize an incorrect posture and provide meaningful feedback to the user. The first step is to pick which posture, movement, or measurement one wants to obtain. Then the system can be mounted as specified in the measurements section.

3.4.1 Complete Posture Monitoring

To monitor the posture of a patient and provide subjective feedback with regards to their entire posture, fuzzy logic can be utilized. Subjective knowledge of the posture provides an easier means of distinguishing between false incorrect posture notifications and intuitive means to evaluate postures. Fuzzy logic will also speed up decisions by reducing calculations. For example, consider the case when a person has his right shoulder elevated for one sample, then at the next sample time he leans to the left so that his spine is in left flexion and his shoulders are not elevated any more. Using fuzzy logic these two events can be observed as sample 1: 'body upright, right shoulder is elevated a lot', sample 2: 'body leaning to left, shoulders not elevated'. It is simpler to evaluate posture using these linguistic concepts and to create a rule base describing posture. If dealing with numerical objective knowledge a mathematical logic model would need to be developed to determine that a position is bad and to compare the previous bad posture against the new bad posture.

Consider the mounting of the system with a receiver on each shoulder and the transmitter on the base of the spine. A single coil from a receiver is mounted with its normal parallel to the y axis between the shoulders in the sagital plane. The received three coil signals and the tilt measurements are used as the inputs to the fuzzy system. Membership functions are created for each of these four signals. Output functions can be created which describe different postures. Rules can then be created. Using logic statements with the inputs, the output feedback can be provided.

Chapter 4[1]

4 SYSTEM THEORY

Several technologies are used to implement the wearable computer for posture monitoring. Their theory is presented here. Recent advances in Microelectromechanical Systems (MEMS) technology have produced low cost accelerometers capable of accurate tilt and motion sensing. This allows angular measures in two dimensions. Electromagnetics can be utilized to create a six-degrees of freedom motion tracking system. In this work it will be used to measure angles, make intelligent decisions based on complex interactions, and to obtain distance measurements.

4.1 Accelerometer Theory

4.1.1 Technology of Accelerometers

Different types of angle sensing devices were evaluated to determine the best sensor technology for obtaining angle measurements with this system. Different types of sensors were evaluated leading to the selection of MEMS accelerometers.

Electrolytic tilt sensors are inexpensive and capable of very accurate angle measurements. They are fluid filled cylindrical glass packages, usually 0.5 to 1 inches in height, containing several electrodes. There are newer polymer packaged electrolytic tilt sensors that are smaller and more rugged. The angle is measured in a potentiometer-like fashion. Using precisely controlled AC excitation, the sensor's resistivity varies

[1] Material in this chapter has been published in: M. Bazzarelli, N. Durdle, E. Lou, V.J. Raso, "A wearable computer for physiotherapeutic scoliosis treatment", *IEEE Transactions on Instrumentation and Measurement*, issue 1, vol. 52, pp. 126-129, February 2003, and in: M. Bazzarelli, N. Durdle, E. Lou, J. Raso, "A low power portable electromagnetic posture monitoring system for scoliosis treatment", in *Proceedings of the 18th IEEE Instrumentation and Measurement Technology Conference*, vol. 1, 2001, pp. 619-623.

with the package's angle as the fluid level between electrodes changes. The support circuitry is more complex than when measuring the resistance of a potentiometer. For example, the number of positive and negative pulses on the AC excitation must be equal to prevent destroying the sensor. This is because an uneven build up of charge causes electroplating on the electrodes leaving the electrolytic liquid non-conducting. The sensors are significantly temperature-sensitive, requiring inversely compensating the gain to the temperature. Although the viscosity of the internal fluid can be changed, the settling time for the fluid is a limiting factor. The settling time limits their use in a constantly moving and jolting environment [60]. For example, a 300 ms settling time to obtain a true measurement is required. Angles could only be obtained when the patient was stationary. Extra overhead would be required to determine if the settling time had elapsed, requiring either extra processing or an additional sensor. These devices are not suited to the posture monitoring environment.

Tilt switches were not used because of their low resolution. Mercury and non-mercury type switches provide an angle threshold detection sensor with performance problems in the presence of jostling movements.

Accelerometers are basically a sensor that consists of two transducers. One transducer converts an acceleration into a displacement, and a second transducer converts a displacement into an electric signal. Piezo electrical elements are primarily used as the second transducer. They provide an electric signal proportional to the strain placed on the piezo element. However, this transducer can not provide a signal under static conditions. The signal is only provided during the time that non-constant acceleration is applied to the piezo element. This makes them unsuitable for a portable posture monitoring device because the system would need to monitor these sensors constantly. A small portable device does not have the battery power required to leave the system on all the time to facilitate constant monitoring. In addition, system complexity increases because errors will sum over time when integrating acceleration measurements to determine velocity and location.

Although there are other types of accelerometer devices that use different technologies for the second transducer, they too cannot sense static acceleration, and are not readily available. Likewise, the ones that can sense static acceleration, such as strain gauge accelerometers, are not readily obtainable and are difficult to make.

A new technology being used in accelerometers that allows static acceleration to be measured are devices that use a capacitive type of transducer based on MEMS technology. MEMS devices are small machines that combine electrical and mechanical components. MEMS devices are characteristically defined as less than 1 mm and greater than 1 μm in length [27].

The devices we considered are made by Analog Devices Inc. and are the first to combine low g sensing with low power, low noise, and digital outputs on one silicon chip [25]. A MEMS structure, called the proof mass, is suspended above the substrate using polysilicon springs. This is illustrated in figure 4-1, where the proof mass is suspended using eight polysilicon springs. The single mass and the spring constant are the two adjustable parameters to change the mechanism of Newton's Second Law, in equation 4.1, and Hooke's Law of deflection of a spring, given in equation 4.2, which control the movement of the mass beam.

$$F = ma \qquad 4.1$$

$$F = kx \qquad 4.2$$

For these equations of force F, m is mass, k is the spring constant, a is acceleration due to gravity, and x is a displacement. The combining of the X and Y axis into one beam, as opposed to using a single beam for each axis, results in a reduction in sensor area, and thus cost, but provides a larger beam mass to enhance resolution.

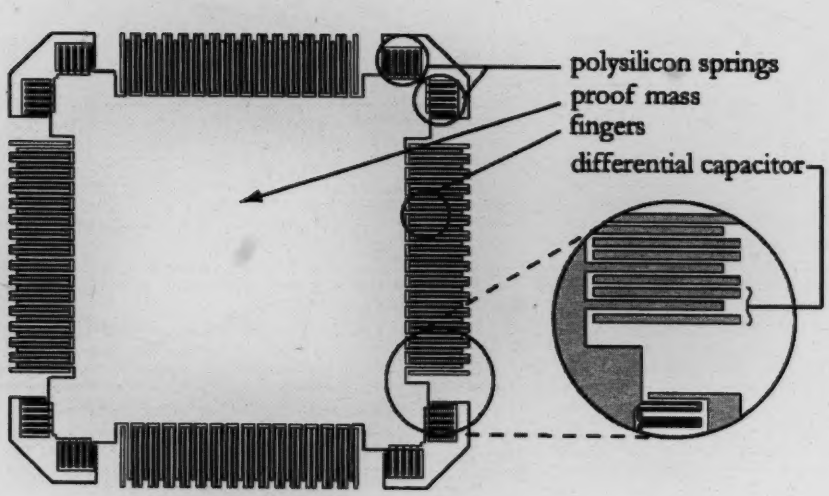

Figure 4-1. Structure of MEMS accelerometer.

The proof mass has 32 separate fingers distributed along its four sides. The fingers are positioned between other plate fingers that are fixed to the substrate. Each finger and two plates create a differential capacitor as shown in figure 4-1. Any movement in the proof mass is detected by measuring the differential capacitance.

The outer finger plates are driven with AC squares waves that are 180 degrees out of phase. The fingers on the proof mass are centered between the two plate fingers and thus the equal capacitance results in an AC voltage of zero. As the proof mass moves the differential capacitance will become unbalanced and there will be an AC signal present proportional to the beam's displacement. The processing of the AC signal involves demodulation before the signal is sent through a 32 kOhm resistor that is accessible outside of the accelerometer's package. This allows for an external capacitor to be used to setup a first-order RC low pass filter. At this point the signal can be used as an analog output from the accelerometer; however, a pulse width modulated signal can be obtained from the accelerometer. Internally the signal is next sent through a duty cycle modulator to create a pulse width modulated signal that corresponds to the

acceleration. The duty cycle of the pulse width modulator is externally adjustable from 0.5 ms to 10 ms.

4.1.2 Calculating Tilt Angles

The theory presented here describes how to obtain the angle from the pulse width modulated (PWM) signal. As discussed in chapter 5, this method was chosen over using the analog signal because it was found to provide better accuracy and resolution. In addition, using this method for a low voltage system is better because, for example, a 3 V system would not have very much range for the analog to digital conversion of the analog signal. Also, it could be possible to remove regulation circuits provided to the microcontroller and accelerometer can operate over the battery discharge range. The duty cycle modulator in the accelerometer has better resolution than the sensor itself, so there is no limitation imposed by the conversion of the signal to a PWM signal.

Figure 4-2 shows the PWM waveform output from both the axes of the accelerometer. There are several ways to calculate acceleration from the sensor's PWM output. Weinberg presents a few ways that vary in accuracy and speed [24]. The method presented here is the most accurate because it removes general assumptions and takes into account the sensor's errors and required calibrations. Also, a novel method to obtain the data will be presented that allows data to be obtained quicker from the accelerometer when using a microcontroller with a counter.

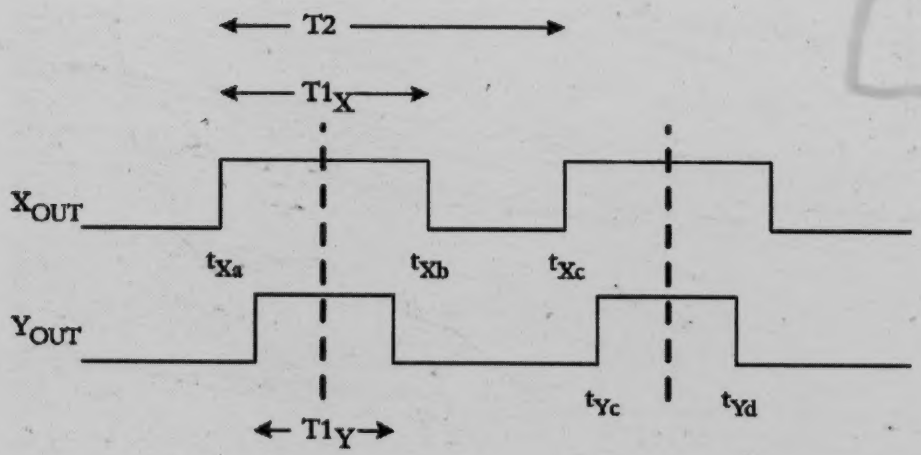

Figure 4-2. Accelerometer PWM output.

The first step is to obtain the transition times of the PWM signal so that the duty cycle of each axis can be computed. Usually when one wants to acquire the rise and fall times of the X axis signal and its period, one would measure the time when the txa signal rises, then the time at txb, and finally the time at txc to obtain the period. Likewise this would then be carried out for the Y axis. Thus, it would take nearly three periods to acquire the times used to decode the PWM signals.

The number of required measurements can be reduced because the duty cycle modulator uses the same reference for each axis. This means that the midpoints of each T1 pulse are coincident. Thus, the period for each channel will be the same and the pulses are center-aligned. This makes it possible to obtain the required times to decode the PWM signal in less than two periods. Using equation 4.3, only the times txa, txb, tyc, and tyd are required to calculate T2.

When all timings are referenced from t1x the pulse times, T1x and T1y, are:

$$T1x = txb$$
$$T1y = tyd - tyc$$

Deriving T2 making use of the coincident midpoints of T1:

$$T2 = T2x = T2y$$
$$T2 = \left(tyd - \frac{tyd - tyc}{2}\right) - \left(\frac{txb}{2}\right)$$
$$T2 = \left(tyd - \frac{T1y}{2}\right) - \left(\frac{txb}{2}\right)$$

Putting this in the best form for a microcontroller calculation:

$$2 \times T2 = (tyd + tyc) - (txb) \qquad 4.3$$

There is an even faster novel method to obtain the signals in one period. It does, however, require a more detailed algorithm. By starting the timer on the first occurrence of a rising edge, the next rising and falling edge that is encountered is recorded as respective times for the other axis. The next falling edge is the end of the original axis' signal. Finally, the next rising edge provides the period of both signals. This method thus provides all the required time measurements within one period. The first requirement when using this method is that you need two external interrupt pins. If the interrupts occur very close together the first interrupt saves the counter. Upon servicing this interrupt, if the second interrupt has occurred, the maximum error will be the number of instructions that have already executed. Retriggering on a second interrupt will not occur because the microcontroller disables interrupts automatically on the first interrupt. Also, the timer value is captured and stored while the timer continues to run preventing any problems with close interrupts. The last issue is to ensure that a false capture is not generated when changing the capture mode from rising to falling edge and vice versa. This can be addressed by clearing interrupt flag bits after the change. In addition, false captures are not generated on the other capture channel that is not having its mode changed. Thus, since one channel will interrupt first followed by the next, there is no need to worry that you are clearing a flag that really did occur right after changing the capture mode.

After obtaining the timing measurements for each axis, the static acceleration can be computed. However, in order to obtain a high resolution and accuracy the method that will be presented here defines how to calculate the acceleration and how to calibrate the sensor. The calibration is required because the period T2 of the waveforms contains some jitter. Also, the value of T2 changes over the operational range of the sensor. Calibration combined with a high accuracy method of calculating acceleration allows the duty cycle change per g to be calculated for each measurement to eliminate error, as opposed to methods that use a constant value.

First the calibration data are obtained from the sensors. This is accomplished by recording the times txa, txb, tyc, and tyd as the accelerometer is rotated through its entire range of motion. The Z axis is kept in the horizontal plane and the accelerometer is rotated through 360 degrees. This is done slowly to minimize centrifugal acceleration contributions. The maximum and minimum durations of the PWM signal are recorded for each axis as T1Xmax, T1Xmin, T1Ymax, T1Ymin. The maximum and minimum values correspond to the +1g and –1g static acceleration forces respectively. The value Zcal is the 0g value of T1 at the time of calibration. This is obtained for both axis and is calculated from equation 4.4.

$$Zcal = \frac{T1\max + T1\min}{2} \qquad 4.4$$

At the time of calibration the period of the pulse width modulated waveform is recorded as T2cal. Again, this values is the same for both axis.

Over the range of tilt angles the period, T2, changes. For each measurement taken the actual 0g value of the duty cycle can be calculated and is called Zact. This is obtained from equation 4.5, which uses the changing ratio consisting of T2 during calibration, T2cal, and the T2 period that was just measured called T2 actual (T2act).

$$Zact = \frac{Zcal \times T2act}{T2cal} \qquad 4.5$$

The following is the derivation of the acceleration for the accelerometer. Equation 4.6 gives the acceleration within the range of +/- 1g. Note that over range values can occur due to shock or vibration and must be dealt with.

$$a = \frac{Duty\,Cycle - 0g\,Duty\,Cycle}{Duty\,Cycle\,Change\,Per\,g}$$

$$a = \frac{\left(\frac{T1}{T2act} - \frac{Zact}{T2act}\right)}{\left(\frac{\frac{T1\max}{T2cal} - \frac{T1\min}{T2cal}}{2}\right)}$$

$$a = 2\left(\frac{T2cal}{T2act}\right)\left(\frac{T1 - Zact}{T1\max - T1\min}\right)$$

$$a = \left(\frac{2T2cal}{T1\max - T1\min}\right)\left(\frac{T1 - Zact}{T2act}\right)$$

To reduce the number of computations required for each static acceleration equation, the constants from the calibration data were factored out as K. This allows K to be computed only once during setup. In addition to this the K value can be multiplied by a constant scaling factor, SF. This factor is useful to scale the final answer as required by your microcontroller. When acceleration is stored as a sign-magnitude integer representation, a final value with more significant figures can be provided reducing round off error. For example by using a SF of 1000 the thousandth digit is obtained, providing a 0.001g resolution.

$$a = K\left(\frac{T1 - Zact}{T2act}\right) \qquad 4.6$$

$$where\ K = \left(\frac{2T2cal}{T1\max - T1\min} \right) \times SF$$

Once the acceleration has been computed the angle can be obtained by taking the arcsine of the acceleration. To obtain the tilt angle of each axis their respective acceleration is substituted into equation 4.7.

$$angle = \arcsin\left(\frac{a}{1g}\right) \qquad 4.7$$

4.2 Electromagnetic Theory

4.2.1 Overview

The ability to determine position and orientation of a sensor is made possible by using electromagnetic (EM) fields. Using a sensor, or receiver, the field of an electromagnetic source can be measured and mapped. Thus it is possible to determine the location of the sensor with respect to the source, or transmitter. However, there are ambiguities in the field that means that more than one position or orientation can appear to be the same. To overcome this, extra information is required to determine the position and orientation of the sensor. This information can be obtained by using any combination of multiple transmission coils, multiple sensing coils, or any known restraints of the system. Electromagnetic field equations will be derived to aid in determining the number of coils required to accomplish a set tracking task.

An electromagnetic field consists of a near field and far field component. This boundary is approximated by equation 4.8 and computes to 3979 m when using a 12 kHz AC signal to generate the EM field. Thus we are in the near field and have a predictable field that follows the theory of a magnetic dipole field. The low frequency field allows quasi-static approximations to be used for the calculations.

$$\text{Near Field and Far Field Boundary} \approx \frac{\lambda}{2\pi} \qquad 4.8$$

When an AC current excites a transmitting coil an EM field is produced. The shape of the coil is not significant provided that the coils are magnetic dipoles and the distance from the transmitter is at least four times the radius of the coil [54]. The near field decreases with the cube of the distance from the source. When the magnetic flux cuts the receiver coil a voltage is induced in the receiver coil. The lines of magnetic flux induce the most voltage, in the receiver, when they are perpendicular to the plane of the coil. As the orientation of the receiver is changes so that the flux lines are parallel to the coil, no voltage is induced. When the receiver is located at a fixed radius from the transmitter, and the orientation is fixed, the flux linkage varies as the receiver is moved. For example, a coil that is a distance r and coaxial to the transmitter will have twice the flux linkage than a coil that is coplanar and at the same distance.

4.2.2 Electromagnetic Dipole Field

The square transmitter coil can be modeled as a dipole in figure 4-3 when excited by a current of $i(t)=I \cos \omega t$. The dipole produces a magnetic field, B, at point P. There is a tangential and radial component of the magnetic field at point P, where P is given in polar coordinates (R,θ,ϕ) [61].

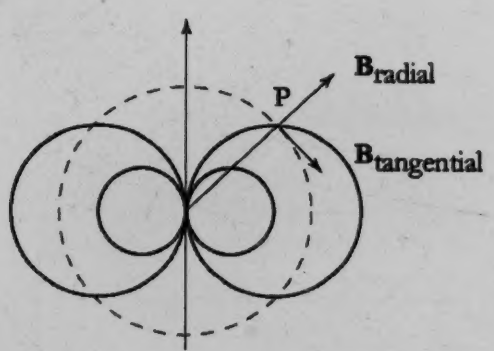

Figure 4-3. Magnetic dipole.

$$\vec{B}_{radial} = \vec{B}_R = \frac{M}{2\pi R^3}\cos\theta$$

$$\vec{B}_{tangential} = \vec{B}_\theta = \frac{M}{4\pi R^3}\sin\theta$$

Combining these equations into one gives

$$\vec{B} = \frac{M}{4\pi R^3}\left[2\hat{a}_R \cos\theta + \hat{a}_\theta \sin\theta\right] \qquad 4.9$$

where,

M = constant equal to μ_0NIA

μ_0=permeability of free-space $4\pi \times 10^{-7}$ (H/m)

N = number of turns in the coil

I = current inside the coil (A)

A = area of coil, for square coil equal to (length of one side (m))^2

B = magnetic flux density (T)

R = distance from dipole to point P (m)

θ = angle from coils axis to point P (rad)

$\hat{a}_R$ = unit vector in direction of R

$\hat{a}_\theta$ = unit vector in direction of θ.

4.2.3 Deriving Position and Orientation Derivation For One Sensor Coil

When a coil is used as a sensor to detect the field given in equation 4.9, the distance and orientation of the coil with respect to the transmitter can be derived. If the position is required then different methods exist to find this by increasing the information. This is generally done by using several generators so that the sensor coil can be triangulated.

To relate the sensing coil's voltage to the magnetic field first the radial and tangential fields can be resolved into Cartesian coordinates. The following derivation makes use of figure 4-4, which defines the vectors and angles in a dipole field at location P.

$$\begin{aligned}\vec{B}_{xy} &= \vec{B}_{Rxy} + \vec{B}_{\theta xy} \\ &= \vec{B}_R \sin\theta + \vec{B}_\theta \cos\theta \\ &= \frac{M}{4\pi R^3}(3\cos\theta\sin\theta) \\ &= \frac{M}{4\pi R^3}\left(3\frac{zR_{xy}}{R^2}\right)\end{aligned}$$

$$\vec{B}_x = \vec{B}_{xy}\cos\phi = \frac{M}{4\pi R^5}(3xz) \qquad 4.10$$

$$\vec{B}_y = \frac{M}{4\pi R^5}(3yz) \qquad 4.11$$

$$\begin{aligned}\vec{B}_z &= \vec{B}_R \cos\theta - \vec{B}_\theta \sin\theta \\ &= \frac{M}{4\pi R^5}\left(2z^2 - y^2 - x^2\right)\end{aligned} \qquad 4.12$$

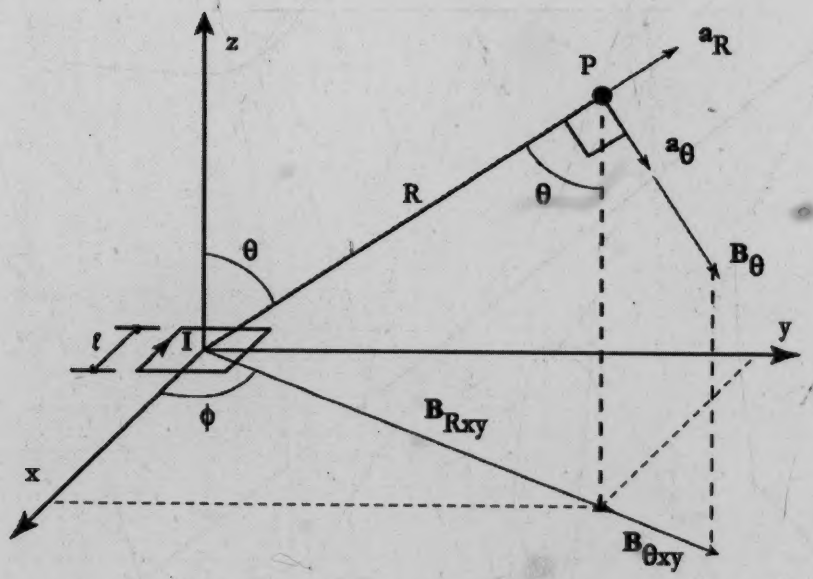

Figure 4-4. Diagram for field derivation.

Combining equations 4.10, 4.11, and 4.12 gives the magnetic field strength at a sensor location P.

$$\vec{B} = \vec{B}_x \cdot \hat{a}_x + \vec{B}_y \cdot \hat{a}_y + \vec{B}_z \cdot \hat{a}_z$$

$$\vec{B} = \frac{M}{4\pi R^5}\left[3z\left(\hat{a}_x x + \hat{a}_y y\right) + \hat{a}_z\left(2z^2 - y^2 - x^2\right)\right] \qquad 4.13$$

Figure 4-5 shows the variables defining the orientation of the sensor coil. Letting the sensor coil axis unit vector be $\hat{a}_s$. The voltage, V_s , that is measured on the sensor is proportional to the magnetic flux resolved to the normal of the sensor coil axis and is expressed as,

$$Vs = C_s \vec{B} \cdot \hat{a}_s . \qquad 4.14$$

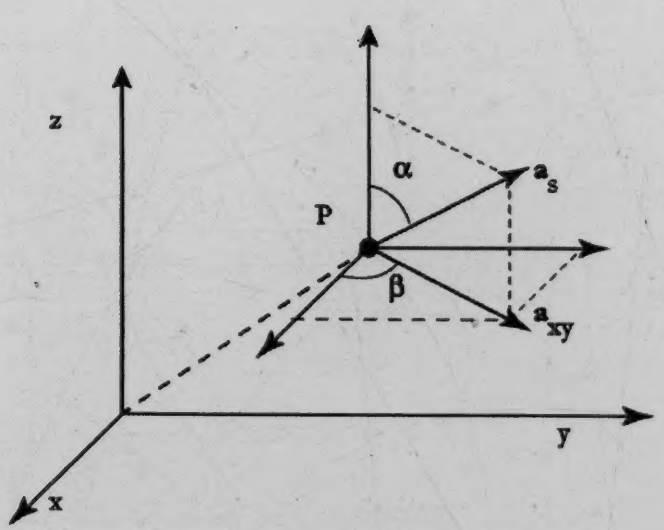

Figure 4-5. Orientation of sensor.

A constant, C_s, is defined for the sensitivity of the sensor coil with units V/T. The polar coordinate angles used in the orientation of the sensor are defined as α for the angle between the coil axis and z axis, and β for the azimuthal angle. The $\hat{a}_s$ unit vector is resolved into Cartesian unit vectors.

$$\hat{a}_s = \sin\alpha \cdot \hat{a}_{xy} + \cos\alpha \cdot \hat{a}_z$$
$$\hat{a}_s = \sin\alpha\cos\beta \cdot \hat{a}_x + \sin\alpha\sin\beta \cdot \hat{a}_y + \cos\alpha \cdot \hat{a}_z$$

The following equation expresses the resulting voltage on the sensing coil.

$$Vs = \frac{C_s M}{4\pi R^5}\left[3z\sin\alpha\cos\beta x + 3z\sin\alpha\sin\beta y + \cos\alpha\left(2z^2 - y^2 - x^2\right)\right]$$

$$Vs = \frac{C_s M}{4\pi R^5}\left[3z\sin\alpha\left(x\cos\beta + y\sin\beta\right) + \cos\alpha\left(2z^2 - y^2 - x^2\right)\right] \qquad 4.15$$

When using three concentric orthogonal coils as the transmitter, the sensor provides three different voltages, V_{si}, where i=1, 2, or 3 representing each of the transmitter's

coils. Thus, equation 4.15 is used to provide three non-linear equations. All equations can be solved for the five unknowns x, y, z, α, and β; however, the results have proven to be unsatisfactory. This equation is best for visualizing what is occurring and to perform calculations if some of the variables are known. For example, using tilt angles the α angle can be solved for.

4.2.4 Reciprocity Principle to Derive Position and Orientation

The form of magnetic field equation that has given the best results for obtaining position and orientation will be described here. It has been because of reciprocity, that is, the idea that if the transmitter and sensor roles were reversed, the transmitter would provide the same results. Thus, we are measuring a single field at multiple points instead of resolving several fields. In practice, three generators are required, each consisting of three orthogonal coils. The sensor can consist of either one or two orthogonal coils. As derived here one sensor coil is used. However, if two sensor coils were to be used it is possible to obtain the distance between a single generator, consisting of three coils, and the sensor.

The magnetic field that is present at the generator, transmitter and receiver roles reversed, will still be equivalent to equation 4.9. This equation can be further simplified as follows,

$$\vec{B}^2 = \left(\frac{M}{4\pi R^3}\right)^2 \left(4\cos^2\theta + \sin^2\theta\right)$$

$$\vec{B} = \frac{M}{4\pi R^3}\sqrt{\left(1+3\cos^2\theta\right)}. \qquad 4.16$$

The magnetic field is proportional to the distance, R, from the field generating sensor. Because the coils of the generator, which is thought to be sensing now, are orthogonal and concentric, the voltages measured can be combined to obtain a measure of the magnetic field.

$$\bar{B} = C_s \sqrt{\left(V^2_{gx} + V^2_{gy} + V^2_{gz}\right)} \qquad 4.17$$

where, Vg_x, Vg_y, Vg_z, are the voltages measured on the x, y, and z coils, respectively. Combining equations 4.16 and 4.17 gives equation 4.18 solvable for the radius between the generator and sensor, R, and the angle between this vector and the coil axis.

$$R^3 = \frac{C_s M}{4\pi} \frac{\left(\sqrt{\left(1+3\cos^2\theta\right)}\right)}{\sqrt{\left(V^2_{gx} + V^2_{gy} + V^2_{gz}\right)}} \qquad 4.18$$

4.3 Network

4.3.1 Communication System

The distributed microcontrollers need the ability to communicate. A communications protocol was needed that would meet several requirements. The protocol needed to lend itself to a wireless hardware platform because future work entails developing a wireless system. This meant that physically a multipoint communications bus should be used, thus simulating the requirements that would be present in a wireless system. For example, the protocol would need to include addressing so that when all microcontrollers receive the same message, they can determine if it is applicable to them. Another required feature is the ability to address all the nodes at the same time. This would speed up the system allowing parallel processing and communication. There also needed to be the ability to easily add or remove distributed microcontrollers from the system. Finally, the microcontrollers should be able to be woken up from a low power state by the communications bus to reduce system power consumption.

A master slave configuration was chosen because the transmitter and receivers would not need to initiate any communications on their own. The master would control the communications and thus the flow of data to or from the transmitter and receivers (slaves). The multipoint bus requirements could all be obtained by using an existing protocol called the Inter-Integrated Circuit Bus (I^2C-Bus).

4.3.2 I²C-Bus Hardware and Protocol

The I²C-Bus was developed by Philips Semiconductor [62]. It is a bi-directional two wire communications bus. The standard has been extended to include different modes allowing different data rates, operation modes, and addressing modes. There is a maximum data transfer rate of 3.4Mbits/s. A maximum of 1024 peripherals can be addressed, however bus capacitance limits the maximum number of peripherals connected to one bus.

The hardware consists of two bus wires called serial data (SDA) and serial clock (SCL), and a common ground. Two pull-up devices are used to pull the lines high to a positive voltage. Typically these are resistors; however, at higher speeds a current source circuit may be required to overcome parasitic problems. Depending on the technology used, open drain or open collector transistors are used as outputs to pull the lines low, or release them. An input buffer is used to read the state of the line. All electrical and timing requirements are given in the I²C-Bus specification.

All devices are connected to the SDA and SCL lines on the I²C-Bus. Each device has an individual address. Some of the addresses are reserved. The address 0000000 is reserved for the General call address. This means that all slaves will respond to this address, although you can still program your slave to ignore this address. The master is the device that starts a data transfer, generates the clock, and terminates a transfer. The slave is the device being addressed by the master. The general communication is explained as follows.

The Master initiates a data transfer by generating a START condition. All devices recognize a START condition as the SDA line being pulled low, followed by the SCL line being pulled low. Thus, it is a transition of the SDA from high to low while the SCL line is high, that is recognised as a START condition.

Next the address of the slave is transmitted. In the seven bit addressing mode the most significant bits contain the address of the slave being addressed. The least significant

bit is the R/W bit. If the R/W bit is set then the slave understands that the master is reading data from it; if it is not set then the master is writing data to the slave. In preparation for the slaves response to this first transmission, the master releases control of the SDA line and keeps the SCL low and monitors the SDA bus.

When the slaves detect an address match they respond to the master with an acknowledge (/ACK) bit. This is done by pulling the SDA line low before the master clocks in the state of SDA. If the Master does not detect an acknowledgment it can handle the error by stopping the transfer or restarting it. The slave releases the SDA line after the master has clocked the SCL line.

The master can now send data to, or read data from the slave. When sending data, 8-bits are sent at a time on the SDA line and the SCL line clocks each bit. The ninth bit is an acknowledge bit from the slave. When reading from the slave, the slave puts the data on the SDA line as the master clocks the SCL line. The data must be stable during the high of the SCL line. The acknowledge bit is set by the master and read by the slave. If the slave sees that the master did acknowledge then it will continue to send the next byte of data. If the master does not acknowledge, then the slave releases the data line so that the master can generate a stop condition.

A stop condition is generated when the SDA line goes high and the SCL line is low. This terminates the communication on the I^2C-Bus. All devices recognise this as a stop.

Arbitration can occur on the buses and is aided by the physical design of the bus. For example, if a slave acknowledges the first transmitted address byte it may then hold the SCL line low while it is getting ready for the next byte. During this time the master might have released the SCL as part of the next clock pulse, however it will monitor if SCL does go high. If it does not go high, the master knows that someone is holding it low and it can wait until the slave has release the line.

5 SYSTEM DESIGN

5.1 System Overview

The objectives of the system design are to create a wearable computer that is discreet, low power, and can be used for posture correction and monitoring in scoliosis treatment. In addition the system should address future development goals where possible, such as facilitating the development of a wireless system and replacing the wiring harness.

A simple to use and small system is important for compliance. In scoliosis treatment a discreet device could elicit better compliance, and provide with a better quality of life and comfort for the patient. These are in addition to the arguments given for its benefits over a brace. A simple to use system will help the clinician and patient through ease of use, mounting, and maintenance.

The low power considerations aid in reducing the system power requirements. This reduces the physical size and weight of the batteries. Lower power requirements allows alternative methods to be investigated to power the system [21, 53]. Also, system maintenance is reduced via infrequent charging times, thus reducing intrusion into the patient's life.

---

[1] Material in this chapter has been published in: M. Bazzarelli, N. Durdle, E. Lou, J. Raso, "A low power hybrid posture monitoring system", in *Canadian Conference on Electrical and Computer Engineering*, vol. 2, 2001, pp. 1373-1377, and in: M. Bazzarelli, N. Durdle, E. Lou, V.J. Raso, "A wearable computer for physiotherapeutic scoliosis treatment", *IEEE Transactions on Instrumentation and Measurement*, issue 1, vol. 52, pp. 126-129, February 2003, and in: M. Bazzarelli, N. Durdle, E. Lou, J. Raso, "A low power portable electromagnetic posture monitoring system for scoliosis treatment", in *Proceedings of the 18th IEEE Instrumentation and Measurement Technology Conference*, vol. 1, 2001, pp. 619-623.

In depth discussion was presented describing how the system can be used for posture monitoring and correction treatment. The focus of this chapter is on the development of a system with three axis orthogonal EM field generation, a single coil EM field sensor, and a 2D tilt sensor. In this configuration both angular and rotational data can be obtained, and distance measurements can be made in both one and three dimensions. The system consists of networked microcontrollers worn by a patient to monitor their posture and provide feedback. The receivers collect EM field and inclinometer data in parallel. The transmitter generates three orthogonal EM fields, and the main controller collects data and oversees system operation. The system can be worn by the patient via a tight fitting t-shirt with small individual pockets that hold the receivers and transmitter. Sewn in piping conceals and protects the wiring harness in the t-shirt. The main controller is mounted on the patient's belt.

A block diagram of the system is shown in figure 5-1. The main controller has an RS-232 interface for configuring and obtaining data from the system via a terminal. The main controller communicates with the receivers using the I^2C protocol and addresses them individually or in parallel. The controller gives the receiver's configuration information, synchronizes their parallel sampling, and polls them for their data. A typical example of data collection entails the main controller waking up the networked processors and synchronizing the EM field generation and sampling. The transmitter generates an EM field sequentially on its orthogonal transmitter coils. A voltage is induced on the receiving coils and this signal is then processed. Next, the receivers obtain inclinometer information and calculate tilt angles in the X and Y planes, where the Z axis is parallel to gravitational force. Finally, the main controller collects the information from the receivers for storage and further processing, such as providing feedback audibly to the patient.

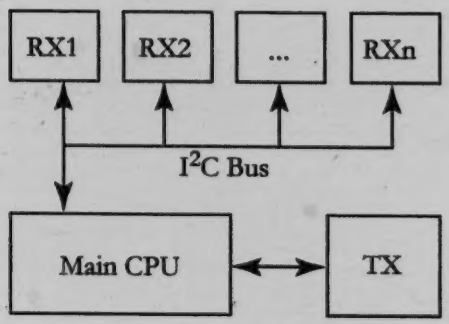

Figure 5-1. System block diagram.

5.2 Hardware Design

5.2.1 Receivers

Figure 5-2 shows a block diagram of a receiver. Each component and its design is discussed in detail in this section. A picture of one of the prototype receivers is shown in figure 5-3. The prototype can be scaled down in size by using surface mount parts as opposed to dual inline package (DIP) parts, optimizing PCB circuit layout and multilayer layout, and removing prototype circuitry not required in the final design.

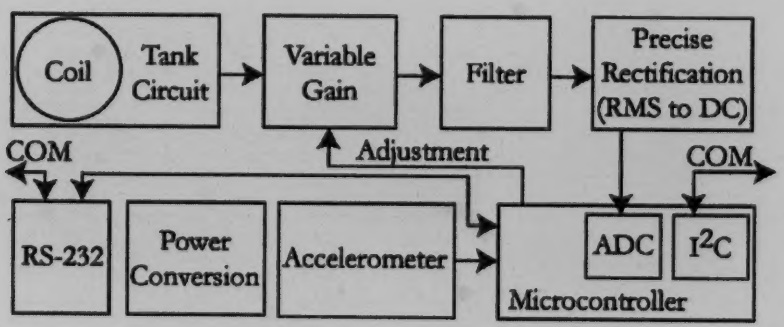

Figure 5-2. Receiver block diagram.

Figure 5-3. Prototype receiver.

5.2.1.1 Sensing Coil and Resonating Circuit

There are several requirements when choosing coils for the system. The size of the coils must be small so that they are not cumbersome to the patient. In addition small coil size allows for a better dipole field approximation as discussed in the magnetic theory section.

In addition coils should be cheap and easy to obtain to facilitate manufacturability of the system. A three axis orthogonal coil cube, called the POCO coil, was developed for the original posture monitoring system. It was 1.5 cm square. These coils were costly to produce and hand wound. When obtaining quotes from coil manufacturing companies to produce the prototype coils several companies turned the job down primarily based on the complexity of the coil bobbin. A company was found that could produce the bobbins with a ferrite core. The unwound coil cores would cost fourteen dollars per unit in low quantities.

The coil excitation frequency needed to be chosen for the system. This should be a frequency with the least noise and interference in a typical everyday environment. In addition a higher frequency was desired to produce a stronger field. This is according to Faraday's law where the voltage induced in a coil is proportional to the frequency.

A frequency of 12 kHz for the EM field of the system was chosen. This was based on previous work that showed this frequency to have little interference in a common everyday environment [54]. In addition, higher frequencies were decided against as experiments showed that the human body interfered with the field. During coil testing it was noticed that the received field increased, distorted or changed phase when a hand was close to the receiving coil at higher frequencies of 169 kHz. A POCO transmitter coil and other receiver coils were tuned for different frequencies from 169 kHz to 26.1 kHz, and tested by placing a hand between the coils. The receiver's signal voltage was monitored on an HP54645D oscilloscope. No effect appeared to be visible with a 26.1 kHz EM field at a received signal magnitude of 91.88 mVpp.

Manufactured coils that could be used in the system were investigated, primarily for providing the benefits previously discussed, and to obtain a single plane coil. A circuit was built, consisting of a current amplifier driven by a signal generator, to provide enough drive current to test the coils. Several different types and shapes of coils from different coil manufacturers, and some hand wound coils, were tested. The original POCO coil was compared to the new coils. Several of the coils were eliminating based on sensitivity and directionality. A change in phase of the observed coil's signal during rotation was used to test if the coil was directional. The remaining few candidates were compared in table 5-1.

	POCO	Ccraft	Bobbin	Large Bobbin	Long Flat Core	Short Flat Core
L(mH)	4.64	1.06	0.17	8.59	35.3	3.19
R (ohm)	46.3	1.7	0.8	11.3	67.4	21.5
Q	7.6	47	16	57.3	39.5	11.2
RX Voltage (mVrms)	27	35	19	539	782	64
Coil Gain/ POCO Coil Gain	1	1.3	0.7	19.96	28.96	2.37
Rise (μs)	732	1900	1150	2900	1740	990
Fall (μs)	652	2000	1200	3300	2350	800
Spurious Free Dynamic Range (dB)	38.12	39.69	31.25	53.12	55.31	44.06
Size (cm) d=diameter h=height	1.5 (cube)	d=1.3 h=0.7	d=1.5 h=1.4	d=2 h=1.3	0.6x1.5x4	0.6x1.5x2

Table 5-1. Coil evaluation.

This was a practical experiment but also necessary as competitive coil manufacturers guard their coil designs and are not eager, nor cooperative, to release the details on the coil and quite importantly its core. In table 5-1 the voltage of the 12 kHz transmitter coil for each test was 16.6 Vrms and it was at a 12 cm distance from the receiving coil being tested. The coils were aligned coaxially.

All the coils used a ferrite type of core. This material has a higher permeability than air. It increases the sensitivity of the coil because the core increases the amount of flux passing through the coil. In coil selection both size and the coil's sensitivity played the biggest role. Important information to note from table 5-1 is that an RLC oscillator circuit with a larger Q value produces larger settling times when a field is applied or removed. Where Q is calculated from equation 5.1.

$$Q = \frac{\omega L}{R} \qquad 5.1$$

The coil that was chosen for use was a Coil Craft coil, part number DO5522P-105. It is a round copper wound coil with a NiZn ferrite having a permeability of approximately 250 H/m. The coil is 1.3 times more sensitive than the custom made coil, it is a small size, and it is commercially available.

A resonating LC circuit was chosen for use with the coil. By tuning this circuit to resonate at 12 kHz a large voltage can be obtained when the 12 kHz EM field induces a voltage in the coil. A parallel LC circuit, as opposed to series circuit, was chosen because it results in less current and more signal voltage. The capacitor value can be calculated from equation 5.2 using the resonant frequency f=12 kHz and the measured coil inductance, L, using an inductance meter. For the 1 mH receiver's coil, a capacitor of approximately 176 nF was required. The tank circuit was tuned for maximum resonance using a capacitor in this range.

$$C = \frac{1}{(2\pi f)^2 L} \qquad 5.2$$

Optionally, the custom three orthogonal coil sensor could be connected to the receiver to create a standard EM 6DOF system. This requires an analog multiplexer to isolate each of the tank circuits, allowing one coil to oscillate and be sampled. The switch is in series with the capacitor. An analog multiplexer with a low on resistance is required. The ADG709 is chosen based primarily on it low power requirements and its very low on resistance. It only requires between 1.8 V to 5.5 V and has an on channel resistance of 3Ω.

5.2.1.2 Electronically Controlled Gain

Due to the possible variations in the distances between the sensors, the gain of the system needs to be adjustable. To make the system more user friendly for a clinician

setting it up, a circuit has been constructed to allow software control of the system's gain. This is simpler than adjusting hardware. In addition this affords the system the ability to intelligently control its gain when attempting to maximize resolution and accuracy.

The EM system was tested to determine the signal levels obtained at the receiver from different distances. This information is used to determine the amount of gain required by the system. Table 5-2 gives the values obtained over the 10-40 cm range. Using the approximation that the signal should drop off proportional to the cube of the distance,

$$V_{RMS} = \frac{Constant}{R^3}, \qquad 5.3$$

the values were verified to this approximation as shown in table 5-2. The total gain required by the system for this range of distances varies from Gain=5V/(Vpp/2) ≈ 36 at 10 cm, to a gain of 1235 at 40 cm.

Distance (cm)	Received Signal		Theoretical (mVrms)
	(mVpp)	(mVrms)	
10	278.1	98.3	98.3
20	34.4	12.2	12.3
30	13.1	4.63	3.64
40	8.1	2.86	1.53

Table 5-2. EM signal measurements.

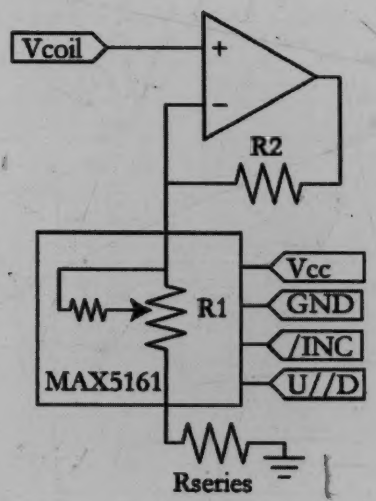

Figure 5-4. Controllable gain circuit.

The adjustable gain circuit is shown in figure 5-4. The voltage from the coil and tank circuit is amplified and buffered using a non-inverting operational amplifier. An LMC7101 amplifier was chosen. The gain for the circuit is given in equation 5.4.

$$Av = \frac{Vout}{Vin} = 1 + \frac{R2}{R1 + Rseries} \qquad 5.4$$

The R2 resistor is 50 kΩ, R_{series} is 1 kΩ, and R1 is a 50 kΩ digital potentiometer to produce a gain from 2.1 to 32. The potentiometer is a MAX5161. It was the only programmable potentiometer commercially available. It can operate in the 2.7 V to 5.5 V supply range. The newest version's incorporate NVRAM with the potentiometer and would be a good replacement. The potentiometer has two control lines that are interfaced to the receiver's microcontroller. These two lines control the movement of the center tap of the digital potentiometer, moving it either up or down to one of thirty-two tap positions. Decoupling capacitors were used with the operational amplifier.

Due to the circuit configuration the resulting gain is inverted and pseudo logarithmic. This means that the lower potentiometer tap points results in larger gain values and decrease in both value and difference between gains, as the upper tap points are approached as shown in figure 5-5. In figure 5-5 series 1 to 3 show an increase in potentiometer R1 resistance from 50 kΩ to 200 kΩ while R2=200 kΩ. Choosing the lowest value of available digital potentiometer R1 resulted in a more linear response. Similarly, increasing R2 produces a more linear response as shown by series 4. This response allows smaller changes in the high gain to be obtained between potentiometer tap locations; however, it increases the minimum gain. For this reason R2 was left as it was to obtain the minimum required gain. The R_{series} resistance was originally used for protection from too much gain, however, it was not required as the digital potentiometer would never go below 0.6 kΩ; the decreased gain only worsens the response curve. For this reason the R_{series} resistance was removed from the circuit. This increased the gain range of the circuit to 2.1 to 83. The gain required to obtain the final gain range comes from the band pass filter's gain of 17.

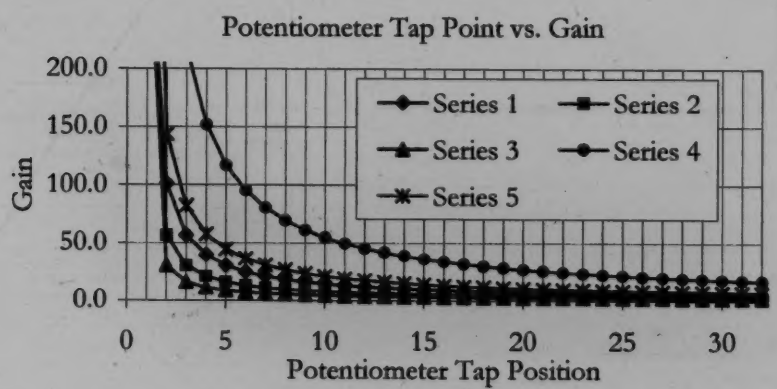

Figure 5-5. Variable gain circuit simulation.

Measurements were taken of the actual circuit using R1=50 kΩ, R2=50 kΩ and R_{series}=0 Ω. The results closely matched the theoretical series 5 curve in figure 5-5.

Slight variations were obtained at the maximum gain primarily due to the estimated value of the digital potentiometers internal wiper resistance. The gain ranged from 1.8 to 71. At the lowest gain setting, the signal was 33 dB above the noise floor when observed with an FFT.

5.2.1.3 Band Pass Filter

Digital and analog filtering were considered for the band pass filter. Digital filtering was ruled out because for real time sampling the microcontroller could only perform a 4^{th} order band pass with a maximum sampling rate of 2.5 kHz using a 16 MHz oscillator. That sampling rate is too low for the 12 kHz signal frequency and would cause aliasing errors. In addition the 16MHz clock speed is not required for all the other operations, and would add an additional 18 mA power requirement to the microcontroller due to the faster clock.

Different methods and selections were considered for analog filtering. Switched capacitor filters were considered, however, due to their inherent noise this was decided against. Synchronous detection was also considered, however, due to the complexity and additional parts requirement this option was rejected. In the future, provided one could overcome the tuning problems, this would be a promising solution as it would allow for the RMS-DC converter circuit to be removed.

A continuous time active band pass filter was chosen, part number MAX275 from Maxim. The most significant reason this integrated circuit was chosen over others, with the same characteristics and specifications, was a price half the amount of the others.

The MAX275 allows for a 4th-order band pass filter to be created by cascading two 2nd-order sections. One of the 2nd-order sections is shown in figure 5-6. The center frequency can be a maximum of 300 kHz and is accurate to ±0.9% over its operating temperature range. It can be operated on a single or dual 5 V power supply.

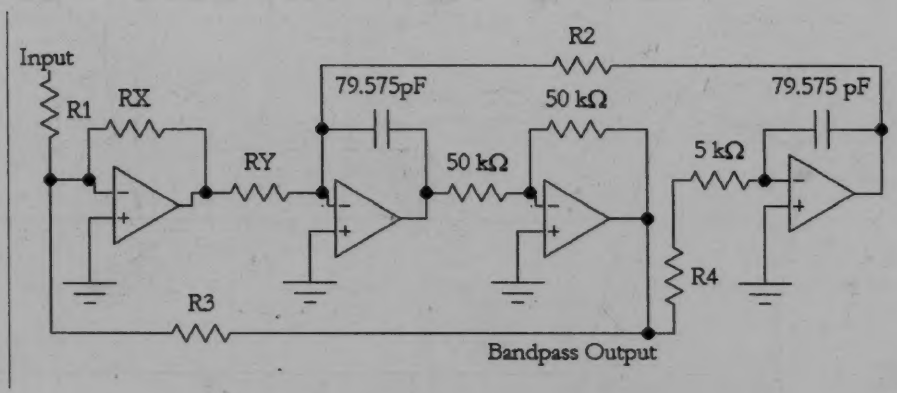

Figure 5-6. Band pass filter first cascadable 2nd-order section.

To calculate the resistor's values for the circuit the datasheet is used. R2 is selected using the formula,

$$R2 = \frac{2x10^9}{F_O} = \frac{2x10^9}{12{,}120} = 165k\Omega, \qquad 5.5$$

where F_O is the center frequency 12.12 kHz. R4 is then obtained from R4 = R2 – 5 kΩ = 160 kΩ. Using a chosen value of Q=10, R3 is calculated using equation 5.6. The quality factor was kept low to reduce the settling time of the signal.

$$R3 = \frac{Q(2x10^9)}{F_O}\frac{Rx}{Ry} = \frac{10(2x10^9)}{12{,}120}\frac{1}{5} = 330k\Omega \qquad 5.6$$

Here the ratio of Rx/Ry is programmed by grounding the frequency control (FC) pin of the integrated circuit. Note that of the three ratio choices, the grounded FC selection minimizes noise in this IC.

Choosing a gain of 10 for the first bandpass output filter section, H_{OBP}, allows R1=33 kΩ to be calculated from equation 5.7.

$$R1 = \frac{R3}{H_{OBP}} \qquad 5.7$$

The second cascaded band pass filter section uses the same computed values except for its gain. A gain of only 1.7 is required, producing an R1 value of 187kΩ. This results in an overall gain of 17 and a Q of 14.1 for the complete 4th order band pass filter. The final combined gain of the band pass filter and adjustable gain circuit was checked and found to meet the requirements. At the lowest input gain setting the signal after the band pass filter was 57 dB above the noise floor when observed using the FFT function of the oscilloscope.

5.2.1.4 RMS to DC Conversion

Root Mean Square (RMS) is a measure of the magnitude of an AC signal. It provides the equivalent DC value required to produce the same heat loss in an equivalent load. Mathematically RMS is defined as,

$$V_{RMS} = \sqrt{\text{average}(V^2)}.$$

When choosing a circuit to perform the RMS conversion power consumption, circuit size, and conversion time are the most important factors. When looking for an integrated solution, to limit the amount of components required, only dual power supply parts were available. Parts that are single supply required the same voltage difference but offset from zero, so they were no real benefit. Also, in general a large power rail difference is required because the peak voltage of the input signal will be converted to a lower RMS voltage. For example, a 5 Vpp sinusoid will result in an RMS voltage maximum of 1.7 V DC. The requirement that proved to be the most important was the conversion time, or settling time, of the RMS to DC converter. Circuits were built for testing three RMS to DC integrated circuits. The test results are given in table 5-3.

Integrated Circuit	Current Draw (mA)	Rise Time / Fall Time (ms)
AD736	0.27*	50 / 50
AD8361	1.1	10 / 15
MX536	0.8	4/5

*=from datasheet, not a bench test measurement

Table 5-3. RMS to DC conversion comparisons.

The integrated circuit MX536, from Maxim, was selected over the others for many reasons: it required only two external passive components in addition to decoupling capacitors, it provides a true RMS conversion, it has a low power requirement, it is available in a small surface mount package, and it has the fastest rise and fall response times. In addition, there is an internal amplifier that can be used to filter the output, thus removing the need for additional low pass filter circuitry.

These features were contrasted by the AD8361, which had an output ripple starting at 1.5 mV and increased when the input was above 1.29 V. It would require the addition of a low pass filter after the converter, which could effect the rise and fall times. Also its transfer function is approximately 7.5 V / 1 Vrms which causes the output signal to be smaller limiting the dynamic range.

From bench test measurements of the MX536 the test circuit was determined to have a linear response and an average percent error of 0.45%. It had a percent error range below ± 1% for the input range of 0.8 Vpp to 9.125 Vpp. Outside of this range the percent error ramped up towards a maximum of 2.5%.

Guidelines are given in the data sheet for choosing capacitor C_{av}, for the averaging circuit, and C_f, for the post filter. A graph provided a starting value, which was then fine tuned via experimental testing. Figure 5-7 shows the final rise time obtained using C_{av}=250 nF and C_f=142 nF. Channel A1 is the received input and channel A2 is the MAX536 output. Increasing C_{av} reduces ripple on the output but increases the settling

times. To reduce C_{av} a one pole low pass post filter utilizing C_f is used. This helps to reduce the settling time and further reduce ripple.

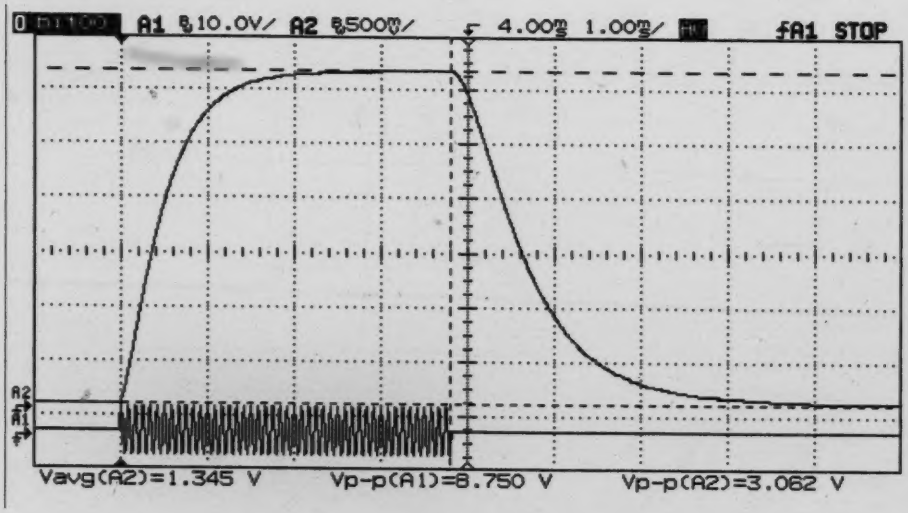

Figure 5-7. RMS to DC rise and settling time.

5.2.1.5 Microcontroller

There are several requirements for selection of the microcontroller. It needs to be a low power, physically small, and a peripheral rich microcontroller. A peripheral makes the receiver smaller by avoiding extra circuitry, such as an analog to digital converter. Some of the peripheral needs include an analog to digital converter (ADC), timers, and communications peripherals.

At minimum a 12-bit analog to digital converter peripheral is required to sample the received analog EM signal. The 12-bit resolution of the analog to digital converter was determined based on the required resolution for the received EM signal. As the angle between the field and the plane of the sensor approaches zero, less change in signal amplitude is available because the induced signal is proportional to the cosine of this angle. For example, between 2 and 5 degrees there is a change of approximately 2 mVrms in this system at a 30cm distance. After the RMS to DC conversion the signal

will be limited to a maximum of 3 V DC, thus using a 12-bit ADC will provide 0.73 mV of resolution.

The microcontroller needs a low pin count and a small package size to occupy the least physical space on the receiver. A low pin count aids in the manufacturability of the device. No more than 14 IO pins are required to implement the system. Two pins are required to have open collector outputs.

To reduce circuit size, code size, and processing overheard, several other peripherals are required. These are timers, capture compares, a universal synchronous asynchronous receiver transmitter (USART), and an inter-integrated circuit (I^2C) peripheral. The USART and I^2C peripherals are used to implement communications busses. The I^2C bus is the two-wire network that is used to communicate between the master computer and the receivers. This allows all the networked processors to share a common bus and protocol, that allows both addressable individual communications or parallel communications. The feature of a networked protocol complements the future goal to integrate a wireless system.

Many microcontrollers were evaluated from several different vendors. Primarily package size, a 12-bit ADC, and an I^2C peripheral became the limiting factors in selection. Parts that did not meet all the peripheral requirements were ruled out. A Xemics XE88LC0X was considered, however, the package had 64 pins. Also, the development tools were expensive. It does however, have a low power requirement at only 0.46 mA at 2 MHz and 3 V. As new packages become available this part would be reconsidered. An ADuC812, from Analog Devices, was smaller, but at 52 pins was still to large. In addition its power requirements were average, with an 8 mA current draw at 1 MHz with a 5 V power supply.

The new PIC16C773 from Microchip was the chosen microcontroller for several reasons in addition to having all the required peripherals. The development assembler tools were free, and a programmer for these microcontrollers was freely available. The

chip is available in a small 28-lead shrink small outline package (SSOP). It was the smallest part found that had a 12-bit ADC. Also, its power supply requirement is low, with a typical current draw of 2 mA at 4 MHz with a 5 V power supply. Finally, it was an easily obtainable part in low quantities.

The PIC16C773 is a 8-bit CMOS microcontroller. Its architecture is based on a high-performance RISC CPU. Also called a Harvard architecture, this allows fast execution speeds to be obtained for a given clock rate. The program memory and its distinct buses are separate from buses used to access the register and data memory. This allows an instruction to be fetched each clock cycle. Once the pipeline is full an instruction executes nearly every clock cycle. A low clock rate reduces the power consumption of the microcontroller, thus the efficient speed at lower clock rates is important. It has 4 kb x 14 of program memory, and 256x8 bytes of RAM data memory. It also has a power saving sleep mode that reduces current consumption to under 1uA.

The 12-bit ADC was tested to evaluate its operation with external and two different internal voltage reference sources. The ADC internal references are taken from either a reference module or the power supply of the ADC. The ADC was tested using the internal ADC power supply references of 0 to 5 V. It was found that the internal references of the ADC power supply produced less variation in the counts of the converter's output than the external references. The variation for the counts using external references for the ADC was 20 counts, however, after software filtering reduced to 7 counts. These results were later improved when the noise was removed form the test signal source resulting in 2 counts variation. The adjustable internal reference module produced very poor results. The counts varied up to 100 counts and this was only reducible to 40 counts via software filtering. Subsequent to these test results, Microchip later confirmed this problem in an errata released for this microcontroller stating that the internal low voltage reference module does not function properly.

An external reference was chosen for use because of these results. With an input voltage of 10 Vpp possible a reference of 3.53 Vrms would provide the best resolution for the ADC. Finally, the ADC was tested along with the MAX536 RMS to DC converter to verify their operation. The reference for the ADC was a 5 V external reference. A 12 kHz input signal was generated using an HP33120A signal generator connected to the RMS to DC converter input. The percent error of this subsystem was measured and is presented in figure 5-8.

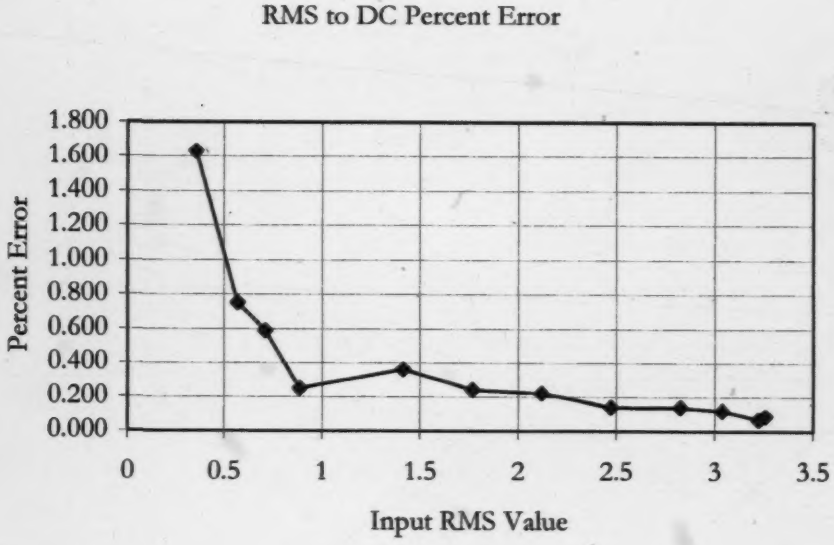

Figure 5-8. ADC and RMS to DC results.

5.2.1.6 Accelerometer

Accelerometer theory was presented in chapter 4 along with reasons for choosing the ADXL202 from Analog Devices. The ADXL's ability to measure static gravity fields in two dimensions was the primary reason for its selection. This allows the system to conserve battery life because it can power down, whereas a regular accelerometer or gyroscope would require continual monitoring.

The choice of the digital output of the accelerometer was influenced by the limitations of the ADC. In order to measure the analog signal produced by the accelerometer the ADC would require the lower reference to be 2.1 V and the higher reference to be 2.9 V. However, as too much error was encountered when testing using the lower reference it was thought that there was a problem with the accelerometer. As stated above, this was later confirmed to be an actual problem with the ADC on this microcontroller. Extra circuitry would have been required to convert the accelerometer's output to a signal between 0 V and 5 V by roughly subtracting 2 V and multiplying by 5. The analog output changed by 20 mV for an angle of 0° to 5°, and 4 mV from 75° to 80°. After converting these measurements to a 5 V range the ADC 1.3 mV/bit resolution would be reaching its limits, for example with 3 counts representing a change of 1 degree at 75°. Using the digital output as opposed to the accelerometer's analog output was a better choice as described in chapter 4.

The selection of the support circuitry involved setting the bandwidth for each axis of the accelerometer and setting the period for the duty cycle modulator. When the accelerometer's differential capacitor is unbalanced due to acceleration, a square wave signal will be generated with its amplitude proportional to the acceleration. After demodulating the signal, an RC low-pass filter for antialiasing and noise reduction is configured so that the capacitor is external. This filter allows the dynamic acceleration to be filtered out. Using an internal R value of 32 kohms±25%, a value of 1 uF was chosen for each channel's C resulting in a 3 dB of 5 Hz from the equation,

$$F_{-3dB_{(x,y)}} = \frac{1}{2\pi(32k\Omega)C_{(x,y)}}.$$

Both of the x and y accelerometer channels use one resistor to set the duty cycle modulator. The duty cycle modulator creates the digital signal output based on the demodulated signal from the RC low-pass filter. Using the formula,

$$T2 = \frac{R_{SET}(\Omega)}{125M\Omega},$$

R_{set} is calculated to be 470 kΩ to give a period of 3.76 ms for the digital output signal sent to the microcontroller. This period was chosen based on measurements of the accelerometers duty cycle changing 0.7% from 0° to 5°, and 0.2% while in the 75° to 80° range. With the microcontroller's counter running at 1μs per count this resulted in a theoretical resolution ranging from 0.15° at 0°, up to 0.56° at 80°.

5.2.1.7 Power Supply

A power supply circuit was built for the receiver. The goal was to create an efficient and clean power supply to provide the required voltages from a single input voltage. This facilitates a wireless system where each receiver will be battery powered, however, for this version a single battery is used to power the entire system. Initially on the first prototype circuit built there were five different voltages required, ±5 V, ±3.3 V, and a +3 V reference. However, as the system design changed only ±5 V supplies and a 3 V reference were required. Due to device limitations an entirely ±3.3 V system could not be realized. Finally, an additional design change removed the need for the remaining 3.3 V parts.

In the selection of the IC for the 5 V supply both switching and linear regulators were considered. A low drop out linear regulator was chosen because it would produce the least noise in the system, and requires less support circuitry thus saving space. The MAX883 is a 5 V, 200 mA regulator that uses internal MOSFET pass transistor technology and requires an input voltage over 6 V. This allows a lengthy battery life because it has a low 11 μA quiescent current over its operating load range. It has an 8 pin small outline package, and it only uses two decoupling capacitors. In addition the part has an integrated low battery detection circuit.

A switching inverter regulator was required to create the –5 V supply. A linear regulator cannot be used to invert voltages. The MAX764 was chosen over other parts because it had an inverter and regulator built into one IC and its switching frequency would not interfere with the EM field signal frequency. However, as a switching part it required more support circuitry. The part takes an input voltage from 3 V to 16 V and converts it into –5 V at up to 250 mA. The quiescent current is around 80 μA. Four capacitors, an inductor, and a Schottky diode are required as support circuitry. The inductor and high valued capacitors are physically large and require more room than the IC itself. An shielded inductor was chosen to reduce EM radiation.

To create the 3 V reference for the ADC on the microcontroller a low noise ultra-low dropout regulator was chosen from National Semiconductor, the LP2980. This part is a tiny 5-pin small outline transistor (SOT) package. It has a fixed 3V, 50 mA output and requires over 4 volts input. Only one external capacitor component is required. In addition it has a sleep mode where it uses less than 1 μA quiescent current.

5.2.2 Transmitter

The transmitter is a microcontroller run device that generates the three orthogonal EM fields. The master computer prompts the transmitter which in turn generates the three 12 kHz fields in sequence. This allows the field generation signals to be generated on the transmitter preventing the cabling from becoming part of the RLC resonating circuit. This adds to the stability of the circuit. A system block diagram is given in figure 5-9, also a picture of the prototype is given in figure 5-10.

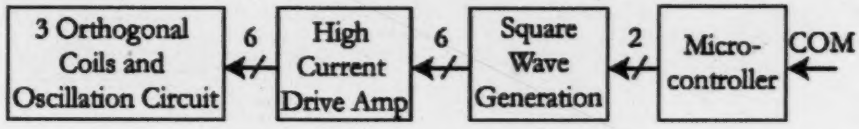

Figure 5-9. Transmitter block diagram.

Figure 5-10. Transmitter prototype.

5.2.2.1 Microcontroller

A PIC16C711 microcontroller was used to control the transmitter. It is a small 18 pin, 8-bit microcontroller. It generates the 12 kHz signal which is altered and used to drive the oscillating circuit to generate the EM field. The microcontroller generator allows the oscillating frequency to be fine tuned. Six outputs from the microcontroller drive the analog circuitry. A single digital input pin is a trigger from the master computer. An external RC low pass filter debounces the input signal from the master computer.

5.2.2.2 Analog Signal Generation

In order to generate the EM field the microcontroller signal is altered into one that can drive the resonating coil circuit. This circuitry is shown in figure 5-11.

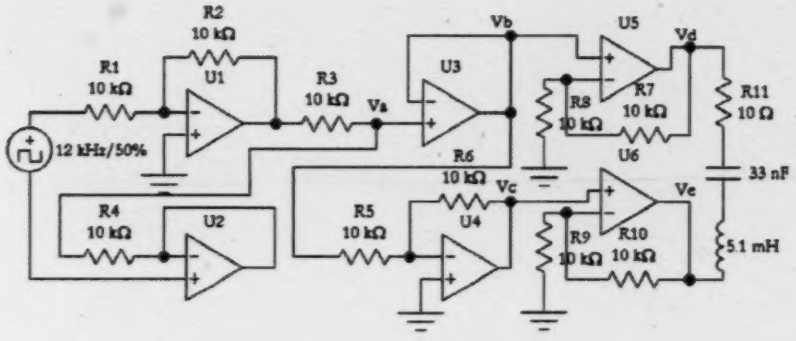

Figure 5-11. Transmitter drive circuit.

The square wave signal generator in figure 5-11 represents the output of the microcontroller. Two output pins, 180 degrees out of phase, each create a square wave signal with a frequency of 12 kHz. U1 is configured as a inverting buffer with a gain of 1. Do to the virtual short at the inverting pin of U2, which is configured as a non-inverting buffer, resistors R3 and R4 act as a voltage divider creating a ±2.5 V square wave at point Va.

Next the single signal is converted into two signals, 180 out of phase, by operational amplifiers U3 and U4. These in turn drive the high current operational amplifiers U5 and U6. These drive the resonating EM field generating circuit. This results in ±5 V switching over the resonant circuit.

Operational amplifiers U1-U4 are LM6132s from National Semiconductor. These are dual low power, rail to rail input and output, small SOIC packaged operational amplifiers. Operational amplifiers U5 and U6 are CLC450s from National Semiconductor. These are small SOT packaged high current output amplifiers capable of 100mA of output to drive the resonating circuit.

5.2.2.3 Transmitting Coils and Circuit

The generation of the EM field utilizes three orthogonal coils which were developed as receiver coils used by [54]. For this thesis these smaller coils were utilized as transmitter coils. These are 1.5 cm hand would coils with a plastic form surrounding a 7 mm ferrite cube from Amidon. Figure 5-12 shows a wound coil form and a coil form that has one of the windings on it.

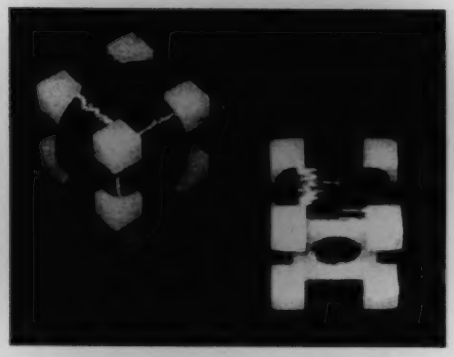

Figure 5-12. Transmitter Orthogonal Coil.

A series LC resonant circuit was chosen to generate the EM field. An LC series circuit is more efficient. By itself an inductor, when driven by a sinusoidal current, stores energy in a magnetic field surrounding the inductor. This means in an ideal case no power is lost in the coil, however, this is not the entire case. Some energy is lost in the coil itself. Also, because voltage leads current by 90 degrees in an inductor there would be a large power loss in the driving amplifier circuit. This is because when zero volts is over the inductor the current is at its maximum value, causing all the power to be dissipated in the driving circuit. A more efficient method is to use a second-order LC circuit where the capacitor is used to store energy.

Choosing a series LC configuration instead of a parallel configuration means that a high current is required to drive the circuit and a low voltage. The resonant frequency is calculated using the same equation as the parallel circuit for the receiver given in equation 5.2. Five hundred turns were hand wound for each of the orthogonal coils. The measured values for one of the coils is 46.2 ohm and an inductance of 5.1 mH. Thus for a 12 kHz resonant frequency, C is calculated to be 34.5 nF.

Two main problems occurred with the transmitter. A printed circuit board problem caused the microcontrollers startup time to be unreliable and random. The characteristics and ratings of discrete parts were changed to overcome a problem that

caused the EM field to initially dip for a few cycles before stabilizing. The final result for the transmitter is shown in Figure 5-13. The 12 kHz 106 Vpp signal is taken from between the series C and L. It shows that the transmitter only takes 5 oscillations, or 390 μs, to stabilize.

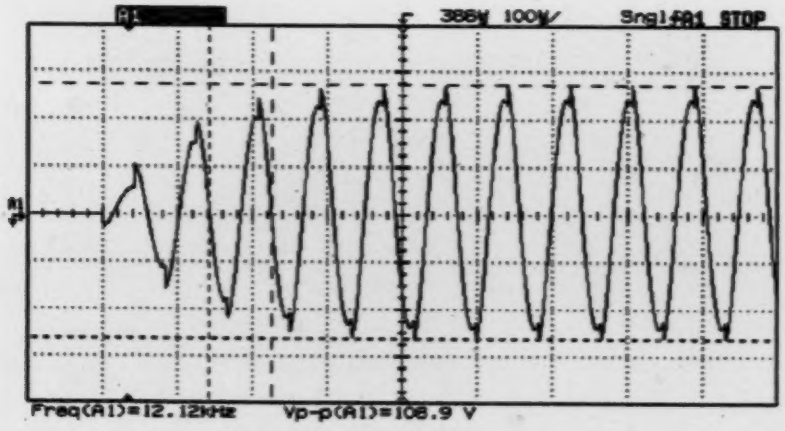

Figure 5-13. Transmitter output.

5.2.3 Master Computer

The master computer is the controller for the entire posture system. For the I^2C network it is the bus master. It synchronizes the system, communicating with the networked receivers and transmitter to facilitate the sampling and collection of the EM and accelerometer information. It keeps time stamped logs of this information and is capable of implementing different algorithms on the data to provide feedback to the patient regarding their posture.

In order to accomplish this, the master computer must have a large amount of non-volatile memory to store the data and to prevent it from being lost. It must be efficient at computations, be able to accurately keep track of time, and be suited to this low power portable application.

To accomplish this a Motorola MC68HC916X1 was used. An existing system was available that could be altered and used for this thesis. This choice was primarily made because the existing system was created by the company funding this work, via the National Research Council's Industrial Research Assistance Program, and they would be the end user of the technology. In addition, because the existing system had already been medically CSA certified, a very costly certification, it was thought this would be the most cost effective device to use.

The microcontroller system met all the requirements desired except it lacked an I^2C peripheral. Thus, an I^2C interface had to be built and an I^2C driver had to be written. The microcontroller has a 16-bit cpu, 2KB SRAM, 2kB block-erasable Flash EEPROM, and 48 KB flash EEPROM. The 5 V microcontroller uses a maximum of 110mA while running and a minimum of 2mA when in low power mode.

The support circuitry consists of a MC68HC68T1 real-time clock (RTC). This devices has a serial three-wire interface that allows the microcontroller to obtain the time (hours, minutes, seconds) and date (day, date, month year) information. This information is saved by the microcontroller for each sample. The RTC generates an interrupt to wake up the microcontroller at a set sample rate.

Battery backed up external 128 K x 16b memory is included for data storage using two 128 K x 8b V62C5181024L-70W SRAM chips from Mosel Vitelic. Another rechargeable battery is used to power the unit and has support circuitry to recharge the device. There are buck and boost converter circuits to create regulated 3.3 V and 5 V power buses.

Figure 5-14 shows the top of the master computer with out a case. Composed of two double layer populated circuit boards the majority of the analog power supply circuitry is on the bottom circuit board. Visible on the top circuit board, is the microcontroller and the battery used to backup the two memory chips, which are located on the bottom of the top board.

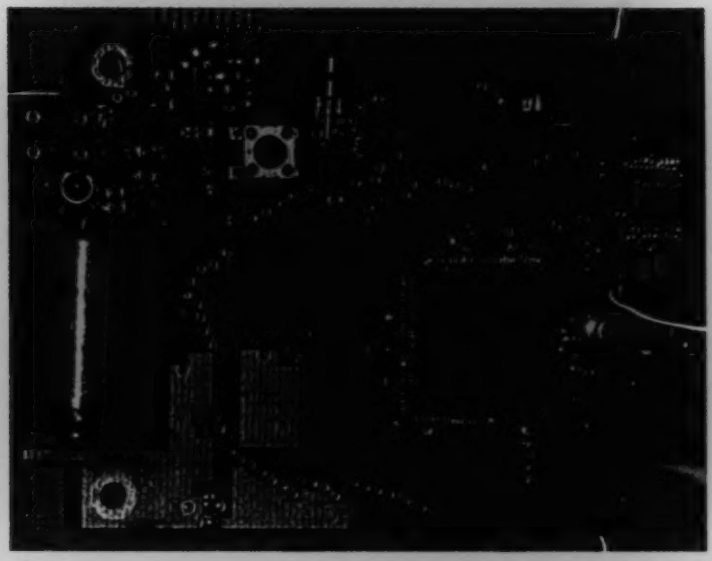

Figure 5-14. Master computer.

The control line to the transmitter is from a totem pole output pin PGP4. Due to noise present during I^2C communication it was discovered that a low pass filter was required on this line to avoid glitches making it to the transmitter. Figure 5-15 shows the interconnect circuitry between the systems. Here the low pass was set to 1 kHz. Open drain outputs were used to connect the master computer to the I^2C bus. Pins PQS4 and PQS5 were connected to the I^2C serial data (SDA) and serial clock (SCL) busses respectively. They are connected through series resistors, which add circuit protection from high voltage spikes and minimize ringing and interference. The bus pull-up resistors are chosen to meet the required current and rise times of the I^2C specification. To calculate the minimum pull-up resistor value a low voltage bus condition of 0.4 V maximum is considered with a required maximum 3 mA sink current. Other factors effecting its selection is the bus capacitance, supply voltage, and number of connected devices. Provided the bus capacitance stays below 400 pF a pull-up resistor can be used. A 1.8 kΩ pull-up was chosen, and 122 Ω used for the series resistors. The rise and fall times were checked to verify operation and compliance.

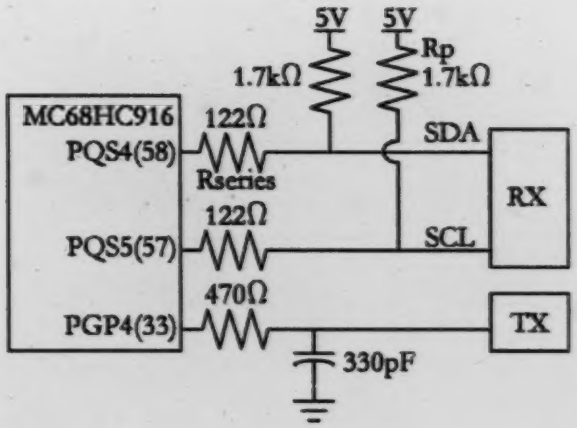

Figure 5-15. System network busses.

5.3 Software Design

Three different pieces of software were written for the three different microcontrollers. The receiver's Microchip PIC16C773 and the master computer's Motorola 68HC916 required the majority of coding all written in assembly language. Assembly was chosen so that the code would be as efficient and as fast possible. In addition there were several time sensitive operations. The code for the transmitter's Microchip PIC16C711 was written in C. This was chosen as an attempt to speed up development and because the code size was not critical.

5.3.1 Receivers

The high level flow chart for the receiver's software is shown in figure 5-16. This provides a general overview of the operation of the receivers. The 4620 lines of assembly code will be summarized for each of the processes listed in the main program flow chart.

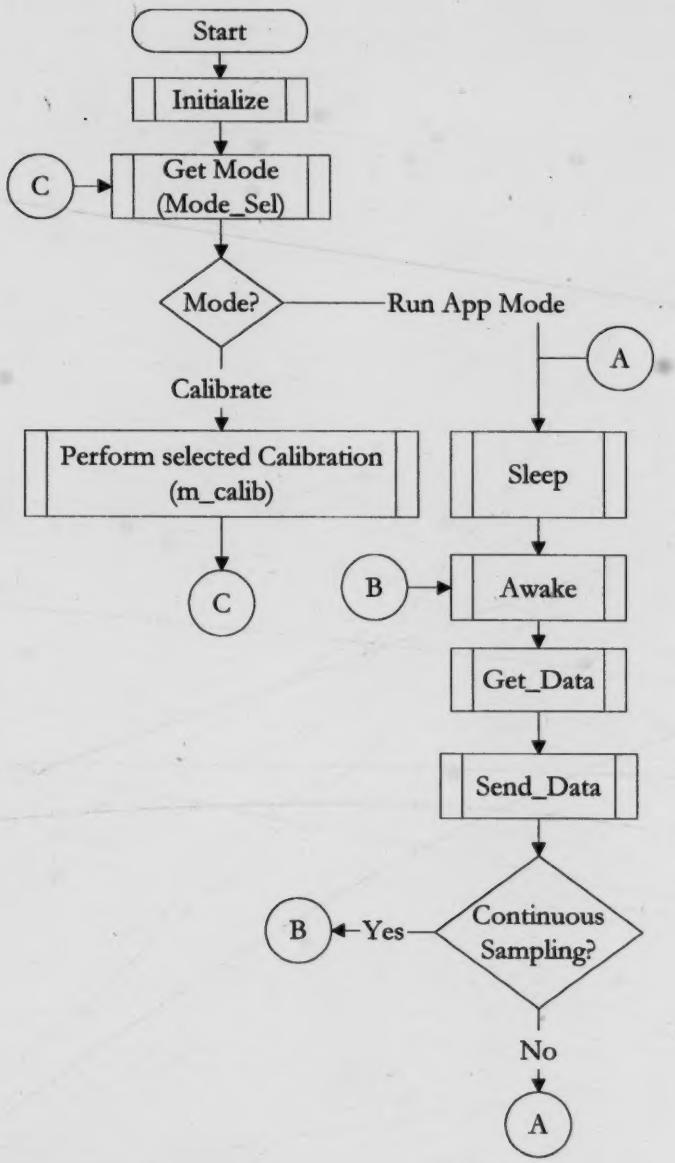

Figure 5-16. Receiver program flow chart.

5.3.1.1 Receiver Initialization Routine

During initial power up the receiver initializes itself. The flow chart for the initialization is shown in figure 5-17. First PORTA of the microcontroller is

configured. This involves clearing its data latches and setting all the pins to digital outputs except for pins A0 and A3. The ADCON1 register is setup to use pin A0 as an analog input pin, which will be used for the ADC. Pin A3 is configured as an analog reference input for the ADC.

PORTB is then configured, first clearing its data latches. Pins B6 and B7 are configured as outputs to control the digital potentiometer. Pin B4 is configured as an output to shutdown the RS-232 transceiver.

Pins C6 and C7 of PORTC are configured for the USART for serial communications. Then the USART is configured for 8 data bit transmission, no parity, asynchronous control, and a speed of 19200 bits per second. Pins C2 and C1 are configured as inputs for the capture module. Pins C4 and C3 are configured for the I^2C bus.

The TIMER2 peripheral is setup for a 2 ms period using pre and post scaling of 4 and 2 respectively. This means that four cycles provide one timer count, and a total of two timer periods are required before an interrupt can be generated. This timer is used for implementing delays in the code. It is also available for resetting the watchdog timer.

The ADC peripheral is setup. The conversion clock is set to 2 μs to allow enough time for a conversion per bit. The total conversion time required is thirteen times the conversion clock. The ADC channel input is set to pin A0.

The 16-bit TIMER1 peripheral is configured to run off the system clock directly. This provides the highest resolution for timing. It is used for timing the digital signals from the accelerometer. Next, the capture modules, CCP1 and CCP2, are setup to capture on the rising edge. Their interrupt flags are cleared. These capture modules are used along with TIMER1 for measuring the accelerometer timing signals. When a capture pin is triggered the capture peripheral stores the value of TIMER1 in its respective registers.

The master synchronous serial port is configured to operate as the I^2C bus. The device is configured as an I^2C slave, and to use 7-bit addressing mode. The receiver's I^2C address is setup.

All the system variables and flags are initialized. Calibration variables for the accelerometers are initialized and are used to calculate other calibration values. Finally all the interrupts are enabled.

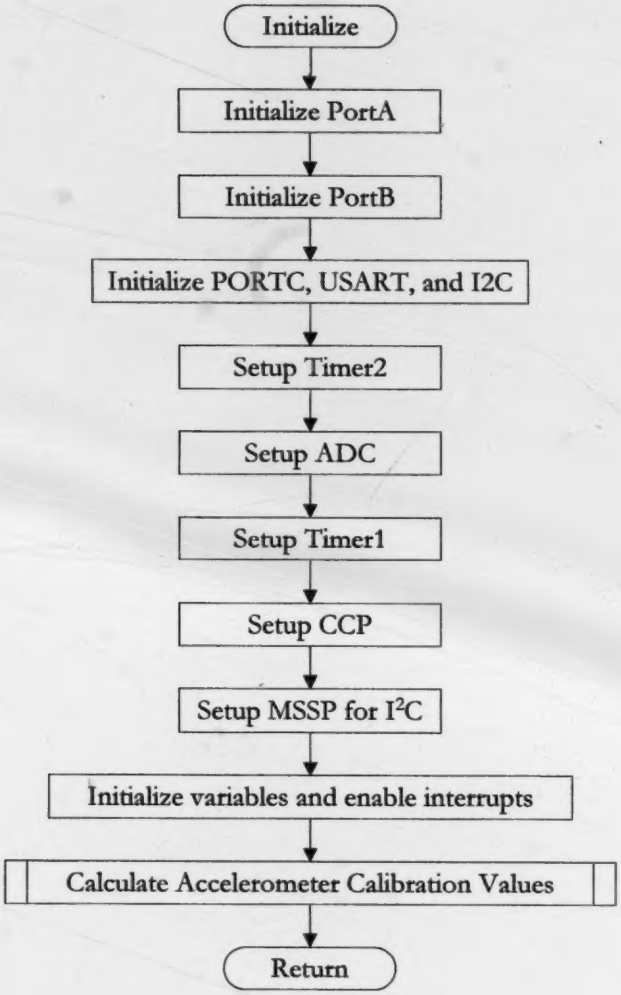

Figure 5-17. Receiver initialization flow chart.

5.3.1.2 Receiver Mode Selection Routine

After initialization the receiver enters a mode selection routine. The program flow for this routine is given in figure 5-18. This function receives information from the master controller communicating what operating mode it should be in. A receive buffer is initialized for I^2C communications then the interrupt is enabled for the I^2C peripheral. The buffer is monitored for an end of message byte. Once this is received the I^2C

interrupt is disabled and the information from the receiver is copied to the appropriate variables in memory, which will be used to determine what the running mode is.

The system operates is either one of three modes. Run mode is the system's normal operating mode. In accelerometer calibration mode the accelerometers can be calibrated. Gain calibration mode allows the gain to be set for the EM signal amplifier. A gain setting is provided along with this mode information.

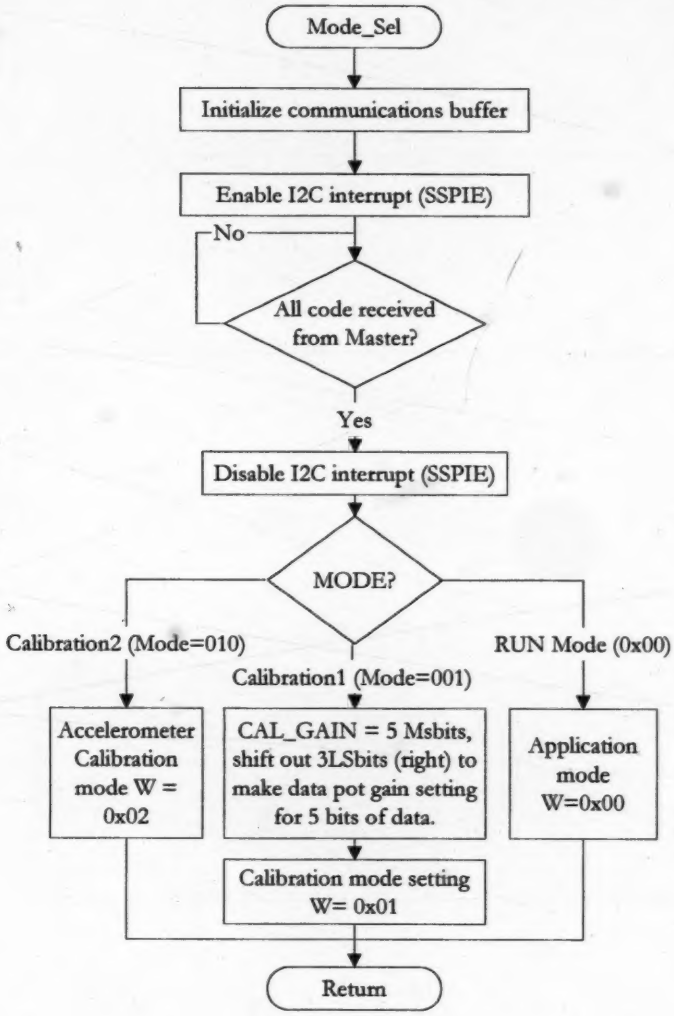

Figure 5-18. Receiver mode selection flow chart.

5.3.1.3 Receiver Calibration Routine

Following the reception of the receiver's mode, the receiver either runs the application or it decides which calibration subroutine to carry out. The m_calib subroutine is called to determine which calibration to carry out. As shown in figure 5-19 either Calibration is called to calibrate the gain setting, or Calibration2 is called to calibrate the accelerometers.

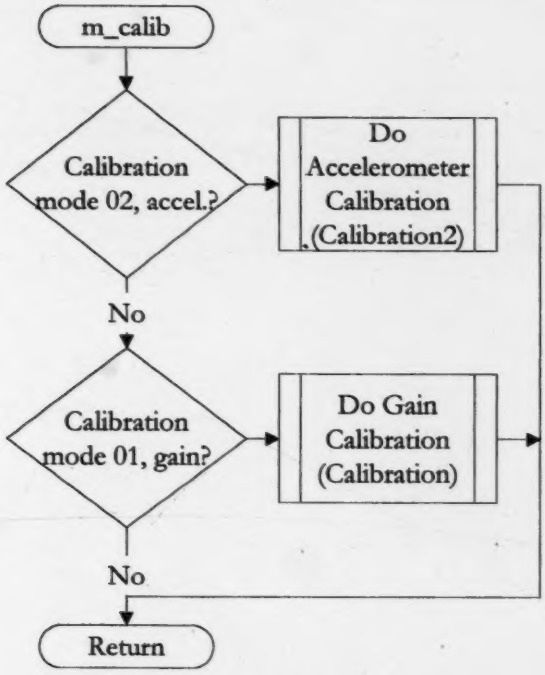

Figure 5-19. Receiver calibration selection flow chart.

If the Calibration subroutine is called the potentiometer is adjusted. The routine initializes the digital potentiometer to its lowest tap position and then increments the tap to the desired gain level utilizing the two control lines.

If the Calibration2 subroutine is called, code is executed to allow the accelerometers to be calibrated. The maximum and minimum pulse width values of the X and Y channels are calculated. While the information is not requested from the receiver, these values are continually obtained, updated, and stored. When a request for the data is received over the I^2C bus, the accelerometer's calibrated period, Tcal, is calculated. It is stored and transmitted back, along with both the maximum and minimum channel values. Finally, four other calibration values are calculated and stored.

5.3.1.4 Receiver Sleep Routine

When the system is instructed to run its application mode code, the first step is to put the receiver to sleep to save power. First, other ICs and peripherals are powered down. Interrupts are disabled to prevent any of them from being serviced after the microcontroller is woken up. Then the I^2C interrupt is enabled and the microcontroller is put into a low power sleep mode.

When it is time for the receiver to start data collection, the master wakes the slave up with an I^2C message. Once the I^2C message is received the receiver will wakeup, acknowledge the master, and continue its code execution without servicing the interrupt. The I^2C peripheral is reset and disabled, the peripherals are turned back on, and the interrupts cleared and reset.

5.3.1.5 Receiver Awake Routine

Once the receiver has been woken up from the power saving sleep mode, it waits for a global multi-receiver command from the master computer to start data collection. This allows for a power up settling time and most importantly allows synchronization of all the receivers. Now all receivers are running and waiting for their queue to start.

5.3.1.6 Receiver Get Data Routine

This subroutine obtains the data from the EM coil and accelerometer, and loads this information into the transmit buffer for the master computer. The flow for this code is given in figure 5-20. Each of the samples that is taken to obtain the received EM field strength from the transmitter's X,Y, or Z coil is obtained from the ADC using the A_D_Conv subroutine. This subroutine takes a chosen number of samples, at a 10 uS interval, and averages them. All of the receivers are synchronized between samplings allowing the transmitter the correct amount of settling time. This is done via global message calls on the I^2C bus that all receivers respond to.

After the EM data is obtained the accelerometer data is acquired. This is performed via the Accel_rtn subroutine. The Accel_rtn subroutine obtains the PWM data from the

accelerometer. The times of the pulses are measured using the Timer1 peripheral with the CCP1 and CCP2 interrupts. A few samples are taken and averaged. The algorithm presented in chapter 4 is used resulting in three 16-bit time variables. The data is stored in a memory array of twelve bytes. The information is then processed, if desired, using the Accel_rtn subroutine. This routine calls a series of subroutines that compute the X and Y channel's acceleration value.

Finally, all the sampled and computed data is stored in big-endian format in memory. The first three 16-bit variables are the X, Y, and Z EM field magnitudes. The next three 16-bit variables are the raw data from the accelerometer. The last two 16-bit variables are the computed tilt angles.

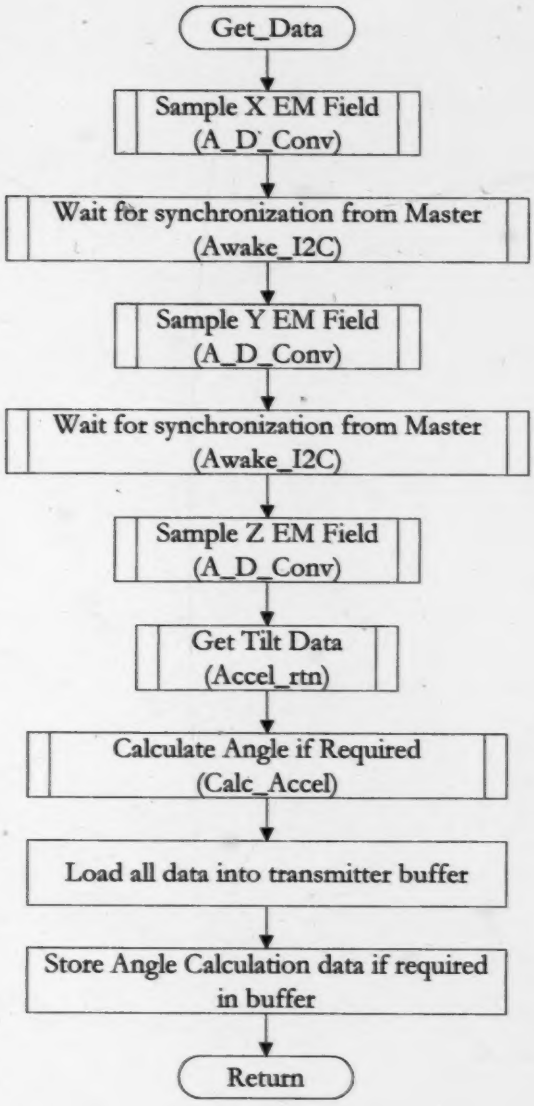
Get_Data
Sample X EM Field (A_D_Conv)
Wait for synchronization from Master (Awake_I2C)
Sample Y EM Field (A_D_Conv)
Wait for synchronization from Master (Awake_I2C)
Sample Z EM Field (A_D_Conv)
Get Tilt Data (Accel_rtn)
Calculate Angle if Required (Calc_Accel)
Load all data into transmitter buffer
Store Angle Calculation data if required in buffer
Return

Figure 5-20. Receiver get data flow chart.

5.3.1.7 Receiver Send Data Routine

After the receiver has completed data acquisition and processing it is ready to transmit the data to the master computer. The receiver configures itself to be ready for an I^2C request and when polled it sends all the information to the master. The subroutine

waits for the interrupt handler routines to complete the transfer because the I^2C communication is completely interrupt driven.

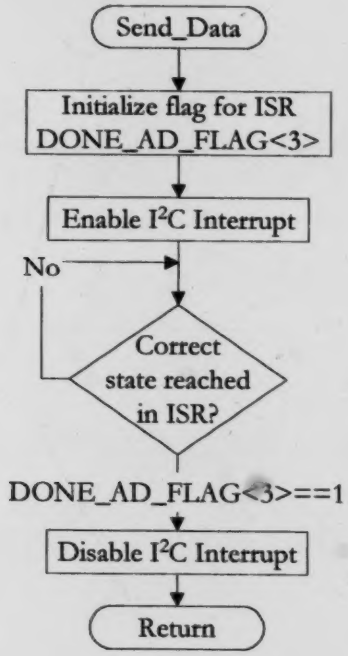

Figure 5-21. Receiver send data flow chart.

5.3.1.8 Receiver Interrupt Service Routine

Interrupts are used extensively throughout the receiver's code to perform time sensitive and asynchronous events. The architecture of the microcontroller uses only one interrupt vector. To determine which service routine to run polling is used. However, both the interrupt flag and the interrupt enable flags must be verified to prevent servicing an interrupt that sets its own flag even when it is disabled. To handle multiple interrupts the polling routine is written in order of precedence.

An overview of the interrupt service routine is provided in figure 5-22. First the interrupt service routine checks what memory bank the microcontroller is in. This allows Bank 0 to be entered to access the working (W) and STATUS registers. The

correct bank to return to is saved in the archived STATUS register. When saving the STATUS register the nibbles are swapped into the storage variable, as opposed to moved, to avoid the possibility of corrupting the Z bit in the STATUS register.

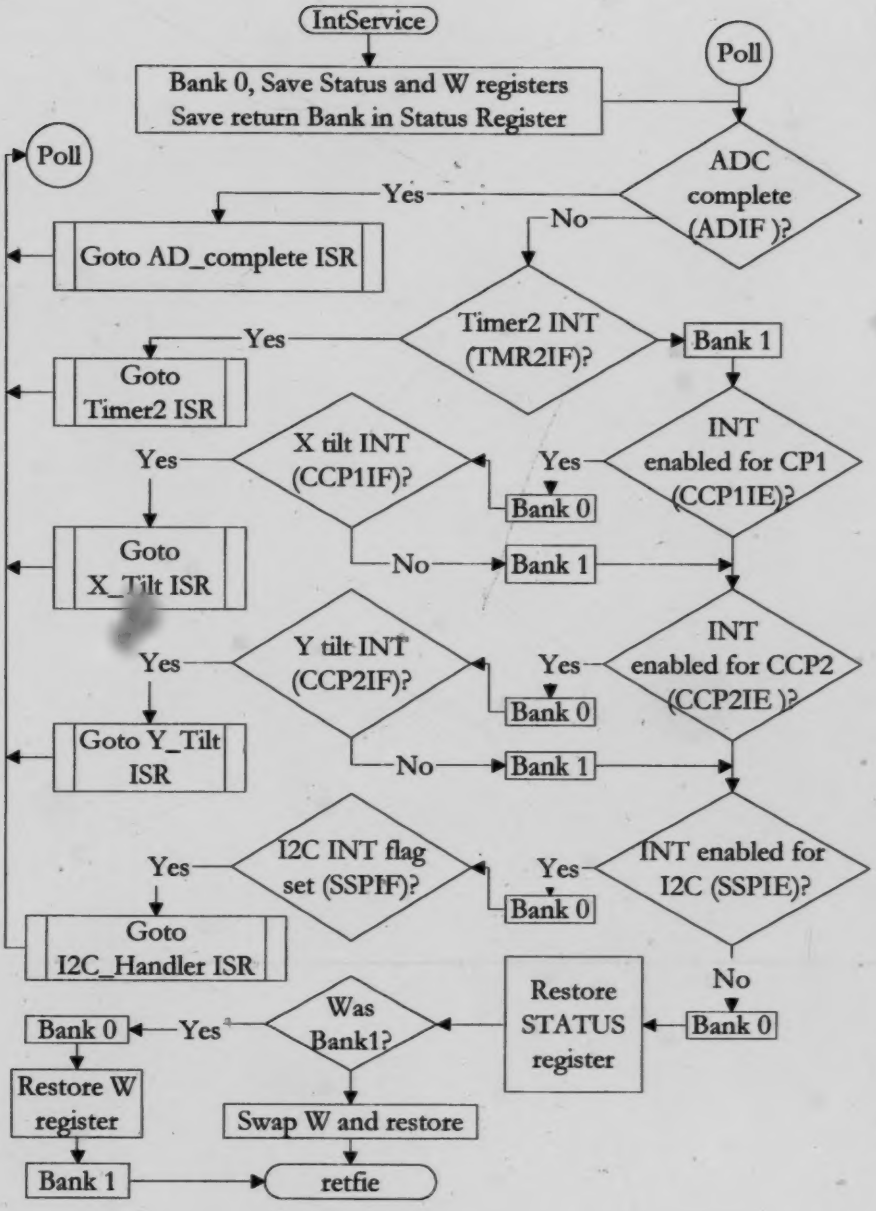

Figure 5-22. Receiver interrupt service routine high level flow chart.

The first interrupt checked is the ADC. If it occurred the interrupt is cleared, a status flag set, and the two byte value from the ADC are stored in memory. The polling routine is entered again to check for other interrupts.

TIMER2 is checked to see if it interrupted. If so, it is cleared and the watchdog timer would be cleared here if required. The polling routine is started again.

The CCP1 and then the CCP2 enables and interrupts are checked. These are interrupts generated by the external pin interfaces to the accelerometer's X and Y axes respectively. Both of these handlers clear the interrupt, set a status flag, and store the two byte TIMER1 value in memory.

The last interrupt enable and flag checked is for the I^2C communication bus. This interrupt is triggered by the MSSP peripheral during an I^2C transfer. A state machine is used to perform the I^2C communication's operations. The state machine determines what event occurred on the I^2C bus from the SSPSTAT register. The six states occur as follows.

The first state detects that the master is writing and the last byte received was an address. In this state the I^2C buffer and its index are setup so that the peripheral is ready to receive data. State 2 detects if the master is writing and the last byte was data. In this state the byte is copied into the buffer, the buffer flag is cleared, and the index incremented. The buffer size is checked to ensure it does not overflow. If it is full the buffer is reset. State 3 detects that the master is reading and that the last byte received was an address. The transmit index is initialized and the first byte from the transmit buffer is sent to the master, then the index is incremented. State 4 occurs when the master is reading and data has been sent to it. First the transmit buffer size is checked to ensure it is not exceeded. A byte is sent to the master followed by incrementing the buffer index. State 5 occurs when the master does not acknowledge the slave thereby terminating the I^2C communication and resetting the slave. A flag variable is set for functions that monitor the I^2C state. State 6 was created because of a possible error

that can occur when a stop command is issued on the I^2C bus before an interrupt has time to capture the SSPSTAT register. This condition could occur during servicing state 2 if the master quickly issues a STOP after it has sent its last data byte to the receiver. This state checks if state 2 code should have run, if it did not there is an error. One method to overcome this is to add delay before STOP commands are sent.

5.3.2 Transmitter

The transmitter is synchronized by the master computer. The transmitter monitors its input from the master computer and sequentially generates the three orthogonal fields. Figure 5-23 shows the flow chart for the transmitter.

Transmitter initialization consists of configuring PORTB[6:0] as logic low outputs with no internal pull-ups. These pins are used to generate the signal to drive the coil. PORTB[7] is configured as a digital input to receive the control signal from the master computer.

Software debouncing is used on this input due to the discovered need to remove glitches caused by the I^2C bus. The signal is monitored for a logic high. Once triggered, the transmitter generates the 12kHz pulse for the X axis coil. Two pins are driven 180 degrees out of phase. If a logic low is detected from the master, the transmitter continues one more oscillation then verifies the logic low signal is still present. If it is low, the X coil outputs are zeroed and generation starts for the Y coil. This process is repeated for the Y and Z coils.

The generated assembly code from the C source code had to be traced through to obtain the correct timings. This is because the timing for the 12 kHz signal generation can not be altered while performing debounce checks. Thus where appropriate, no operation (NOP) instructions were inserted to ensure the same delay times for the loops regardless of the results of the logical glitch tests. This is because an assembly test instruction results in a different number of execution cycles depending if it resolves as true or false.

Later this code was completely rewritten using assembly, counters, and interrupts to allow greater flexibility. Interrupts ensure the event times, thereby allowing code changes with out worrying about effecting the loop timing. In addition, this aids easier expansion to utilize the I^2C bus with the transmitter. Although this code was fully tested, which included testing the sleep mode and its operation with the system, the original code presented was used for this thesis.

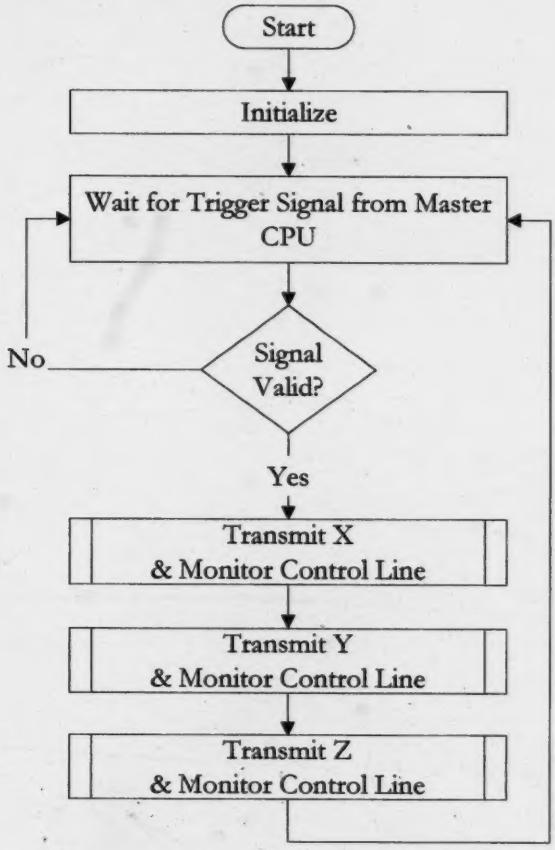

Figure 5-23. Transmitter flow chart.

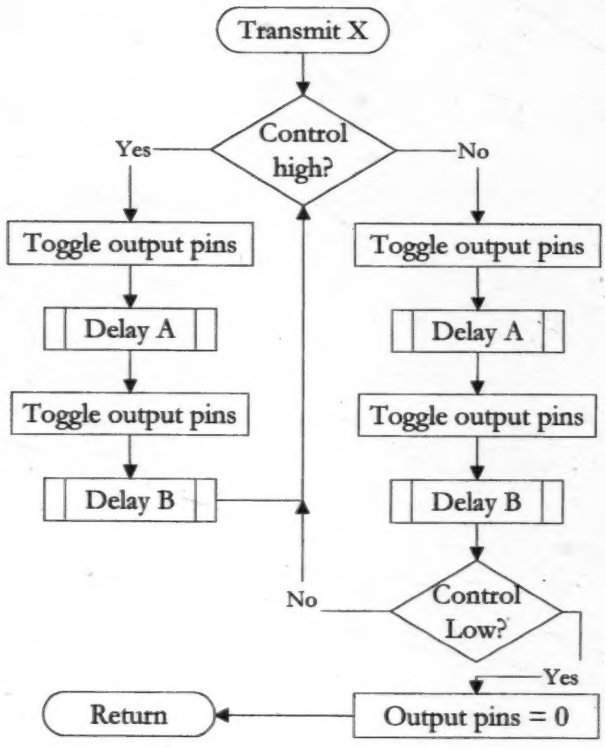

Figure 5-23. Transmitter flow chart (continued).

5.3.3 Master Computer

The software for the master computer was written using Motorola's assembly language for the 68HC16 microcontroller. The high level flow chart is given in below.

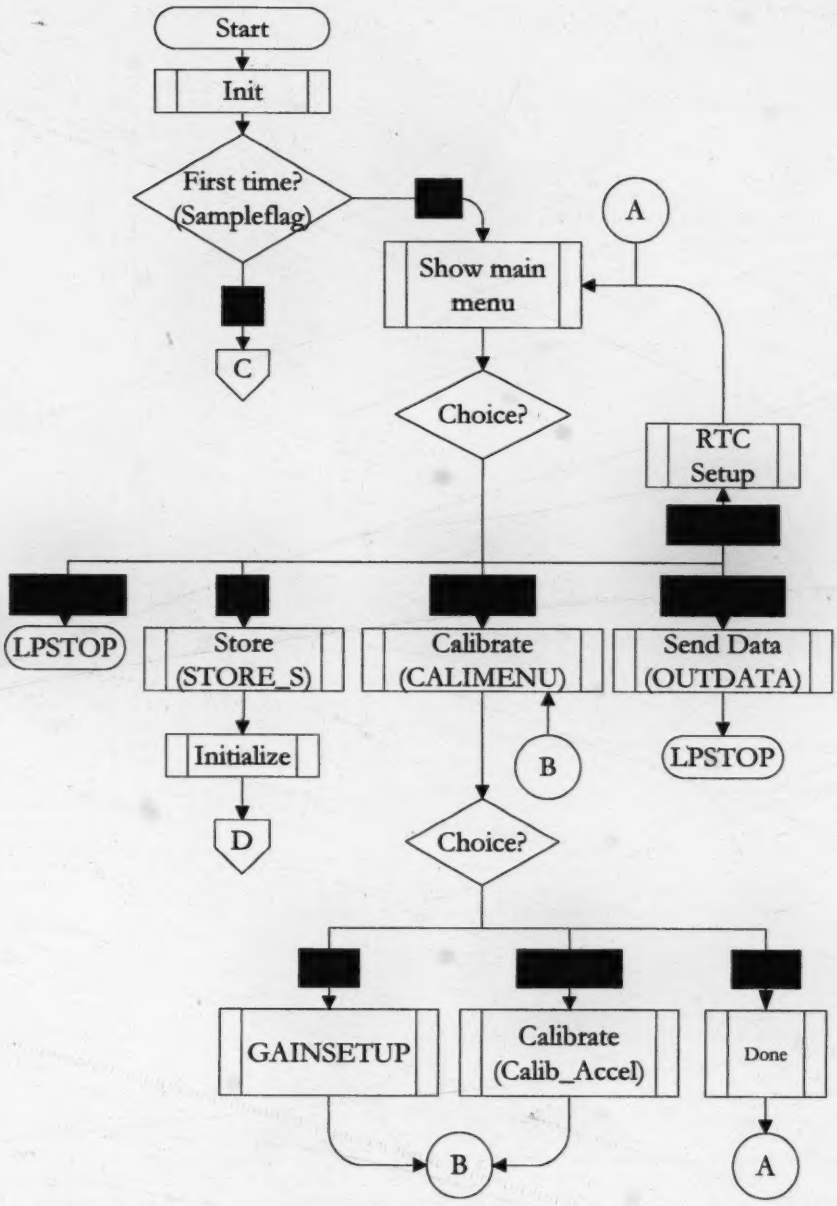

Figure 5-24. Main computer high level flow chart.

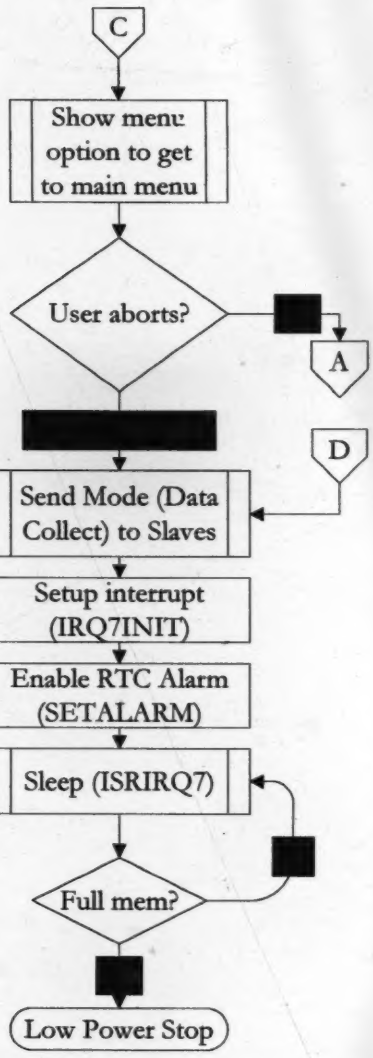

Figure 5-24. Main computer high level flow chart (continued).

5.3.3.1 Initialization

At power up the microcontroller is initialized. This involves configuring internal and external peripherals and memory. Care must be taken when addressing memory and registers. An extension field nibble is concatenated to form a 20-bit address. The external RAM was mapped from $40000 to $7FFFF, and internal RAM was mapped

from $8000 to $87FF. Internal memory is used for variable storage and the system stack. External memory is used for storing application data. Both memories are battery backed up. Interrupts and all communication buses are configured.

5.3.3.2 Configuration

After initialization the system determines if it has already been configured. If it is starting again after having already been configured and collecting data, it gives the user an option to access the control menu. However, if no input is received it continues with system operations from where it left off. If it is the first time the system is turned on a control menu is presented to the user. If an option is not selected the system will shut itself down and enter the low power stop mode. The menu choices are to set the real time clock (RTC), to calibrate the system, to start the system running, or to download the data.

When the user chooses to setup the RTC they are prompted to enter the time, date, and sample time for the system. This time is stored with each sample acquired. The user is then returned back to the main menu.

If calibration is selected the user is prompted to either calibrate the receiver's accelerometer or to set the receiver's gain. When calibrating the accelerometer the user is instructed on what actions to perform to complete the calibration. This allows the calibration values of the accelerometer to be determined. The gain calibration asks the user for the receiver's address and its respective gain.

When calibrating either of these, the system communicates to the receivers individually using the I^2C bus. Due to the lack of an I^2C peripheral on this microcontroller the entire protocol had to be written resulting in an 1800 assembly line I^2C driver.

The option to download the system data allows the clinician to obtain the collected information from the system. The entire external memory is sent to a personal computer via an RS-232 serial port. The format is an ASCII text file. Each line

contains the date and time the sample was obtained followed by each receiver's data. Each receiver's data consists of first the received EM signals, then the raw accelerometer's data values, then the calculated X and Y tilt angles.

5.3.3.3 System Operation

The final option for the user to select is the system run mode. This mode resets the memory so previous data is over written. A flag is set that is used to determine if the system was already running in this mode. If after a system reset this flag is detected execution continues from this point.

The master computer communicates the current operating mode to the receivers. Then it enables the interrupt that is triggered by the RTC. Next it enters into a low power sleep mode. The system is awoken when the RTC interrupt occurs.

The interrupt service routine first synchronizes the receivers and transmitter through the sampling of the transmitted X, Y, and Z fields. After this the receivers will acquire their tilt data. Via the I^2C bus, the master will read back each receiver's data and store it in memory along with the time and date the sample was obtained.

After the interrupt hander finishes the amount of memory left is checked. Provided the memory is not full, the system enters the low power sleep mode again, and waits for the next interrupt. If the memory is full the system will turn itself off.

6 RESULTS AND DISCUSSION

This chapter presents the test methods, results, and discussion for the posture monitoring system.

6.1 Test Methods

The system was tested to determine the performance characteristics of the system and sensors, and thus its ability to detect postural and scoliotic specific features. Each of the test methods is presented here.

6.1.1 Angle Detection Test Methods

The system utilizes both electromagnetic sensors and accelerometers to measure angles. Specifically the accelerometers are used to obtain tilt angles in 2D. An electromagnetic sensor can be used to measure a rotational, or yaw, angle. The methods used to test both of these angle sensors follows.

The system's accelerometer angle measurements were evaluated using several different tests. First the stability of the system's angle measurements was tested. Samples were obtained using a 10ms sampling period. A range of 122 to 983 samples were taken for each test while the accelerometers were fixed at a stationary position and angle. The test was performed at approximately 0, 20, 60, and 80 degrees. This provides the variance of the static tests as a standard deviation from the average value.

---

[1] Material in this chapter has been published in: M. Bazzarelli, N. Durdle, E. Lou, J. Raso, D. Hill, "Physiotherapeutic scoliotic treatment using networked MEMS and EM sensors", in *International Research Society of Spinal Deformities Symposium 2004*, Vancouver, BC, 2002, pp. 166-169 and in: M. Bazzarelli, N. Durdle, E. Lou, V.J. Raso, "A wearable computer for physiotherapeutic scoliosis treatment", *IEEE Transactions on Instrumentation and Measurement*, issue 1, vol. 52, pp. 126-129, February 2003

The repeatability of the angle measurements was obtained by securing the sensors to a balanced beam. The beam was fixed at an arbitrary angle and a measurement was taken. The beam was then moved and returned back to its original at rest position and another measurement was taken. The process was repeated. This experiment checked for static repeatability error and repeatability between sensors.

To test the accuracy of angle measurements from the accelerometer sensors, a test device was built. It consisted of a plumb line and a protractor fixed to a tiltable platform. Using fluid filled levels the platform was leveled off and the protractor was adjusted so that the plumb line corresponded with zero degrees. The plumb line is a metal thread the width of the protractor's markings. The protractor has an accuracy of ± 0.25 degrees. The sensors are mounted on the platform. Adjusting the platform produced an angle between the platform's protractor and the earth's gravitational field vector or plumb line. This provides the true tilt angle of the platform. To obtain an overview of the tilt measurements, one degree increment measurements were taken from a range of 0 to 90 degrees. To obtain accuracy and repeatability measurements, incremental 10 degree samples were taken in the 0 to 90 degree range. Starting at 0 degrees one sample was taken, then consecutive samples at 10 degree increments were taken until 90 degrees was reached. Direction was reversed and a sample was taken at 10 degree intervals back down towards 0 degrees. This was repeated ten times.

An additional resolution test was performed for the accelerometer tilt measurements. At increasing 10 degree intervals, measurement groupings of 0.5 degrees were taken. For example 9.5, 10, and 10.5 degrees measurements were taken followed by 19.5, 20, 20.5 degrees. A sample size of ten was used for each angle.

The EM systems were tested to determine their performance characteristics. First the receivers were tested to evaluate the stability of the circuitry that measures the EM field strength. This includes the gain circuit, filter circuit, RMS to DC circuit, and analog to digital conversion circuit. Using an HP33120A signal generator, a 100mVpp

12.3 kHz AC signal was coupled directly to the receiver's EM sensor input. The system collected 215 samples over an hour time frame to determine the system's stability. Finally, with the receivers and transmitter in fixed positions, a closed loop system test was performed over a five hour interval, with a sample rate of one minute.

A test jig was constructed to test the accuracy of detecting angles using the EM system, in particular for measuring yaw angles. The device, shown in figure 6-1 consists of a machined 18 cm diameter acrylic protractor disc that rotates in a machined acrylic base. The receiver's sensing coil is attached to a moveable bracket on the disk to center the coil on the test jig. Using a shelved acrylic box, the entire test jig was mounted above the transmitter coil to simulate the location of the sensor's position as it would be worn by a patient.

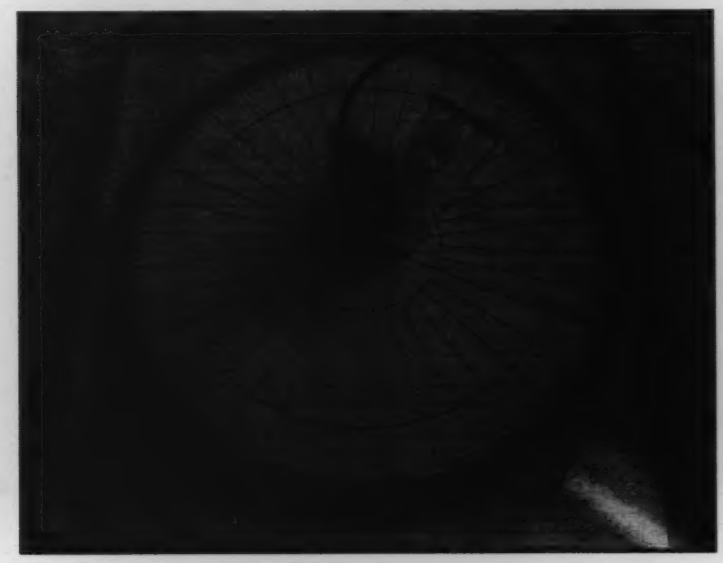

Figure 6-1. EM rotational test fixture.

To obtain an overview of how the EM system operates, tests were performed using rotational yaw movements with the sensors located in different locations in space. A receiver was placed 30 cm above the transmitter to simulate a receiver located on the

thoracic spine, and one was placed to the left of this receiver to simulate a placement on the left shoulder. This provided a useful intuitive reference to how the coupling works with the EM sensors, and a verification of the system in general. In addition it aids with deriving tests that can be created, depending on the required movement or position to be tracked.

To test the accuracy of the system, measurements were made at 10 degree intervals with a receiver located vertically above the transmitter. By calibrating to the maximum received signal, the angle can be calculated from the arcsine or arccosine of the received normalized EM signal. This is because the voltage induced in the coil is proportional to the angle the lines of flux make with the coil. Thus, depending on the orientation of the coils when they are mounted, one can determine if an arcsine or arccosine is used.

Additional resolution tests of the system were performed to check the system's ability to measure changes in angle of 0.5 degrees. Using the same test apparatus developed for the accuracy measurements, five angles were chosen in the range of 0 to 50 degrees. At each of these angles, nine consecutive 0.5 degree angle measurements were taken. For example, 9.5 was measured followed by 10, 10.5, 11, 11.5, 12, 12.5, 13, and 13.5 degrees.

6.1.2 Distance Test Methods

The EM measurement system was tested to verify it could measure and produce an EM field. Ideally this EM field would mirror an ideal dipole field and the magnitude of the field would decrease proportionally to the inverse cube of the radius. A single receiver was a tested for its ability to measure the field in one dimension. If data is obtained from two receivers with their coils mounted orthogonally, a radius in three dimension could be obtained using the algorithm by Paperno [23].

A test jig, shown in figure 6-2, consists of a positionable plastic U-shaped block that straddles a wooden board. The transmitter is placed at one end of the board and the

receiver coil is mounted on the moveable plastic block. This allows the receiver coil to be moved in a controlled fashion a fixed radius from the transmitter.

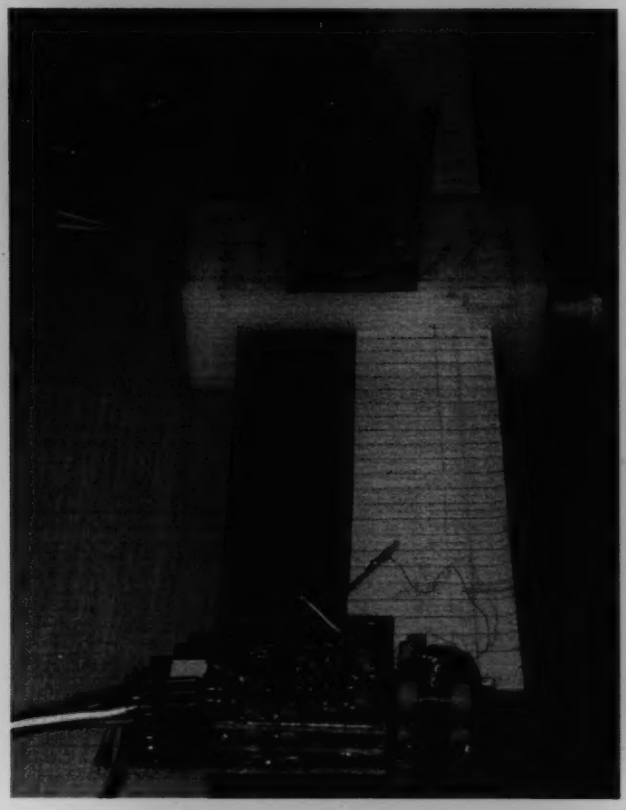

Figure 6-2. EM distance test fixture.

First, repeatability was tested. This was performed by moving the receiver through three different distance measurements of 28, 33, and 38 cm. At each distance five measurements were taken. This process was repeated four times.

To test the accuracy of the distance measurement, first the EM system was calibrated. Then seven points were chosen at random by moving the receiver an unknown distance. Ten sample points were taken at each random point and the distance to that position was marked and measured using a digital calliper.

6.2 Test Results

6.2.1 System Accelerometer Angle Measurement Stability Test Results

The static acceleration computed by the system for the X axis has an average standard deviation of 0.0023 g over the measurable sensor range of ± 90 degrees. The precision, or significant digits, of the system is 0.001 g. Taking the arcsine of 0.001 g gives an angle of 0.057 degrees. The distribution of the results are close to a normal distribution allowing the Empirical Rule to be used and thus ±2 standard deviations contain 95 percent of the measured values. The standard deviation ranges from 0.0022 g to 0.0026 g over the 0 to 90 degrees range as shown in figure 6-3 which illustrates the standard deviation measurements over a range of angles from several tests for one receiver's X axis. The average standard deviation for the Y axis is 0.0022 g.

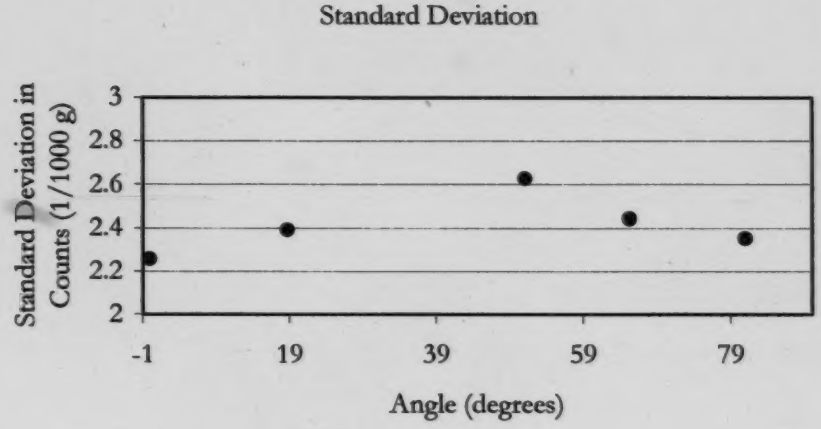

Figure 6-3. Standard deviation.

The error in the angle in degrees is not constant and increases towards ± 90 degrees. This is due to the nature of the arcsine function and the precision of the system. As 90 degrees is approached, smaller changes in magnitude produce a larger variation in the corresponding angle. Increasing error is depicted below in figure 6-4 showing the

round-off error that occurs in the arcsine function due to the standard deviation as 90 degrees is approached. The graph was constructed by: computing the theoretical count value, rounding to the same precisions as the system, adding a standard deviation, converting back to an angle in degrees, and finding the error. A comparison of actual measured error values is presented in table 6-1. They are close to the given theoretical error values.

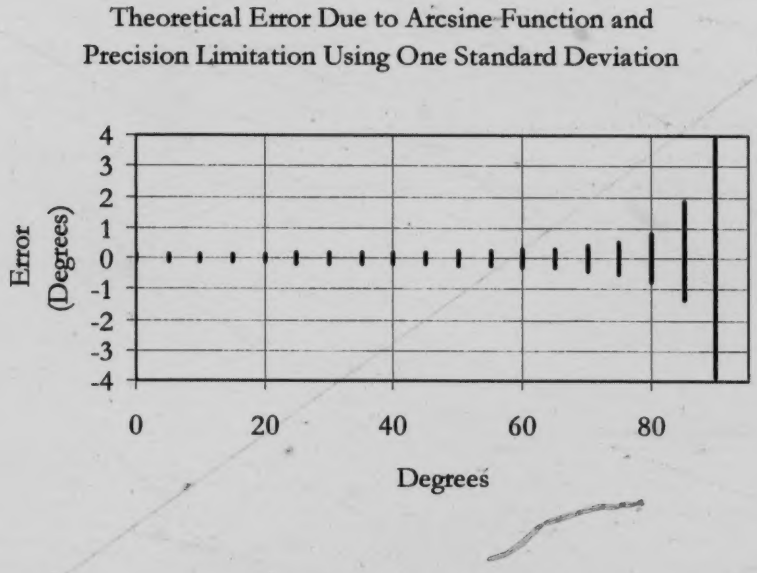

Figure 6-4. Theoretical angle error.

Comparison of Measured and Theoretical Error Using One Standard Deviation

Mean Angle (Degrees)	Measured Error (Degrees)	Theoretical Error (Degrees)
-0.09	0.129	-0.132/+0.132
18.7	0.145	-0.139/+0.139
51.05	0.239	-0.209/+0.210
65.28	0.335	-0.313/+0.317
80.96	0.882	-0.803/+0.881

Table 6-1. Actual and theoretical error comparison.

6.2.2 System Accelerometer Repeatability Test Results

The average standard deviation in the repeatability test for the X axis is 0.0023 g which is the same as the static tests. The Y axis standard deviation was 0.0019 g. The tests were carried out for the X axis at 9.8, 76.4, -14.2, and -73.6 degrees. The standard deviation for each test is given in table 6-2. The repeatability error of 0.002 g was the same between different accelerometer sensors and receivers.

Repeatability Test Standard Deviation

Mean Angle (Degrees)	Standard Deviation (g)
9.8	0.0025
76.4	0.0021
-14.2	0.0022
-73.6	0.0022

Table 6-2. Repeatability test.

6.2.3 System Accelerometer Accuracy Test Results

A strong positive correlation of 0.999 is obtained from the acceleration data for the tilt angles of the accelerometer at 1 degree increments from 0 to 90 degrees in Figure 6-5.

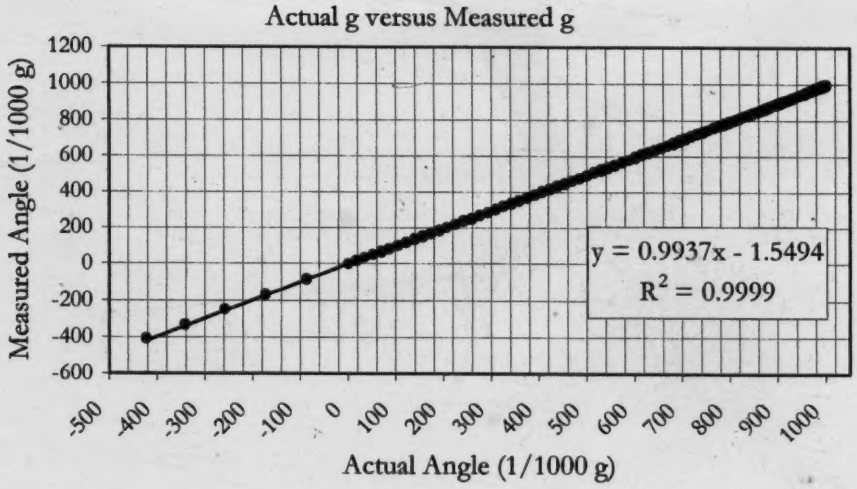

Figure 6-5. Accelerometer acceleration data.

Table 6-3 lists a range of mean absolute errors and standard deviations for the static acceleration data obtained by repetitively sampling the 0 to 90 degree range in 10 degree intervals. The absolute error ranges from -0.014 g to 0.002 g and has a mean absolute error of -0.005 g with a standard deviation of ± 0.002 g.

System Acceleration Data Accuracy Ten Degree Increments

Actual Angle ±0.25 (Degree)	Actual Angle ± Error (1/1000 g)	Measured Mean Angle ± SD (1/1000 g) (n=20)	Mean Absolute Error ± SD (1/1000 g) (n=20)	Percent Error (%)
0	0 ± 9	0 ± 1.34	0 ± 1.34	-
10	174 ± 9	171 ± 2.27	-2 ± 2.27	-1.35
20	342 ± 8	338 ± 2.18	-4 ± 2.18	-1.26
30	500 ± 8	492 ± 2.61	-8 ± 2.61	-1.58
40	643 ± 7	634 ± 1.6	-8 ± 1.6	-1.30
50	766 ± 6	759 ± 1.6	-7 ± 1.6	-0.87
60	866 ± 4	858 ± 2.5	-8 ± 2.5	-0.90
70	940 ± 3	933 ± 2.04	-6 ± 2.04	-0.69
80	985 ± 2	979 ± 1.54	-6 ± 1.54	-0.63
90	1000 ± 0	997 ± 2.46	-3 ± 2.46	-0.34

Table 6-3. Acceleration data analysis.

The arcsine of the static acceleration provides the tilt angle in degrees. However, it introduces more error as 90 degrees is approached due to the system's three decimal place precision for static acceleration. The error in g, as given in table 6-3, contributes greater to the error as 90 degrees is approached. Thus an error in g is more tolerable at lower angles. Table 6-4 lists the absolute mean error over the 0 to 90 degree range. The theoretical error due to the precision of the static acceleration using three standard deviations (3SD) is also given as a comparison to show that the system performs within the expected error.

Accuracy of System Tilt in Degrees Ten Degree Increments

Actual Angle ±0.25 (Degree)	Measured Mean Angle ± SD (Degrees) (n=20)	Absolute Mean Error ± SD (Degrees)	± Theoretical Error Due to Rounding in g Value (Degrees) (using 3SD)
0	-0.01 ± 0.08	-0.014 ± 0.077	0.395
10	9.86 ± 0.13	-0.137 ± 0.132	0.402
20	19.86 ± 0.13	-0.263 ± 0.133	0.421
30	29.48 ± 0.17	-0.521 ± 0.172	0.458
40	39.38 ± 0.12	-0.624 ± 0.119	0.518
50	49.41 ± 0.14	-0.588 ± 0.141	0.619
60	59.12 ± 0.28	-0.867 ± 0.279	0.800
70	68.9 ± 0.32	-1.058 ± 0.324	1.19
80	78.13 ± 0.43	-1.867 ± 0.431	2.616
90	85.9 ± 2.47	-4.102 ± 2.475	6.735

Table 6-4. Accelerometer angle error.

6.2.4 System Accelerometer Resolution Test Results

The system's average standard deviation is 0.0023 g; this is the system resolution. This test confirmed this value giving an average standard deviation of static acceleration of 0.0021 g. Taking the average of the maximum static acceleration measurements over the operational range, gives 0.0066 g.

As the upper 90 degree limit is approached the resolution in degrees becomes greater due to smaller changes in the static acceleration values between equal angle increments. Table 6-5 shows this. For example, the average standard deviation around 0 degrees is 0.1 degrees of resolution with the maximum range of data between ±0.2 degrees. At 60 degrees, the average standard deviation has increased to 0.25 degrees and the maximum range of data has increased to +0.4 and -0.5 degrees.

Change of Accelerometer Resolution in Raw Data and Degrees

Actual Angle ± 0.25 (Degrees)	Mean Measured Angle ± SD (1/1000 g)	Mean Measured Angle ± SD (Degrees)	Measured Range (1/1000g)
-0.5	-7.2±2.57	-0.4 ± 0.15	8
0	0.2±0.63	0 ±0.04	2
0.5	8.64±1.75	0.5 ± 0.1	6
9.5	165.55±1.81	9.5 ± 0.11	6
10	173.55±2.70	10 ± 0.16	10
10.5	183.00±1.55	10.5 ± 0.09	4
19.5	332.55±2.34	19.4 ± 0.14	9
20	340.91±2.70	19.9 ± 0.16	8
20.5	350.73±1.85	20.5 ± 0.11	6
29.5	490.18±1.40	29.4 ± 0.09	4
30	496.18±2.27	29.7 ± 0.15	8
30.5	504.91±1.64	30.3 ± 0.11	6
39.5	631.91±1.58	39.2 ± 0.12	4
40	639.27±2.05	39.7 ± 0.15	6
40.5	645.27±3.26	40.2 ± 0.24	10
49.5	756.09±1.87	49.1 ± 0.16	6
50	762.45±1.57	49.7 ± 0.14	4
50.5	768.64±2.34	50.2 ± 0.21	8
59.5	859.36±1.69	59.2 ± 0.19	6
60	864.18±2.23	59.8 ± 0.25	8
60.5	867.91±1.7	60.2 ± 0.2	6
69.5	936.18±2.09	69.4 ± 0.34	6
70	939.45±2.54	70 ± 0.43	8
70.5	942.18±2.09	70.4 ± 0.36	6
79.5	984.55±2.38	79.9 ± 0.77	8
80	984.91±2.74	80.1 ± 0.94	8
80.5	988.55±2.38	81.4 ± 0.91	8

Table 6-5. Change of accelerometer resolution.

Figure 6-6 shows nine groups of angles plotted. Each group consists of 3 angles 0.5 degrees apart. For example 9.5, 10, and 10.5 degrees make up one group. The error bars indicate the average standard deviation of each set of measurements. This shows

the relationship of the resolution for each group over the range of degrees. For example, at 60 degrees it can be seen that the resolution of 0.5 degrees is undecipherable because the errors, or standard deviations, overlap. This graph also provides another look at the accuracy of the system. Ideally the second data point of each group of three should be centered at zero. However, any deviation from this is an error in accuracy of the system and the test method. The initial deviation in accuracy is acceptable and within the experimental error, however the larger deviation towards 90 degrees is the accuracy error as previously explained in the accuracy section.

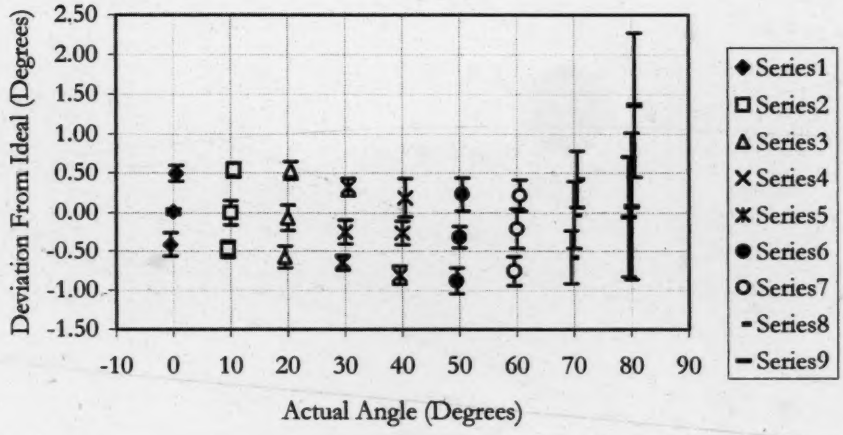

Figure 6-6. Accelerometer resolution measurements.

6.2.5 System Electromagnetic Stability Test Results

The receiver's EM circuitry has standard deviations of 1.7, 1.5, and 1.6 counts for the received X, Y, and Z channels, respectively. For the full scale analog signal conversion there are 4095 counts in a 3.0 V range. If the sensor's full scale value is 3 V then a deviation of 1.7 counts corresponds to a voltage of 1.2 mV or 3.39 mVpp of signal voltage after gain. The received signal magnitude relative to the angle at which the flux cuts the receiver's coil, is proportional the absolute value of a sinusoid. This means that the resolution will provide different accuracies depending if you are near zero or

near 90 degrees. That is because there is less change in signal magnitude near 90 degrees. Figure 6-8 shows this clearly and is elaborated on later.

For the five hour closed loop test the standard deviation of each received channel is given in table 6-6. The data were obtained after a fixed settling time. This settling time requirement was discovered when tests were done using faster sample periods. It was observed that the EM field was dropping a considerable amount and was dependent on the sample rate of the system as shown in figure 6-7. The fast sample rate has a larger signal drop from an initially larger EM field reading. The settling times were similar.

Receiver Channel	X1	Y1	Z1	X2	Y2	Z2
Standard Deviation (Counts)	3.6	3	3.3	3.3	1.6	2.2

Table 6-6. Five hour EM standard deviations.

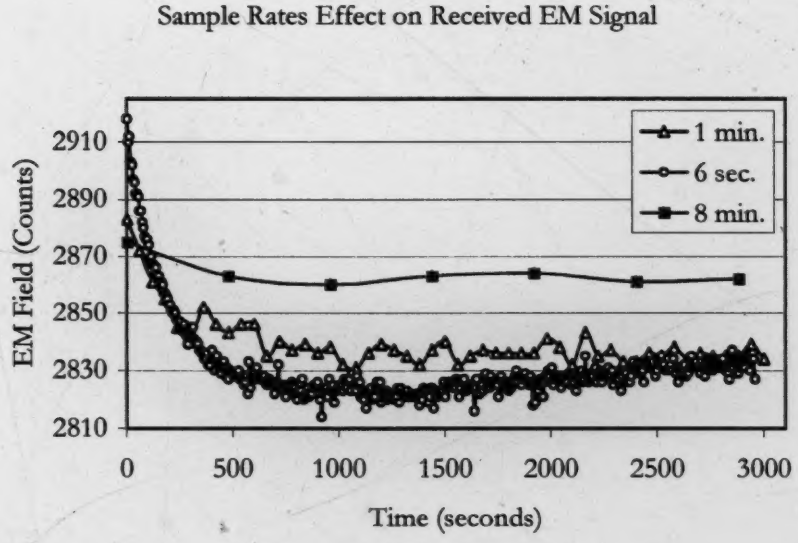

Figure 6-7. Sample rate effect on droop and settle time.

Debugging this EM field generation problem was a lengthy process. It was found that the resonant frequency of the RLC circuit was shifting up depending on the amount of current in the RLC circuit. However, this observation and the way it masked itself as a thermal problem, due to core and copper losses, was not actually the cause. The final solution was to replace the capacitors in the RLC circuits with 400V metallized polyester capacitors, with a low equivalent series resistance (ESR) rating. After fixing the transmitter, its field strength increased approximately by 1.4 times and the field was steady regardless of the sample period.

6.2.6 System Electromagnetic Angle Accuracy Test Results

Figure 6-8 shows the results obtained from a preliminary EM system overview test. Sensors were located to simulate a left shoulder position and a position vertically above the transmitter on the thoracic spine. The sensors were rotated to confirm system operation and gain further insight into the field coupling. The signals were as expected and they aided in visualizing the EM system.

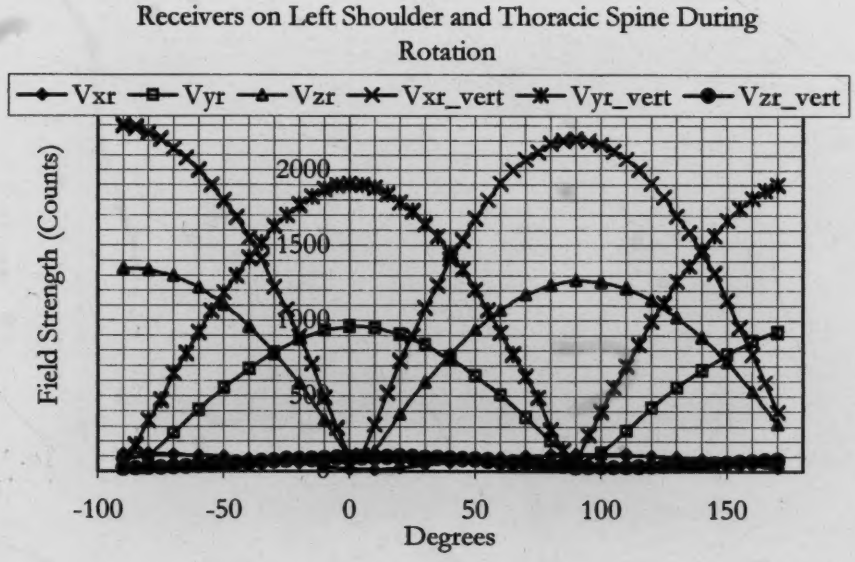

Figure 6-8. Overview of EM system.

Table 6-7 shows the results of the accuracy test. The transmitter and receiver were placed 31.5cm apart. Since the coils are not coaxial the amount of coupling is at half strength and the highest count value of the field was 1141.

Note that when calibrating the system it is possible to have some offset with the zero degree measurement. Factors that cause this are system noise, test equipment alignment, and imperfectly wound coils. When an EM field cuts a coil normal to its axis (coplanar) some voltage can still be induced if some of the coil windings are not completely coplanar. It is most important that the changes in angle are detected accurately. This is shown in table 6-7 where the change in consecutive angle measurements of 10 degree angle increments are detected very accurately. They are within error until 90 degrees is approached, as expected and previously explained. In addition, in practical use it is not expected that a patient will twist their torso to near 90 degrees. Also, if it is required the sensors can be mounted so this does not occur.

Actual Angle (degrees) (±0.25 degrees)	Measured Angle (degrees)	Change Between Consecutive Angle Measurements (degrees)
0	0.0	
10	9.81	
20	19.84	10.03
30	29.79	9.95
40	39.81	10
50	49.82	10.02
60	59.68	9.86
70	69.72	10.04
80	79.73	10.01
90	88.51	8.78

Table 6-7. EM accuracy test results.

6.2.7 System Electromagnetic Angle Resolution Test Results

A summary of the results is shown in Figure 6-9. Between each adjustment of 0.5 degrees the system's measured error ranged from 0.10 degrees to -0.15 degrees, with an average error of 0 degrees. This error range is within the ±0.25 degrees error of the

test equipment itself. The offset angle corresponds to the next measured consecutive angle, ideally 0.5 degrees.

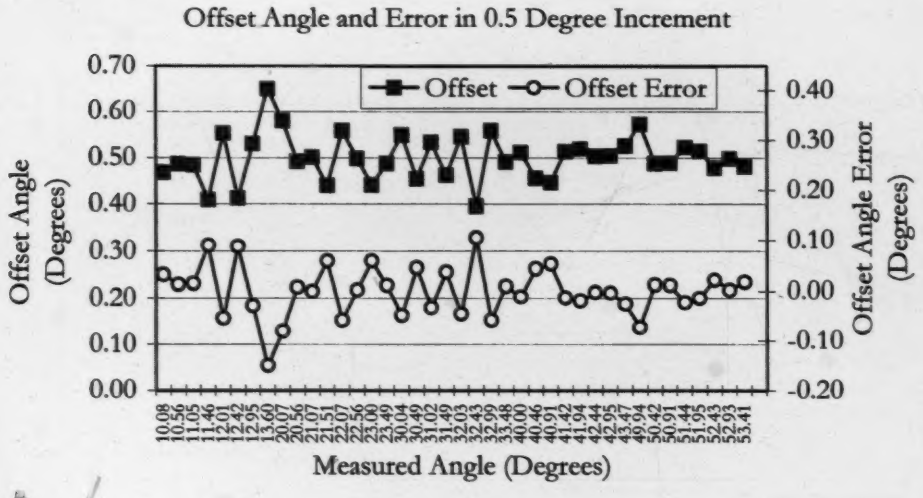

Figure 6-9. EM angle resolution test results.

6.2.8 System Electromagnetic Distance Test Results

The repeatability test results are given in table 6-8. The data reflects the increased resolution of the system as the receiver is brought closer to the source. Any error in placing the receiver back in the same position for each consecutive trial results in a larger signal difference, closer towards the transmitter, due to this resolution. This is observed with the standard deviation of the trial's results increasing the closer the receiver was to the transmitter. In like manner, the average standard deviation for each individual trial decreased as the receiver moved farther from the transmitter.

Radius (cm)	Trial1±SD (counts)	Trial2±SD (counts)	Trial3±SD (counts)	Trial4±SD (counts)	Average SD (counts)	Trial SD (counts)
28	3763.8±2.2	3763.4±2.3	3765.6±2.4	3770±3.2	2.5	3
33	2276±0.7	2277.8+3.9	2277.6±0.5	2277.2±1.8	1.7	0.8
38	1483±2	1483.2±1.3	1482.4±1.7	1484±1.2	1.6	0.7

Table 6-8. Repeatability of EM distance tests.

To perform a distance measurement test the receiver was first calibrated. Figure 6-10 shows the curve obtained for the receiver by taking measurements at 1cm intervals. This curve closely agrees to what is expected for the near dipole EM field.

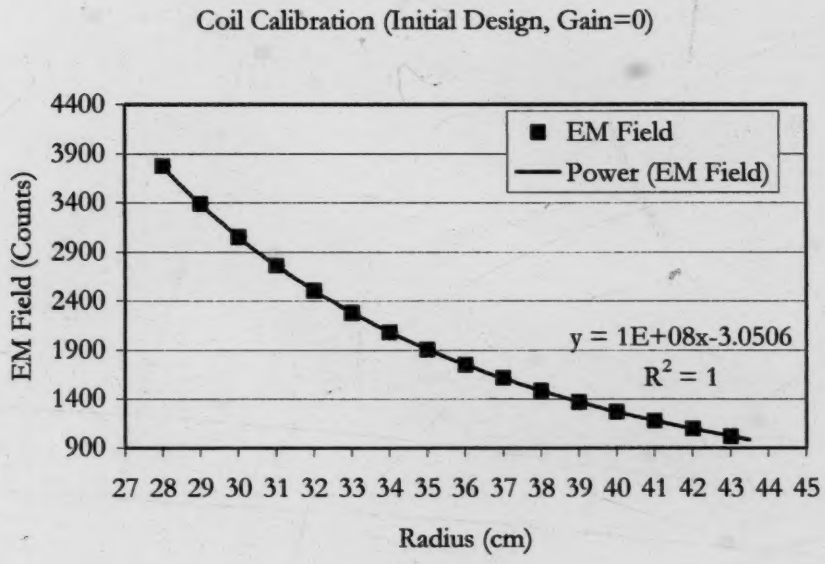

Figure 6-10. EM coil calibration.

Actual Distance±0.001 (cm)	Measured±SD (counts)	Calculated Distance±SD (cm)	Percent Error	Error±SD(cm)
29.737	3137.5±2.2	29.757±0.006	0.067	0.020±0.006
32.269	2442.6±3.2	32.279±0.014	0.031	0.010±0.014
34.207	2043.2±2.4	34.228±0.013	0.061	0.021±0.013
36.94	1615.1±3.0	36.986±0.022	0.125	0.046±0.022
39.647	1303.4±2.1	39.677±0.02	0.076	0.030±0.02
42.709	1040.9±1.7	42.705±0.021	0.009	-0.004±0.021
43.286	999.7±1.3	43.288±0.021	0.004	0.002±0.021

Table 6-9. Distance measurement test summary.

Table 6-9 summarizes the distance measurement results for seven random points used to test the system. The largest error seen was 0.46±0.22 mm. This is more than adequate for the application of this system as mounting error and skin movement will contribute to greater errors in measurement.

Chapter 7

7 CONCLUSIONS AND RECOMMENDATIONS

This thesis explores the requirements and application of posture monitoring to idiopathic scoliosis (IS) treatment. The results from this thesis show that the developed portable posture monitoring system is capable of being used for further research in IS development and treatment, improving treatment studies, and implementing new treatment methods. This thesis demonstrates the benefit of utilizing networked microcontrollers to increase system performance and expandability. It introduces a new hybrid approach to portable posture monitoring and explores the methods that can be used to intuitively and quantitatively monitor an IS patient's posture.

7.1 Conclusions and Results

This thesis examined and presented the need for a wearable system that can monitor posture and record postural information for IS patients. The literature revealed that there is a lack of quantitative data in many IS treatment studies. The system can benefit IS research by providing insight into IS development and the mechanisms of treatment, by reducing the unknowns in treatment studies. In addition it can be used to investigate alternative treatments to bracing and to improve existing, or create new, IS treatment methods. For example existing behaviour programs could be enhanced, and progress and compliance accurately verified. Likewise, new treatment programs could be created, such as a physiotherapeutic treatment program and proprioceptive training. It was determined such a system would require a small, low power, discrete device capable of posture monitoring and providing feedback for posture correction.

To accomplish these goals a novel hybrid networked posture monitoring system was designed, tested, and built. The hybrid design gives the system the benefits of two

technologies. This allows both fast and intuitive setup and calculations, while maintaining the ability to obtain accurate high-resolution measurements. The networked architecture also used parallel processing and acquisition to increase system performance and efficiency. The system is no longer limited to a set number of receivers because each receiver can sample data in parallel. This is opposed to previous systems with a limited number of sensors resulting from sequential polling and a small sampling window. Also, each microcontroller can process its data reducing the computational load on the main controller. The networked architecture and protocol allows for easier integration of a radio frequency transmitter in the future.

Position sensors were evaluated that would be best suited to the system. Accelerometers were investigated and one selected that is capable of measuring yaw angles, yet it does not require constant computations and power. In addition, a single accelerometer package acquires two tilt angles. Coils were evaluated that could be used to detect an EM field. The coils were used in a method that allows yaw angle measurements to be obtained without integration.

A list of movements and postures specific to IS was created in order to summarize the type of motions and postures that need to be monitored. This allowed for the development of different methods to detect postures. Methods were presented to allow the system to quickly determine if a posture is incorrect by monitoring a specific movement. This removes excessive coordinate calculations, speeds up the system, and also allows the system to be set up and configured in an easy intuitive manner. At the same time, the data that are collected are of high resolution, for example, and can be used to calculate clinical measures. Methods were also presented for obtaining clinical measurements specifically.

The methods already presented for posture monitoring aid in developing alternative treatments for IS. The promising literature for behavioural treatment specifically requires training with feedback and reinforcement. Thus the system is suited to this

treatment method as it would reduce training time, and would provide continual reinforcement and proprioceptive training.

Testing was performed to verify the system's ability to measure and detect incorrect posture. In addition, extensive testing was performed at the component level for optimizing the design. The system's angle measurements using the accelerometer resulted in a resolution of ±0.002 g. As explained in the thesis, the resolution in degrees varies over the measurable range, increasing towards 90°. For example, at 0° the resolution is 0.04° and at 70° it is 0.43°. The accuracy of the accelerometer measurement test produced a mean average error of -0.005 g. At 0° this corresponded to -0.0014°, and -1° at 70°. The EM system was tested for both its angle and distance measurements. For the angle test the EM system accuracy is below the test equipment's error of ±0.25°. Likewise the resolution test is below the test equipment error of ±0.25° and is capable of detecting angular changes of 0.5 degrees. Finally for the distance measurement the EM system has higher resolution towards the transmitter and varies as presented. For accuracy, the largest error observed is 0.46±0.22 mm and the mean error of the tests is 0.18±0.17 mm.

7.2 Future Recommendations

To further develop the posture system, clinical trials would be required. Initially a patient's posture could be monitored. Next, a clinic involved in behavioural IS treatment could incorporate the system into its training program. Following the fine tuning from these trials and the quantification of success in the behavioural program, other treatment programs could be developed.

Some improvements that could be made to the system include repackaging the system and creating a new printed circuit board incorporating the smallest surface mount packages available. The digital potentiometers could also be replaced with the new non-volatile digital potentiometers so that their settings are static after power is

removed. This would remove the need for their initialization, saving power and time. The RMS-DC circuit that was used allowed conversion times much faster than previous parts. However, this part requires dual power supplies and thus increases the support circuitry. Specifically, the –5 V switching power supply requires a large inductor and the supply's removal would reduce noise. If synchronization problems with synchronous detection could be overcome, synchronous detection might be a cleaner solution. This would also remove the analog band pass filter circuit that requires the most power on the receiver. This front end could be simplified if a small higher power microcontroller was found with the required peripherals. Provided the higher speed did not increase power requirements digital filtering could then be used. This processor selection could now be simplified as new high bit ADCs are being produced that have a very small 2.9 mm^2 package. Finally, any of the electronics could be integrated into a single IC, such as the analog front end.

The transmitter's power supply could be changed to remove the dual power supply requirement. Due to new, smaller, higher current drive amplifiers it could be possible to produce the same EM field at a lower voltage. This would simplify power supply design and reduce the physical size.

The microcontroller on the main controller unit could be replaced with a lower powered microprocessor. Or, consideration should be given to a modern personal pocket computer, or wearable computer, as their processing power has drastically increased and their prices have decreased. The networked architecture helps facilitate a simple interface for this.

Consideration could be given to implementing a wireless system so that all three devices can communicate without wires. In the simplest form the existing protocol can be transmitted wirelessly with the addition of radio frequency transceivers.

Future researchers might choose to consider a few suggestions to simplify development. The microcontrollers used for the receiver and transmitter should be

changed to a Flash ROM type. This allows code changes to be made much faster. In addition, emulators or in-circuit debuggers for debugging would be beneficial. The microprocessor on the main controller was a flash type; however, it has such a low number of Flash ROM rewrite cycles that several boards were used to finish development because the fine pitch part could not be replaced after the chip was unable to be reprogrammed.

REFERENCES

[1] D. M. Ford, K. M. Bagnall, K. D. McFadden, B. J. Greenhill, V. J. Raso, "Paraspinal muscle imbalance in adolescent idiopathic scoliosis," *Spine*, vol. 9, no. 4, pp. 373-376, 1984.

[2] J. E. Lonstein, R. B. Winter, "Adolescent idiopathic scoliosis: Nonoperative treatment," *Orthopedic Clinics of North America*, vol. 19, no. 2, pp. 239-246, 1988.

[3] N. N. Byl, S. Holland, A. Jurek, S.S. Hu, "Postural imbalance and vibratory sensitivity in patients with idiopathic scoliosis: Implications for treatment," *Journal of Orthopedic and Sports Physical Therapy*, vol. 26, no. 2, pp. 60-68, 1997.

[4] C. Ferraro, S. Masiero, A. Venturin, M. Pigatto, N. Migliorino, "Effect of exercise therapy on mild idiopathic scoliosis: Preliminary results," *Europa Medicophysica*, vol. 34, no. 1, pp. 25-31, 1998.

[5] N. Birbaumer, H. Flor, B. Cevey, B. Dworkin, N. E. Miller, "Behavioral treatment of scoliosis and kyphosis," *Journal of Psychosomatic Research*, vol. 38, no. 6, pp. 623-628, 1994.

[6] B. Dworkin, N. E. Miller, S. Dworkin, N. Birbaumer, M. L. Brines, S. Jonas, E. P. Schwentker, J. J. Graham, "Behavioral method for the treatment of idiopathic scoliosis," *Proceedings of the National Academy of Sciences of the United States of America*, vol. 82, no. 8, pp. 2493-2497, 1985.

[7] M. S. Wong, A. F. T Mak, K. D. K. Luk, J. H. Evans, B. Brown, "Effectiveness of audio-biofeedback in postural training for adolescent idiopathic scoliosis patients," *Prosthetics and Orthotics International*, vol. 25, no. 1, pp. 60-70, 2001.

[8] D. E. Rowe, S. M. Bernstein, M. F. Riddick, F. Adler, J. B. Emans, D. Gardner-Bonneau, "A meta-analysis of the efficacy of non-operative treatments for idiopathic scoliosis," *The Journal of Bone and Joint Surgery – America Volume*, vol. 79-A, no. 5, 664-674, 1997.

[9] J. B. Emans, A. Kaelin, P. Bancel, J. E. Hall, M. E. Miller, "The Boston bracing system for idiopathic scoliosis: Follow-up results in 295 patients," *Spine*, vol. 11, no. 8, pp. 792-801, 1986.

[10] E. Ascani, P. Bartolozzi, D. A. Logroscino, P. G. Marchetti, A. Ponte, R. Savini, F. Travaglini, R. Binazzi, M. Di Silvestre, "Natural history of untreated idiopathic scoliosis after skeletal maturity," *Spine*, vol. 11, no. 8, pp. 784-789, 1986.

[11] R. B. Winter, J. E. Lonstein, J. Drogt, D. A. Noren, "The effectiveness of bracing in the nonoperative treatment of idiopathic scoliosis," *Spine*, vol. 11, no. 8, pp. 790-791, 1986.

[12] V. Mooney, J. Gulick, R. Pozos, "A preliminary report on the effect of measured strength training in adolescent idiopathic scoliosis," *Journal of Spinal Disorders*, vol. 13, no. 2, pp. 102-107, 2000.

[13] B. Stone, C. Beekman, V. Hall, V. Guess, H L. Brooks, "The effect of an exercise program on change in curve in adolescents with minimal idiopathic scoliosis," *Physical Therapy*, vol. 59, no. 6, pp. 759-763, 1979.

[14] R. A. Dickson, "Spinal deformity – Adolescent idiopathic scoliosis," *Spine*, vol. 24, no. 24, pp. 2601-2606, 1999.

[15] F. A. Focarile, A. Bonaldi, M Giarolo, U. Ferrari, E. Zilioli, C. Ottaviani, "Effectiveness of nonsurgical treatment for idiopathic scoliosis: Overview of available evidence," *Spine*, vol. 16, no. 4, pp. 395-401, 1991.

[16] A. Negrini, N. Verzini, S. Parzini, A. Negrini, S. Negrini, "Role of physical exercise in the treatment of mild idiopathic adolescent scoliosis: Review of the literature," *Europa Medicophysica*, vol. 37, no. 3, 181-190, 2001.

[17] M. J. Eliason, L. C. Richman, "Psychological effects of idiopathic adolescent scoliosis," *Journal of Developmental and Behavioral Pediatrics*, vol. 5, no. 4, pp. 169-172, 1984.

[18] M. H. Mehta, "Active correction by side-shift: An alternative treatment for early idiopathic scoliosis," in *Scoliosis Prevention: Proceedings of the 7th Phyillip Zorab Symposium*, 1983, pp. 126-140.

[19] M. A. Herbert, "The treatment of scoliosis using electrical stimulation of muscle," *IEEE Engineering in Medicine and Biology Magazine*," vol. 2, no. 3, pp. 43-49, 1983.

[20] M. A. Herbert, W. P. Bobechko, "Scoliosis treatment in children using a programmable, totally implantable muscle stimulator (ESI)," *IEEE Transactions on Biomedical Engineering*, vol. 38, no. 7, pp. 801-802, 1989.

[21] G. K. Ottman, H. F. Hofmann, A. C. Bhatt, G. A. Lesieutre, "Adaptive piezoelectric energy harvesting circuit for wireless remote power supply," *IEEE Transactions on Power Electronics*, vol. 17, no. 5, pp. 669-676, 2002.

[22] E. Lou, D. L. Hill, V. J. Raso, N. G. Durdle, "A posture measurement system for the treatment of scoliosis," in *Proceedings of IEEE Instrumentation and Measurement*, 1999, pp. 354-358.

[23] E. Paperno, (personal communication), April 29, 2003.

[24] H. Weinberg, *Using the ADXL202 Duty Cycle Output*, Application Note 604, Analog Devices, 2002.

[25] H. Weinberg, "Dual Axis, Low g, Fully Integrated Accelerometers," *Analog Dialogue*, no. 1, pp. 23-24, 1999.

[26] W. Keessen, A. Crowe, M. Hearn, "Proprioceptive accuracy in idiopathic scoliosis," *Spine*, vol. 17, no. 2, pp. 149-155, 1992.

[27] M. Gad el Hak, "Introduction," in *The MEMS handbook*, M. Grad el Hak, Ed., Boca Raton, FL: CRC, 2002.

[28] V. J. Raso, E. Lou, D. L. Hill, J. K. Mahood, M. J. Moreau, N. G. Durdle, "Trunk distortion in adolescent idiopathic scoliosis," *Journal of Pediatric Orthopedics*, vol. 18, no. 2, pp. 222-226, 1998.

[29] P. Anderson, (personal communication), May 2, 2003.

[30] J. W. Wiley, J. D. Thomson, T. M. Mitchell, B. G. Smith, J. V. Banta, "Effectiveness of the Boston brace in treatment of large curves in adolescent idiopathic scoliosis," *Spine*, vol. 25, no. 18, pp. 2326-2332, 2000.

[31] C. L. George, "The posture monitor: An automated prompting device for body alignment," in *Proceedings of the Johns Hopkins National Search for Computing Applications to Assist Persons with Disabilities*, 1992, pp. 143-145.

[32] H. R. Weiss, "Influence of an in-patient exercise program on scoliotic curve," *Italian Journal of Orthopedic Traumatology*, vol. 18, no. 3, pp. 395-406, 1992.

[33] P. D. Sponseller, "Sizing up scoliosis," *Journal of the American Medical Association*, vol. 289, no. 5, pp. 608-609, 2003.

[34] S. L. Weinstein, L. A. Dolan, K. F. Spratt, K. K. Peterson, M. J. Spoonamore, I. V. Ponseti, "Health and function of patients with untreated idiopathic scoliosis: A 50-year natural history study," *Journal of the American Medical Association*, vol. 289, no. 5, pp. 559-567, 2003.

[35] F. Schwab, A. Dubey, M. Pagala, L. Gamez, J. P. Farcy, "Adult scolisis: A health assessment analysis by SF-36," *Spine*, vol. 28, no. 6, pp. 602-606, 2003.

[36] J. A. Lerman, E. Sullivan, R. J. Haynes, "The pediatric outcomes data collection instrument (PODCI) and functional assessment in patients with adolescent or juvenile idiopathic scoliosis and congenital scoliosis or kyphosis," *Spine*, vol. 72, no. 18, pp. 2052-2058, 2002.

[37] D. L. Skaggs, G. S. Bassett, "Adolescent idiopathic scoliosis: An update," *American Family Physician*, vol. 53, no. 7, pp.2327-2334, 1996.

[38] T. Karachalios, J. Sofianos, N. Roidis, G. Sapkas, D. Korres, K. Nilolopoulos, "Ten-year follow-up evaluation of a school screening program for scoliosis: In the forward-beading test an accurate diagnostic criterion for the screening of scoliosis?" *Spine*, vol. 24, no. 22, pp. 2318-2324, 1999.

[39] R. T. Morrissy, "School screening for scoliosis," *Spine*, vol. 24, no. 24, pp. 2584-2591, 1999.

[40] C. J. Goldberg, M. kaliszer, D. P. Moore, E. E. Fogarty, F. E. Dowling, "Surface topography, cobb angles, and cosmetic change in scoliosis," *Spine*, vol. 26, no. 4, pp. E55-E63, 2001.

[41] L. A. Karol, "Effectiveness of bracing in male patients with idiopathic scoliosis," *Spine*, vol. 26, no. 18, pp. 2001-2005, 2001.

[42] K. Felton, "The use of adherence monitors with orthoses," *Journal of Prosthetics and Orthotics*, vol. 11, no. 4, pp. 98-100, 1999.

[43] A. L. Nachemson, L. E. Peterson, "Effectiveness of treatment with a brace in girls who have adolescent idiopathic scoliosis: A prospective, controlled study based on data from the brace study of the Scoliosis Research Society," *Journal of Bone & Joint Surgery – American Volume*, vol. 77-A, no. 6, pp. 815-822, 1995.

[44] W. A. den Boer, P. G. Anderson, J.v. Limbeek, M. A. P. Kooijman, "Treatment of idiopathic scoliosis with side-shift therapy: An initial comparison with a brace treatment historical cohort," *European Spine Journal*, vol. 8, no. 5, pp. 406-410, 1999.

[45] P. Bylund, S. Aaro, B. Gottfries, E. Jansson, "Is lateral electrical surface stimulations an effective treatment for scoliosis?" *Journal of Pediatric Orthopaedics*, vol. 7, no. 3, pp. 298-300, 1987.

[46] W. S. Marras, F. A. Fathallah, R. J. Miller, S. W. Davis, G. A. Mirka, "Accuracy of a three-dimensional lumbar motion monitor for recording dynamic trunk motion characteristics," *International Journal of Industrial Ergonomics*, vol. 9, no. 1, pp. 75-87, 1992.

[47] Y. Nishida, M. Takeda, T. Mori, H. Mizoguchi, T. Sato, "Monitoring patient respiration and posture using human symbiosis system," in *Proceedings of the 1997 IEEE/RSJ International Conference on*, 1997, pp. 632-639.

[48] S. Tanaka, K. Yamakoshi, P. Rolfe, "New portable instruments for long-term ambulatory monitoring of posture change using miniature electro-magnetic inclinometers," *Med Biol Eng Comput*, vol. 32, no. 3, pp. 357-60, 1994.

[49] M. Neuwith, *The Scoliosis Handbook*. New York: Henry Hold, 1996.

[50] G.C. Robin, *The Aetiology of Idiopathic Scoliosis*. Boca Raton, Florida: CRC, 1990.

[51] W.P. Blount, J.H. Moe, *The Milwaukee Brace, 2nd Edition*. Baltimore: Williams and Wilkins, 1980.

[52] K.D. Leatherman, R.A. Dickson, *The Management of Spinal Deformities.* London: Butterworth & Co. Ltd., 1988.

[53] S.S. Shenk, J.A. Paradiso, "Energy scavenging with shoe-mounted piezoelectrics," *IEEE Micro*, vol.21, May and June, pp. 30-42, 2001.

[54] E. Lou, "An EM Approach to the Treatment of Scoliosis," Ph.D. Dissertation, University of Alberta, Edmonton, AB, Canada, 1998.

[55] A. State, G. Hirota, D. T. Chen, W. F. Garrett, M. A. Livingston, "Superior Augmented-Reality Registration by Integrating Landmark Tracking and Magnetic Tracking," in *Computer Graphics Proceedings Annual Conference Series*, 1996, pp. 429-438.

[56] B. Kemp, A.J.M.W. Janssen, B. van der Kamp, "Body position can be monitored in 3D using miniature accelerometers and earth-magnetic field sensors," *Electroencephalography and clinical Neurophysiology*, vol. 109, no. 6, pp. 484-488, 1998.

[57] Virtual Corset, [Online], [cited 2000 July 17], Available WWW: http://www.microstrain.com/vcorset.htm.

[58] J.J. Bray. *Prosthetic principles upper extremity amputations, Fabrication and fitting principles.* University of California, Los Angeles: Prosthetics-Orthotics Education Program, n.d.

[59] Dryver R. Huston, Bruce Beynnon, Martin Krag, "Smart structures technology and biomechanics research", in *Smart Structures and Materials 1996*, SPIE Proceedings, 1996, pp. 523-529.

[60] W.B. Powell, D. Pheifer, "The Electrolytic Tilt Sensor", *Sensors*, vol. 17, no. 5, May, pp.120-125, 2000.

[61] D. K. Cheng. *Fundamentals of Engineering Electromagnetics.* Reading, Mass.: Addison-Wesley Pub. Co., 1994.

[62] Philips Semiconductor, "I2C Specification," [Online Document], 2000 (Version 2.1), [cited 2004 September 10], Available WWW: http://www.semiconductors.philips.com/acrobat/literature/9398/39340011.pdf.